Modal coupling in the damped structures

Auteur : Mayou, Anass
Promoteur(s) : Denoel, Vincent
Faculté : Faculté des Sciences appliquées
Diplôme : Master en ingénieur civil des constructions, à finalité spécialisée en "civil engineering"
Année académique : 2018-2019
URI/URL : http://hdl.handle.net/2268.2/8013

FACULTY OF APPLIED SCIENCES
UNIVERSITY OF LIÈGE

Modal coupling in the damped structures

Effect of the coupling on the vibration behavior of footbridges

Graduation work carried out to obtain
the Master's degree Civil Engineer in Construction
By Anass Mayou

Supervisor :
Vincent Denöel
Readers :
Vincent De Ville De Goyet
Yves Duchêne
Peter Van Den Broeck

Academic year : 2018-2019

Acknowledgements

I would like to thank Professor Vincent Denoël, Professor at the University of Liège, who mentored me throughout this thesis and shared with me his brilliant insights, and his research themes that inspired this thesis. May he also be thanked for his kindness, his permanent availability and for the many encouragement he has given me.

I thank Mr Vincent De Ville De Goyet, Mr Yves Duchêne (Engineers at Bureau Greisch), and Mr Peter Van Den Broeck (Professor at the KU Leuven), for the honour they have bestowed upon me by agreeing to be the readers of this thesis.

I would like to thank the members of the Dynamics' team and especially Mrs Margaux Gueuzaine, who has been a huge support during these two years of Master's, responding calmly and patiently to my questions.

I would like to thank all the friends with whom I shared my studies and especially those from the years of Master's, who welcomed me and helped me quickly integrate the Belgian life.

Finally, I cannot thank enough my family who gave me the opportunity to study in Europe, and offered me all the conditions to succeed : morally and financially.

University of Liège

Liège, August 2019

Abstract

English version

TMDs (Tuned Mass Dampers) are renowned for vibration control under dynamic loading, and aim at maintaining the acceleration of the main structure below the thresholds defined by guidelines. They are particularly essential when it comes to lightweight and slender structures such as modern footbridges, where "lock-in" effects may manifest under the loading of pedestrians, and create situations of discomfort. Belonging to the category of passive control devices, the TMDs offer the advantage to not require external power supply. Their applicability is nevertheless limited for economic and aesthetic reasons essentially, when large mass ratio is demanded. Also, when simplified approaches are adopted that neglect the modal coupling, requiring the association of a damper to each structural mode.

This work examines the feasibility of damping two frequency-nearby modes of vibration with a single TMD, when a MDOF system is subjected to crowd excitation. Considering the crowd motions as a stationary phenomenon, stochastic tools are engaged so as to extract directly the steady-state of the response. The variables of the problem (acceleration, displacement and loading) are treated as random variables, characterized by their PSDs (Power Spectral Densities). The design of the TMD is then founded on the minimization of the response's variance until meeting the comfort criteria. The modal coupling is considered and pointed out by analytical expressions derived thanks to perturbation methods. These techniques are also essential to determine the TMD's optimal parameters : mass ratio, tuning ratio and damping ratio.

Keywords – TMD design, Modal coupling, Perturbation techniques, Random stochastic variables

Version française

Les AMA (Amortisseurs à Masse Accordée) sont renommés pour le contrôle des vibrations sous chargement dynamique, maintenant l'accélération de la structure principale en dessous des seuils prédéfinis par les guides. Ils sont particulièrement essentiels lorsqu'il s'agit de structures légères et élancées, comme le sont les passerelles modernes. Particulièrement, lorsque les effets de "lock-in" peuvent se manifester sous le chargement des piétons, et créer des situations d'inconfort. Appartenant à la catégorie des amortisseurs de type passif, les TMD offent l'avantage de n'exiger aucune alimentation externe. Néanmoins, leur applicabilité reste limitée pour des raisons essentiellement économiques et esthétiques lorsqu'un grand rapport de masse est requis. Elle est également limitée lors de l'adoption d'approches simplifiées qui négligent le couplage modal, nécessitant l'association d'un amortisseur à chaque mode structurel.

Ce travail examine la faisabilité d'amortir deux modes de vibration de fréquences propres voisines, avec un seul TMD attaché à un système MDOF soumis à l'excitation d'une foule. Considérant les mouvements de foule comme un phénomène stationnaire, des outils de type stochastique sont engagés de manière à extraire directement la réponse de la structure. Les variables du problème (accélération, déplacement et chargement) sont traitées comme des variables aléatoires, caractérisées par leurs DSP (Densités Spectrales de Puissance). Le dimensionnement du TMD reposera ensuite sur la minimisation de la variance de la réponse, jusqu'à atteindre les critères de confort. Le couplage modal est pris en compte et mis en évidence par des expressions analytiques obtenues grâce à des méthodes par perturbation. Ces techniques sont également essentielles pour déterminer les paramètres optimaux du TMD : masse, fréquence propre et coefficient d'amortissement.

Mots-clés – Dimensionnement du TMD, Couplage modal, Méthodes par perturbation, Variables aléatoires

Contents

List of Figures

List of Tables

List of Symbols

$R_{x,x}(t_1, t_2)$	Auto-correlation function of the random variable x
$R_{x,y}(t_1, t_2)$	Cross-correlation function between the random variables x and y
$S_{x,x}$	Power Spectral density (PSD) of the random process, defined as the Fourier transform of its auto-correlation function
$S_{x,y}$	Power Spectral density (PSD) of the random processes x and y, defined as the Fourier transform of its cross-correlation function
m_i	Spectral moment of order i, representing the shape of a spectral power density
σ_x	Variance of the random variable x
$\sigma_{x,y}$	Covariance of the random variables x and y
$\underline{\underline{M}}$	Mass matrix
$\underline{\underline{K}}$	Stiffness matrix
$\underline{\underline{C}}$	Damping matrix
$\{x\}$	Nodal displacement vector
$\{\dot{x}\}$	Nodal velocity vector
$\{\ddot{x}\}$	Nodal acceleration vector
$\{p(t)\}$	External loads vector
$\underline{\underline{M}}^*$	Generalized Mass matrix : Mass matrix projected in the modes' basis
$\underline{\underline{K}}^*$	Generalized Stiffness matrix : Stiffness matrix projected in the modes' basis
$\underline{\underline{C}}^*$	Generalized Damping matrix : Damping matrix projected in the modes' basis
ξ^*	Equivalent damping ratio of the structure
$\{p^*(t)\}$	Modal forces
Φ	Matrix containing the eigenvectors (modes)
$\{q\}$	Modal displacement vector
$\{\dot{q}\}$	Modal velocity vector
$\{\ddot{q}\}$	Modal acceleration vector
$\{Q\}$	Fourier transformation of the modal displacement
$\{\dot{Q}\}$	Fourier transformation of the modal velocity
$\{\ddot{Q}\}$	Fourier transformation of the modal acceleration
$H(\omega)$	Frequency Reponse Function (FRF) or Transfer function
$H^*(\omega)$	Transfer function projected in the modes' basis
μ	Mass ratio : mass of the damper over the mass of the structure (or first modal mass)
$\overline{M_2}$	Mass ratio : mass of the second modal mass over the first modal mass
α	Tuning ratio : natural frequency of the damper over the natural frequency of the structure
β	Ratio of the second natural frequency over the first natural frequency
(φ_1, φ_2)	Coordinates in the modes : position of the damper
ξ_s	Damping ratio of the structure
ξ_{TMD}	Damping ratio of the damper
μ_1,b,ν_2	Dimensionless parameters of $ord(1)$

1 Introduction

1.1 Contextualization

The vibrations are by definition periodic movements occurring around an equilibrium position, characterized by a frequency. In the construction field, these movements are undesirable, especially when it comes to low frequencies. Indeed, the (1 to 10 Hz) range is considered as the most threatening, leading to considerable displacements which current constructions are seriously sensitive. It is more critical for lightweight structures as the vibration frequency can match the resonant frequencies. The footbridges serve as a good example of structures subjected to vibration issues, the source of disturbance can appear under wind, seismic or crowd loading engendering significant lateral and vertical displacements and accelerations, resulting in safety problems.

In the recent years, the discomfort occasioned constitutes a topic of growing concern, because of the conception of sophisticated bridges where the aesthetic aspect and the environmental integration constitute essential features especially in urban context. More slenderness and bigger spans are requested, motivating a flexible behavior of the footbridges, and a bigger ratio live loads over permanent loads.

The disposition of external dampers is aimed to limit the vibrations undergone by the primary system. These devices are characterized by a mass, a damping (viscosity) and a spring (stiffness), and are placed at the position where the maximum displacement is reached. The damper has its natural frequency adjusted with the fundamental mode of the vibrating structure. This tuning allows the transfer of the vibrating energy to the absorber. The transmitted energy is higher when the added mass is increased, which contributes to reduce more the discomfort.

The discomfort is generally expressed in terms of acceleration, thresholds are given by guidelines like Hivoss [4] and Sétra [8], to avoid phenomenons like the *Lock-in* effect. This effect is related to lateral vibrations, that occurs when there is a partial synchronization between the pedestrian motion and the footbridge motion. The well-known illustration of this phenomenon is given by the Millenium bridge in London the day of its inauguration on the 10th of June 2000, where 2000 pedestrians were walking on it at the same time, inducing significant and increasing displacements in the lateral direction.

The structural modes can be found very close in the frequency domain. A classical solution is to dedicate a damper for each mode, giving birth to a non-optimal solution. Indeed, since the implemented equipment is significant and thus expensive in terms

of labour as well. It is also not slender and not optimal regarding the weight added on the supposed lightweight structure. The damping devices are thus designed on the basis of simplified assumptions not taking into account modal coupling. A considerable number of practical cases call for the consideration of the interaction of multiple structural modes of the mutual influence of several dampers. For instance, structures with close natural frequencies, where the mentioned assumptions are not valid for the design of the dampers.

The numerical tool based on the finite element method, is nowadays developed to include the damping devices in the modelling phase. It constitutes the privileged solution when it comes to problems of this complexity. However, the increase of the number of elements and parameters can be time and memory consuming, also the understanding of the results can no more still intuitive. The development of the analytic tool based on mathematical methods, can provide approached results, giving a first idea of the quantity and the mass of the dampers needed. The feasibility of a solution is evaluated quickly, without having to go through a complete modelling of the structure, which is costly in terms of time and investment. The use of analytic forms, how accurate they may get, makes also possible the understanding of the real dynamics behind a structure.

1.2 Motivation

The appreciation of the modal coupling raises the capacity to simultaneously dampen a number of vibration modes with a lower number of dampers, which is different from traditional damping strategies. This work aims attention to 2DOF (2 Degree-Of-Freedom) structures, and examines the ability of a single damper to dampen both structural modes at the same time.

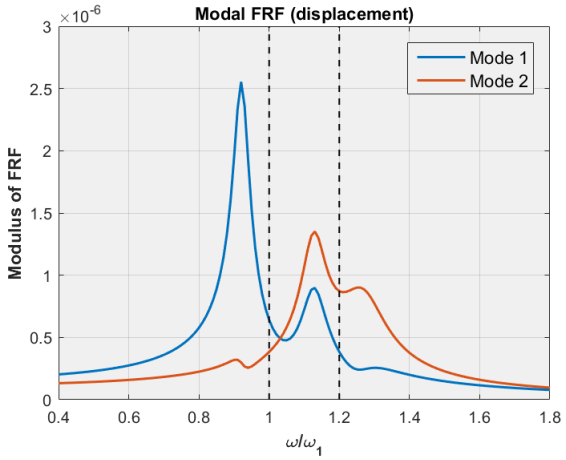

Figure 1.1: FRF of a damped system

The figure above illustrates well the phenomenon of modal coupling. The transfer functions in the first and second mode present 2 bumps in the right of the natural frequencies. It is observed that the position of the right bump of the first transfer function, coincides with the left bump of the second. Meaning two things : First, the damper tuned to the first mode, have also an effect on its neighbour, which is not the case in an uncoupled situation. Second, that the transfer functions have a common pole coming from the implementation of the damper.

A first investigation has been carried out by Loore [5] where the influence of the modal coupling is studied in a MDOF (Multi-Degree-Of-Freedom) structure under a deterministic approach. A simplified and completely analytic expression of the transfer function of the damped system is established. The strategy implemented is to verify that the nodal transfer function admits its optimum values $(\theta_1^{**}, \theta_2^{**})$ below comfort limits (θ_1, θ_2), involving conditions to be fulfilled (**Figure 1.2**).

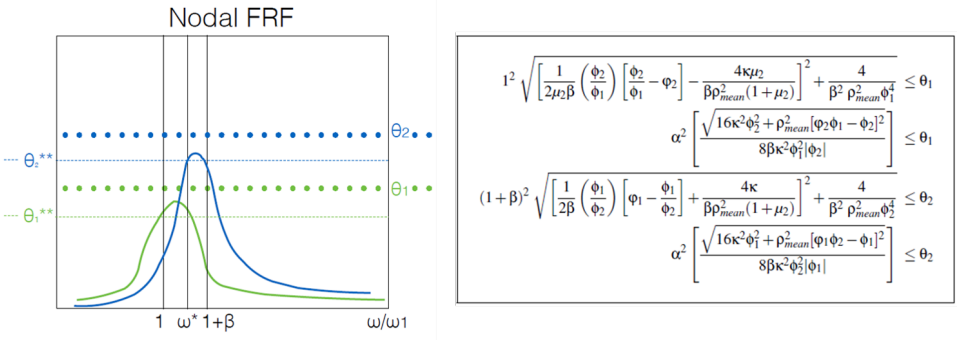

Figure 1.2: Strategy of Loore [5]

Meanwhile, the current document suggests a spectral analysis, involving a stochastic approach for the optimum design of the TMD (Tuned Mass Damper). The crowd loading is assimilated to a simple stationary stochastic process (such as a white noise), the response (acceleration or displacement) is treated as random variable, characterized by its PSD (Power Spectral Densities). The study is in this case, interested in keeping the variance of the response below the thresholds, and not concern the transfer function. The purpose is to reach expressions that are light and meaningful, where the influence of the TMD's parameters appears clearly.

1.3 Organization of the text

This work provides a solution to the questions outlined above, while meeting the practical need for simple analytic formulations. The development of the analytic model is employed for the investigation and the development of new results.

The content is divided into 3 main parts :

The first section introduces the spectral model established, with the analytic treatment of the stochastic operators allowing to link the response of the structure (displacement and acceleration) to the wideband excitation applied to it.

The second section provides a presentation of the technology of passive dampers as TMDs with its main characteristics, moving on to the determination of the modal properties after the implementation to the main structure. The idea is to develop thanks to a perturbation method analytic formulations for the natural frequencies and the damping ratio of the damped system, evidencing the interaction of the structural modes.

The third section gathers the results of the first and second section, to produce a method that predicts the serviceability state of the footbridge. The method is subjected to a validation procedure through an example of a real-life structure. The performance of the TMD in the vibration mitigation is then discussed in function of its mass, position and frequency ratio.

2 Dynamic analysis with stochastic methods

The idea is to develop the stochastic tools necessary for the resolution of the equation of motion, where the walking action is treated like a random variable, as the walking characteristics remains a specificity of the single pedestrian. A spectral analysis is performed where the random variables are characterized by their PSD[1] (Power Spectral Density). Going from the crowd excitation treated as a stationary phenomenon, the purpose is to figure out easily the steady-state of the structure, and reach the cumulants of the response such as the variance. The variance is no other than the result of the integral of the spectra considered in a frequency domain.

This chapter aims attention in the first place to the displacement, going through the development of the analytic approximation of its variance, armed with the methods developed by Denoël ([1] and [10]). Secondly, the focus is translated to the acceleration, maintaining the same reasoning with the integration of some adaptations, to find the variance as final outcome. The validity of the analytic results is discussed comparing it with numerical integration's result. The resolution is possible in both time and frequency domain, the transition from one to another simply requires a Fourier Transformation. The establishment of the equations is done in the time domain first, then in the frequency domain.

2.1 Analytic resolution of the equation of motion

2.1.1 Time domain

The time domain is much more attractive when it comes to a deterministic approach. Indeed, the solicitation is generally given in function of the time.

$$\underline{\underline{M}}\{\ddot{x}(t)\} + \underline{\underline{C}}\{\dot{x}(t)\} + \underline{\underline{K}}\{x(t)\} = \{p(t)\} \tag{2.1}$$

For the resolution of the equation of motion, a step-by-step approach is used. The time is discretized into finite intervals, in which relationships exist between the displacements, the velocities and accelerations. The goal is to simplify the implicit relationships between the different variables.

Starting from integration methods that are based on approximations of integrals

[1] The PSD of a signal describes its mean-square value in function of the frequency, such that the magnitude is normalized to a single hertz bandwidth. It gives the image of the frequency distribution of the energy contained in the process.

(EQUATION (2.2) and (2.3)), simple analytic expression can be derived of $\{\ddot{x}(t)\}$ that allows to solve the equation in an explicit way (found in [2]).

$$\{\dot{x}\}_{t+\Delta t} = \{\dot{x}\}_t + \int_t^{t+\Delta t} \{\ddot{x}\}_{t+\Delta t}\, \mathrm{d}t \tag{2.2}$$

$$\{x\}_{t+\Delta t} = \{x\}_t + \int_t^{t+\Delta t} \{\dot{x}\}_{t+\Delta t}\, \mathrm{d}t \tag{2.3}$$

At the beginning of the step, $\{x\}_t$, $\{\dot{x}\}_t$ and $\{\ddot{x}\}_t$ are considered as known. As it is a stable and quite precise method, the Newmark method is chosen which is based on the assumption :

$$\{\dot{x}\}_{t+\Delta t} = \{\dot{x}\}_t + [(1-\delta)\{\ddot{x}\}_t + \delta\{\ddot{x}\}_{t+\Delta t}] \cdot \Delta t \tag{2.4}$$

$$\{x\}_{t+\Delta t} = \{x\}_t + [(1/2-\alpha)\{\ddot{x}\}_t + \alpha\{\ddot{x}\}_{t+\Delta t}] \cdot \Delta t^2 \tag{2.5}$$

$$\underline{\underline{M}}\{\ddot{x}\}_{t+\Delta t} + \underline{\underline{C}}\{\dot{x}\}_{t+\Delta t} + \underline{\underline{K}}\{x\}_{t+\Delta t} = \{p\}_{t+\Delta t} \tag{2.6}$$

As the variables $\{x\}_{t+\Delta t}$ and $\{\dot{x}\}_{t+\Delta t}$ are expressed in function of $\{\ddot{x}\}_{t+\Delta t}$, the latter remains the only unknown of the problem. Thanks to the equation of motion expressed at $t+\Delta t$, and the replacement of $\{x\}_{t+\Delta t}$ and $\{\dot{x}\}_{t+\Delta t}$ by their expressions above, the variables can be computed at the end of the step. Considering 3 equations per degree of freedom, $3N$ relationships are derived for the N degrees of freedom problem.

A constant acceleration corresponds to the couple $(\alpha, \delta) = (\frac{1}{4}, \frac{1}{2})$, while the linear acceleration is considered in the case of $(\alpha, \delta) = (\frac{1}{6}, \frac{1}{2})$. The first scheme is chosen, since it is recommended for its performances in terms of stability and precision.

The modal decomposition is written : $\{x(t)\} = [\Phi]\{q(t)\}$, the replacement in (2.1) gives an equation of equilibrium that has the same physical meaning, but this expressed in a modal basis :

$$\underline{\underline{M}}[\Phi]\{\ddot{q}(t)\} + \underline{\underline{C}}[\Phi]\{\dot{q}(t)\} + \underline{\underline{K}}[\Phi]\{q(t)\} = \{p(t)\} \tag{2.7}$$

The components of the combination of the natural modes are contained in the vector $\{q(t)\}$. The modes ϕ_j such that $\Phi = [\phi_1 \phi_2 \ ... \ \phi_N]$, are normalized for a unitary maximum ($max_j|\phi_{j,i}| = 1$), the coefficients become the modal amplitudes. Multiplying the EQUATION (2.1) by $[\Phi]^T$ means that the equations are projected in the modes' basis, which makes appear the generalized matrix $\underline{\underline{M^*}} = [\Phi]^T\underline{\underline{M}}[\Phi]$, $\underline{\underline{C^*}} = [\Phi]^T\underline{\underline{C}}[\Phi]$, and $\underline{\underline{K^*}} = [\Phi]^T\underline{\underline{K}}[\Phi]$, as well as the generalized force $\{p^*\} = [\Phi]^T\{p\}$.

The modal decomposition offers to convert the problem from 1 equation of N unknowns to a problem of N equations of 1 unknown, the problem is said "uncoupled".

Another advantage is that it allows to work with diagonal matrices (it is automatically the case for $\underline{\underline{M}}^*$ and $\underline{\underline{K}}^*$, but not for $\underline{\underline{C}}^*$ where assumptions have to be made).

$$\underline{\underline{M}}^*\{\ddot{q}(t)\} + \underline{\underline{C}}^*\{q(t)\} + \underline{\underline{K}}^*\{q(t)\} = \{p^*(t)\} \tag{2.8}$$

Stepping back to the modal decomposition :

$$\{x(t)\} = [\Phi]\{q(t)\} = \int_0^t [h(t-\tau)]\{p(\tau)\}\,\mathrm{d}\tau \tag{2.9}$$

The solicitation is represented by a PSD, the variables $\{\ddot{x}(t)\}$, $\{\dot{x}(t)\}$, $\{x(t)\}$ and $\{p^*(t)\}$ become random processes, and get characterized by their $PSDM$.

To compute the mean of the signal, the operator $E[\,]$ is introduced in order to detect the regularities and repeated profiles in the output process $\{x(t)\}$ through the time.

$$E[\{x(t_1)\}\{x(t_2)\}^T] = \int_0^{t_1}\int_0^{t_2} [h(t_1-\tau_1)]\ E[\{p(\tau_1)\}\{p(\tau_2)\}^T]\ [h(t_2-\tau_2)]^T\,\mathrm{d}\tau_1\mathrm{d}\tau_2 \tag{2.10}$$

This is therefore the definition of the auto-correlation function. It represents the temporal mean of the product of the signal by itself shifted by a time $\Delta t = t_2 - t_1$.

As long as the process is stationary, it is possible to replace $E[\{p(\tau_1)\}\{p(\tau_2)\}^T]$ by the auto-correlation function $R_p(\Delta\tau)$.

$$R_x(t_1,t_2) = \int_0^{t_1}\int_0^{t_2} [h(t_1-\tau_1)]\ R_p(\Delta\tau)\ [h(t_2-\tau_2)]^T\,\mathrm{d}\tau_1\mathrm{d}\tau_2 \tag{2.11}$$

Fourier's transformation serve as the link between $R_x(\tau)$ and its associated PSD $S_x(\omega)$, like it stated by the theorem of Wiener-Khintchine here below :

$$S_x(\omega) = \frac{1}{2\pi}\int_{-\infty}^{+\infty} R_x(\tau)\cdot e^{-i\omega t}\mathrm{d}\tau\ ;\ R_x(\tau) = \int_{-\infty}^{+\infty} S_x(\omega)\cdot e^{i\omega t}\mathrm{d}\omega \tag{2.12}$$

A very important result that emerges from those equations is that : when τ equals 0, the auto-correlation function becomes equal to the squared variance of the process considered. It is also the area below the curve of $S_x = fct(\omega)$.

$$R_x(0) = \int_{-\infty}^{+\infty} S_x(\omega)\cdot\mathrm{d}\omega = \sigma_x^2 \tag{2.13}$$

Going back to (2.11), and considering a white noise as an input, the PSD $S_x(\omega) = S_0 = cst$, the auto-correlation function associated is a Dirac impulsion centered at the origin : $R_p(\Delta\tau) = 2\pi S_0\delta(\Delta\tau)$. The introduction of the Dirac function, simplifies

the equation to a single integral :

$$R_x(t_1,t_2) = \int_0^{t_1} [h(t_1-\tau_1)]\ R_p\ [h(t_2-\tau_1)]\,\mathrm{d}\tau_1 \tag{2.14}$$

$$\sigma_x^2(t) = R_x(0) = R_x(t,t) = R_p \int_0^t [h(t-\tau)]^2\,\mathrm{d}\tau \tag{2.15}$$

For a simple oscillator, the variance of the displacement x is written :

$$\sigma_x^2(t) = \frac{R_p}{4\xi\omega^3 m^2}[1 - e^{-2\xi\omega t}(\frac{1}{1-\xi^2} - \frac{\xi^2}{1-\xi^2}cos(2\omega_d t) + \frac{\xi^2}{\sqrt{1-\xi^2}}sin(2\omega_d t))] \tag{2.16}$$

At the permanent stage (when $t \to +\infty$), the variance tends to a constant value :

$$\boxed{\sigma_x^2 = \frac{R_p}{4\xi\omega^3 m^2} = \frac{S_0}{K^{*2}_{m,m}} \cdot \frac{\pi\omega}{2\xi}} \tag{2.17}$$

The variance is expressed in function of the physical parameters of the problem, where the external force represents the motor of the acceleration against the stiffness and the damping ratio that are supposed to limit it.

2.1.2 Frequency domain

In practice, the frequency domain remains more interesting, owing to the simplicity of the link between the input $Q(\omega)$ and the output $P(\omega)$, where the convolution corresponds to a multiplication. However, the representation of instationary mechanisms in the frequency domain is much more complicated than in the time domain. The following investigation concerns exclusively the stationary problems.

$$Q(\omega) = \int_{-\infty}^{+\infty} q(t)\cdot e^{-i\omega t}\,\mathrm{d}t\ ;\ P(\omega) = \int_{-\infty}^{+\infty} p(t)\cdot e^{-i\omega t}\,\mathrm{d}t \tag{2.18}$$

The velocity and the acceleration are derived from the displacement as following :

$\dot{Q}(\omega) = (i\omega)Q(\omega)$ and $\ddot{Q}(\omega) = (i\omega)^2 Q(\omega) = -\omega^2 \cdot Q(\omega)$

The FRF is then expressed as the ratio of the output of the problem over it's input $H(\omega) = Q(\omega)/P(\omega)$, the development leads to the EQUATION 4.4.

$$\underline{\underline{H}}(\omega) = (-\underline{\underline{M}}\omega^2 + i\omega\underline{\underline{C}} + \underline{\underline{K}})^{-1} \tag{2.19}$$

Pre-multiplying the EQUATION (2.1) by $[\Phi]^T$, converts from nodal expressed in function of $\{x\}$ to modal basis in function of $\{q\}$, with $\{x\} = [\Phi]\{q\}$. Generalized

matrix $\underline{\underline{M}}^*$, $\underline{\underline{C}}^*$, and $\underline{\underline{K}}^*$ make their appearance, as well as the generalized force $\{P^*\}$, and $\underline{\underline{H}}^*(\omega)$:

$$\underline{\underline{M}}^*\{\ddot{Q}(\omega)\} + \underline{\underline{C}}^*\{\dot{Q}(\omega)\} + \underline{\underline{K}}^*\{Q(\omega)\} = \{P^*(\omega)\} \tag{2.20}$$

$$\underline{\underline{H}}^*(\omega) = (-\underline{\underline{M}}^*\omega^2 + i\omega\underline{\underline{C}}^* + \underline{\underline{K}}^*)^{-1} \tag{2.21}$$

Owing to **Property 1**[2], with the consideration of the link between $\{P^*\}$ and $\{P\}$ written in a vectorial form, the PSDM of the generalized forces is naturally obtained from the PSDM of the nodal forces :

$$\{P^*\} = [\Phi]^T\{P\} \Rightarrow [S_{p^*}] = [\Phi]^T[S_p][\Phi] \tag{2.22}$$

Using **Property 2**[3], the PSDM associated to the displacement can be derived, where all the components of (2.24) are henceforth known :

$$\underline{\underline{Q}}(\omega) = \underline{\underline{H}}^*(\omega) \cdot \underline{\underline{P}}^*(\omega) \Rightarrow [S_q] = \underline{\underline{H}}^*(\omega) \cdot [S_{p^*}] \cdot \overline{\underline{\underline{H}}^*(\omega)}^T \tag{2.23}$$

$$[S_q] = \begin{bmatrix} S_{q_{1,1}} & S_{q_{1,2}} & \cdots & S_{q_{1,M}} \\ S_{q_{2,1}} & S_{q_{2,2}} & \cdots & S_{q_{2,M}} \\ \vdots & \vdots & \ddots & \vdots \\ S_{q_{M,1}} & S_{q_{M,2}} & \cdots & S_{q_{M,M}} \end{bmatrix} \tag{2.24}$$

2.2 Developments for the displacement

The field of study is limited to linear stationary problems, the developments are thus conducted in the frequency domain. On account of the direct computation of the steady-state, by means of a simple multiplication. Besides, the stochastic loading is already expressed in this domain, which is encouraging to maintain it.

2.2.1 Determination of the variance

In the case of a uncoupled system, each mode is treated separately : the relationship between the mass, stiffness and damping are simple. The correspondent FRF matrix is diagonal, and offers a single-peak curve when represented in function of ω, a result similar to an SDOF (Single-Degree-Of-Freedom) system.

[2]**Property 1 :** Knowing $[S_x]$ the PSD associated to the random process $\{x(t)\}$, the PSD $[S_y]$ of the random process $\{y(t)\}$ defined by : $\{y(t)\} = [Z]\{x(t)\}$ is also known : $[S_y] = [Z][S_x][Z]^T$

[3]**Property 2 :** Knowing $[S_x]$ the PSD associated to the random process $\{X(\omega)\}$ and the transfer matrix $[H(\omega)]$, the PSD $[S_y]$ of the random process $\{Y(\omega)\}$ defined by : $\{Y(\Omega)\} = [H(\omega)]\{X(\omega)\}$ is also known : $[S_y] = [H(\omega)][S_x]\overline{[H(\omega)]}^T$

The variance of the displacement in the mode m is obtained by the integration of the PSD component $S_{q_{m,m}}(\omega)$:

$$\sigma^2_{q_{m,m}} = \int_{-\infty}^{+\infty} S_{q_{m,m}}(\omega)\,\mathrm{d}\omega = \int_{-\infty}^{+\infty} |H^*_{m,m}(\omega)|^2 \cdot S_{p^*_{m,m}}(\omega)\,\mathrm{d}\omega \tag{2.25}$$

With :

$$H^*_{m,m}(\omega) = \frac{1}{K^*_{m,m}} \cdot \frac{1}{1 - (\frac{\omega}{\omega_m})^2 + 2i\xi^* \frac{\omega}{\omega_m}} \tag{2.26}$$

Given a generalized loading approximated to a white-noise, $S_{p^*_{m,m}}(\omega)$ becomes a constant, guiding to the following simplification :

$$\sigma^2_{q_{m,m}} = S_{p^*_{m,m}} \int_{-\infty}^{+\infty} |H^*_{m,m}(\omega)|^2\,\mathrm{d}\omega \tag{2.27}$$

Owing to a perturbation method, the previous integral can be approximated to a simple analytic expression, which avoids heavy numerical integration, like it can be operated in time domain reasoning (The demonstration is available in Appendix A1).

$$\boxed{\sigma^2_{q_{m,m}} = \frac{S_{p^*_{m,m}}}{K^{*2}_{m,m}} \cdot \frac{\pi\omega_m}{2\xi^*}} \tag{2.28}$$

2.2.2 Determination of the covariance

When it comes to a coupled system, the S^*_p which is a $M \times M$ matrix, contains :

- Diagonal components $S^*_{p_{m,m}}$ representing the independent modal contributions, as if the modal responses were uncoupled in the natural modes' basis (like in (2.28)).
- Non-diagonal components $S^*_{p_{m,n}}$ representing the interactions between different modes.

  The covariance $\sigma_{q_{m,n}}$ associated is computed as the integral of $S_{q_{m,n}}(\omega)$:

$$\sigma_{q_{m,n}} = \int_{-\infty}^{+\infty} S_{q_{m,n}}(\omega)\,\mathrm{d}\omega = \int_{-\infty}^{+\infty} H^*_{m,m}(\omega) \cdot S_{p^*_{m,n}}(\omega) \cdot \overline{H^*_{n,n}(\omega)}\,\mathrm{d}\omega \tag{2.29}$$

Assuming a white-noise approximation of the generalized loading, the following simplification is suggested :

$$\sigma_{q_{m,n}} = S_{p^*_{m,n}} \int_{-\infty}^{+\infty} H^*_{m,m}(\omega) \cdot \overline{H^*_{n,n}(\omega)}\,\mathrm{d}\omega \tag{2.30}$$

Similarly to the formulae (2.28), a perturbation technique is employed in order to find an explicit equation describing the covariance in function of the parameters of

the system (The demonstration is available in APPENDIX A2) :

$$\sigma_{q_{m,n}} = \frac{1}{K^*_{m,m}K^*_{n,n}}\ Re\Big(\frac{S_{p^*_{m,n}}(\omega_m) + S_{p^*_{m,n}}(\omega_n)}{2}\frac{\omega_m+\omega_n}{2}\frac{\pi(\xi^* - i\varepsilon)}{2(\varepsilon^2+\xi^{*2})}\Big) \tag{2.31}$$

Where $\varepsilon = \frac{\omega_m-\omega_n}{\omega_m+\omega_n} \in [-1;1]$ represents a dimensionless unit that measures the distance between the modal frequencies m and n. $S_{p^*_{m,n}}(\omega)$ is a real constant, it can be derived a simpler relationship (2.28). The replacement of ω_n by ω_m recapture the expression of the modal variance $\sigma^2_{q_{m,m}}$ (2.28).

$$\boxed{\sigma_{q_{m,n}} = \frac{S_{p^*_{m,n}}}{K^*_{m,m}K^*_{n,n}}\ \frac{\omega_m+\omega_n}{2}\frac{\pi\xi^*}{2(\varepsilon^2+\xi^{*2})}} \tag{2.32}$$

Stepping back to the modal decomposition, the nodal displacement x is written :

$$x = \phi q = \sum_{i=1}^{n} \phi_{i,x} q_i \tag{2.33}$$

The variance is expressed as the mean of x^2, evidencing a combination of the modal quantities found in (2.28) and (2.32) :

$$\boxed{\sigma_x^2 = E[x^2] = \sum_{i=1}^{n} \phi_{i,x}^2 \sigma_{q_i}^2 + 2\sum_{i=1}^{n}\sum_{j\neq i}^{n}\ \phi_{i,x}\ \phi_{j,x}\sigma_{q_{i,j}}} \tag{2.34}$$

2.2.3 Correction of the uncoupled approach

The uncoupled approach based on neglecting non-diagonal components, provides a rough approximation of the exact behaviour of the system, since the modal coupling is not taken into account. The interest in this section is to include it in the analysis, without the need to inverse the complete matrices, thanks to the use of the developments furnished by [9]. Before that, it is important to restate the arguments engendering $\underline{\underline{M}}^*$ and $\underline{\underline{K}}^*$ diagonal matrices.

The generalized matrices : $\underline{\underline{M}}^* = [\Phi]^T \underline{\underline{M}}[\Phi]$ and $\underline{\underline{K}}^* = [\Phi]^T \underline{\underline{K}}[\Phi]$, such that : $M^*_{i,j} = \phi_i^T M \phi_j$, $K^*_{i,j} = \phi_i^T K \phi_j$, and ϕ_j the normalized natural modes. A normalization for a unitary maximum is adopted : $max_j|\phi_{j,i}| = 1$. Those natural modes are orthogonal via mass and stiffness matrices. This postulate can be demonstrated considering two different modes i and j, with distinct natural pulsations $\omega_i \neq \omega_j$.

Starting from the modal relationships, the next step is to make appear the generalized matrices. A pre-multiplication by ϕ_j^T is made for the first equation, and by ϕ_i^T for the second equation. The subtraction member-to-member of those equations gives

(2.35):

$$\begin{cases} K\phi_i = \omega_i^2 M\phi_i \\ K\phi_j = \omega_j^2 M\phi_j \end{cases} \Rightarrow \begin{cases} \phi_j^T K\phi_i = \omega_i^2 \phi_j^T M\phi_i \\ \phi_i^T K\phi_j = \omega_j^2 \phi_i^T M\phi_j \end{cases}$$

$$\phi_j^T K\phi_i - \phi_i^T K\phi_j = \omega_i^2 \phi_j^T M\phi_i - \omega_j^2 \phi_i^T M\phi_j \tag{2.35}$$

Focusing on the LHS of the equation (2.35), the transpose of the first term gives its neighbour : $(\phi_j^T K\phi_i)^T = \phi_i^T K\phi_j$. Differently, considering that $\phi_j^T K\phi_i$ is a scalar, $\phi_j^T K\phi_i$ is equal to its transpose. Employing the same reasoning for the RHS gives :

$$0 = (\omega_i^2 - \omega_j^2)\phi_j^T M\phi_i \tag{2.36}$$

Finally, for $(i \neq j)$: $\phi_j^T M\phi_i = \phi_i^T M\phi_j = 0$, this induces $\phi_j^T K\phi_i = \phi_i^T K\phi_j = 0$ from (2.35).

The matrices $\underline{\underline{M}}^*$ and $\underline{\underline{K}}^*$ are thus diagonal, however nothing can be stated for $\underline{\underline{C}}^*$.

A non-diagonal generalized damping matrix prohibit the decoupling of modal equations. The most common way to deal with this matter, is to neglect the off-diagonal components. One of the other ways is decompose the damping matrix to an exclusively diagonal matrix and an off-diagonal matrix.

An asymptotic expansion of the FRF is proposed by [9]. It is an intermediate approach between 2 cases : the case where the FRF is approximated to a diagonal matrix (decoupling assumption), and the case considering the inversion of a non-diagonal matrix.

The normalization used of the $\underline{\underline{M}}^*$ and $\underline{\underline{M}}^*$ matrices in the aforementioned method, is done through the mass matrix such as : $[\Phi]^T \underline{\underline{M}}[\Phi] = \underline{\underline{I}}$. The following developments are the adaptation of the method to our case, where a unitary maximum normalization is chosen.

Going from the equation of motion expressed in the modal basis, the factorization by $\underline{\underline{M}}^*$ in the expression of the FRF gives :

$$\underline{\underline{H}}^*(\omega) = (-\underline{\underline{I}}\omega^2 + i\omega\underline{\underline{D}} + \underline{\underline{\Omega}})^{-1}\underline{\underline{M}}^{*-1} \tag{2.37}$$

Where : $\underline{\underline{D}} = \underline{\underline{M}}^{*-1}\underline{\underline{C}}^*$ and $\underline{\underline{\Omega}} = \underline{\underline{M}}^{*-1}\underline{\underline{K}}^*$.

The generalized damping matrix $\underline{\underline{D}}$ is established as the sum of a diagonal matrix $\underline{\underline{D_d}}$ and an off-diagonal matrix $\underline{\underline{D_0}}$ providing :

$$\underline{\underline{H}}^*(\omega) = (\underline{\underline{J_d}} + \underline{\underline{J_0}})^{-1}\underline{\underline{M}}^{*-1} \tag{2.38}$$

Where : $\underline{\underline{J_d}} = -\underline{\underline{I}}\omega^2 + i\omega\underline{\underline{D_d}} + \underline{\underline{\Omega}}$ and $\underline{\underline{J_0}} = i\omega\underline{\underline{D_0}}$.

(2.38) becomes (2.39) after the factorization by $\underline{\underline{H_d}}^* = \underline{\underline{J_d}}^{-1}$:

$$\underline{\underline{H}}^*(\omega) = (\underline{\underline{I}} + \underline{\underline{J_d}}^{-1}\ \underline{\underline{J_0}})^{-1}\underline{\underline{H_d}}^*\ \underline{\underline{M}}^{*-1} \tag{2.39}$$

→ To be able to find an approximate expression of $(\underline{\underline{I}} + \underline{\underline{J_d}}^{-1}\ \underline{\underline{J_0}})^{-1}$ via an expansion method[a]. First, it is required to demonstrate that the quantity $\underline{\underline{J_d}}^{-1}\ \underline{\underline{J_0}}$ is one order inferior than $\underline{\underline{I}}$.

$$\underline{\underline{J_d}}^{-1}\underline{\underline{J_0}} = i\omega(\underline{\underline{\Omega}} - \underline{\underline{I}}\omega^2 + i\omega\underline{\underline{D_d}})^{-1}\underline{\underline{D_0}} \tag{2.40}$$

The factorization by $i\omega D_d$ inside the parenthesis gives :

$$\underline{\underline{J_d}}^{-1}\underline{\underline{J_0}} = (\frac{1}{i\omega}\underline{\underline{D_d}}^{-1}(\underline{\underline{\Omega}} - \underline{\underline{I}}\omega^2) + \underline{\underline{I}})^{-1}\underline{\underline{D_d}}^{-1}\underline{\underline{D_0}} \tag{2.41}$$

Otherwise, from the definition of the diagonality index : $\rho(D) = max(|eig\ \underline{\underline{D_d}}^{-1}\underline{\underline{D_0}}|)$, that represents the biggest eigenvalue of $\underline{\underline{D_d}}^{-1}\underline{\underline{D_0}}$, it can be written that : $\underline{\underline{D_d}}^{-1}\underline{\underline{D_0}} = \Psi\underline{\underline{\lambda}}\Psi^{-1}$. Where $\underline{\underline{\lambda}}$ is a diagonal matrix containing the eigenvalues, and Ψ containing the eigenvectors.
If the maximum eigenvalue is small, all the others are small. In other words, for a diagonality index of order ε, it can be written that : $\underline{\underline{\lambda}} = \varepsilon\underline{\underline{\Lambda}}$, with $\underline{\underline{\Lambda}} = ord(1)$;
The substitution of $\underline{\underline{D_d}}^{-1}\underline{\underline{D_0}}$ leads to the following expression :

$$\underline{\underline{J_d}}^{-1}\underline{\underline{J_0}} = \varepsilon(\frac{1}{i\omega}\underline{\underline{D_d}}^{-1}(\underline{\underline{\Omega}} - \underline{\underline{I}}\omega^2) + \underline{\underline{I}})^{-1}\Psi\underline{\underline{\Lambda}}\Psi^{-1} \tag{2.42}$$

The squared natural frequencies are collected in the diagonal of $\underline{\underline{\Omega}}$. Therefore at the resonance : $\underline{\underline{\Omega}} - \underline{\underline{I}}\omega^2 \simeq 0$ leading to the wanted result :

$$\underline{\underline{J_d}}^{-1}\underline{\underline{J_0}} = \varepsilon\Psi\underline{\underline{\Lambda}}\Psi^{-1} \tag{2.43}$$

[a] **Explanatory example:** $\frac{1}{x}$ being a known quantity, the goal is to compute $\frac{1}{x+y}$ for $y << x$:

$$\frac{1}{x+y} = \frac{1}{x}\frac{1}{1+\frac{y}{x}} = \frac{1}{x}\frac{1}{1+\varepsilon} \simeq \frac{1}{x}(1-\varepsilon)$$

Thanks to this result, it is possible to access an approximated expression of $\underline{\underline{H}}^*$ called $\underline{\underline{H_c}}^*$. The c-index stands for *correction* as it is an enrichment of the diagonal FRF matrix assumption :

$$\underline{\underline{H_c}}^*(\omega) = (\underline{\underline{I}} - \underline{\underline{H_d}}^*\ \underline{\underline{J_0}})\underline{\underline{H_d}}^*\ \underline{\underline{M}}^{*-1} \tag{2.44}$$

The response $\underline{Q_c}$ is then computed by post-multiplying by the generalized forces $\underline{P}^*$, such that $\underline{P}^*_{bis} = \underline{\underline{M}}^{*-1}\underline{P}^*$:

$$\boxed{\underline{Q_c} = \underbrace{\underline{\underline{H_d}}^* \ \underline{P}^*_{bis}}_{\underline{Q}_d} + \underbrace{\underline{\underline{H}}^*_d \ \underline{\underline{J_0}}(\overbrace{\underline{\underline{H_d}}^* \ \underline{P}^*_{bis}}^{\underline{Q}_d})}_{\underline{\Delta Q}}} \tag{2.45}$$

$\underline{Q}_d$ representing the response corresponding to the uncoupled approach, completed by a residual $\underline{\Delta Q}$ computed in function of the first term, where $\underline{\underline{J_0}}\underline{Q}_d$ represents modal forces.

The PSDM of the corrected response is the result of the combination of the pure contributions of $\underline{Q}_d$ and $\underline{\Delta Q}$, adding to it the terms of interaction :

$$S_{Q_c} = S_{Q_d} + S_{\Delta Q} + S_{Q_d \Delta Q} + S_{\Delta Q Q_d} \tag{2.46}$$

The development of each of these terms is suggested below :

$$\begin{cases} S_{Q_d} = E[\underline{Q_d}^2] = \underline{\underline{H_d}}^* \ [S_{p^*_{bis}}] \ \overline{\underline{\underline{H_d}}^*}^T \\ S_{\Delta Q} = E[\underline{\Delta Q}^2] = \underline{\underline{H_d}}^* \ \underline{\underline{J_0}} \ \underline{\underline{H_d}}^* \ [S_{p^*_{bis}}] \ \overline{\underline{\underline{H_d}}^*}^T \ \overline{\underline{\underline{J_0}}}^T \ \overline{\underline{\underline{H_d}}^*}^T \\ S_{Q_d \Delta Q} = E[\underline{Q_d} \ \overline{\underline{\Delta Q}}^T] = \underline{\underline{H_d}}^* \ [S_{p^*_{bis}}] \ \overline{\underline{\underline{H_d}}^*}^T \ \overline{\underline{\underline{J_0}}}^T \ \overline{\underline{\underline{H_d}}^*}^T \\ S_{\Delta Q Q_d} = E[\underline{\Delta Q} \ \overline{\underline{Q}_d}^T] = \underline{\underline{H_d}}^* \ \underline{\underline{J_0}} \ \underline{\underline{H_d}}^* \ [S_{p^*_{bis}}] \ \overline{\underline{\underline{H_d}}^*}^T \\ [S_{p^*_{bis}}] = \underline{\underline{M}}^{*-1} \ [S_{p^*}] \ [\underline{\underline{M}}^{*-1}]^T \end{cases}$$

2.2.4 Comparison with numerical integration

This new approach is supposed to offer a better approximation, due to the enrichment of the uncoupled model manifested by the presence of the residual term.

It is considered an SDOF structure of mass M equipped with a damper of mass m, such that the mass ratio of $\mu_{TMD} = m/M = 5\%$.

The components of the PSD are illustrated in the following figure. For each component, three curves are displayed : the 'Exact' plot represents the coupled system, the 'Diagonal' plot corresponds to the uncoupled approximation, and the 'Corrected' plot speaks for the asymptotic approximation method.

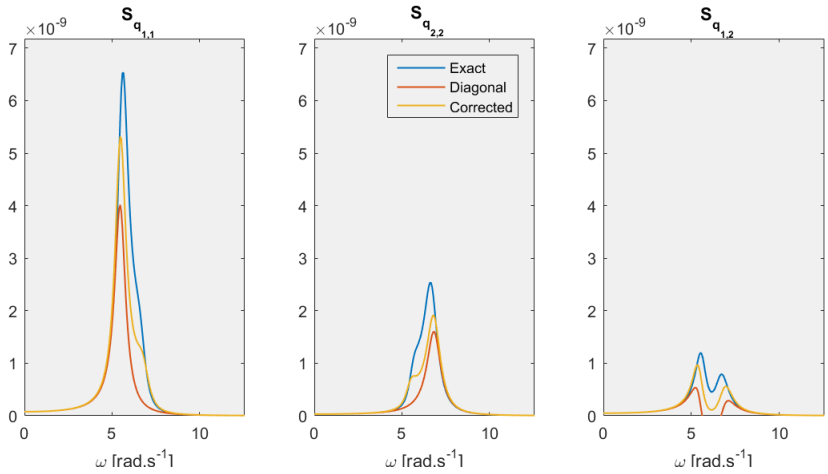

Figure 2.1: PSD of the displacement in the different configurations for $\mu_{TMD} = 5\%$

The corrected plot reproduces better the shape of the exact solution, the amplitude is also well approximated. The variance corresponding to the area under the curve, is naturally more accurate than the diagonal result, as it is showed in the **Figure 2.3**.

It is noticed a drop of the ampltiude of the PSD's peak (and thus the variance), for an increasing mass ratio. The added mass brings more damping to the system, which can explain this tendency. Indeed, the literature get along to reveal that the damping ratio of the damper is an increasing function of the mass ratio, for the case of a random excitation [4]. The equivalent damping being a linear combination of the structural damping ratio and the damping ratio provided by the TMD[5], it is verified by the formula (2.28) that the more important is the damping ratio, the lower is the variance.

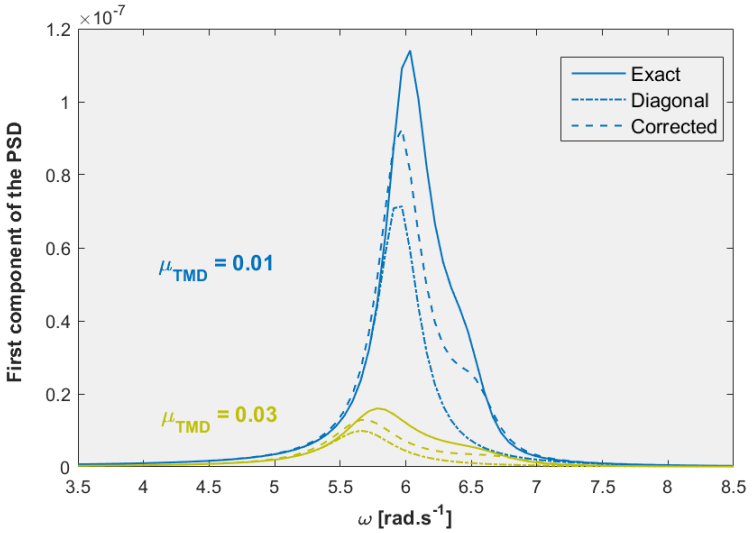

Figure 2.2: Evolution of $S_{Q_{1,1}}$ for different values of the ratio mass μ_{TMD}

[4]The propositions of the literature are presented in the next chapter
[5]This statement is also be demonstrated further in the document in the next chapter

The analytic expressions of the variance coming from (2.32) and (2.28) are constructed on the uncoupled approach. They are thus an approximation the 'Diagonal' curves seen above. The relative error of the analytic variance with respect to the numerical variance, is displayed in the following figure in function of the mass ratio. It doesn't exceed 2.5% for a ratio mass of 5%.

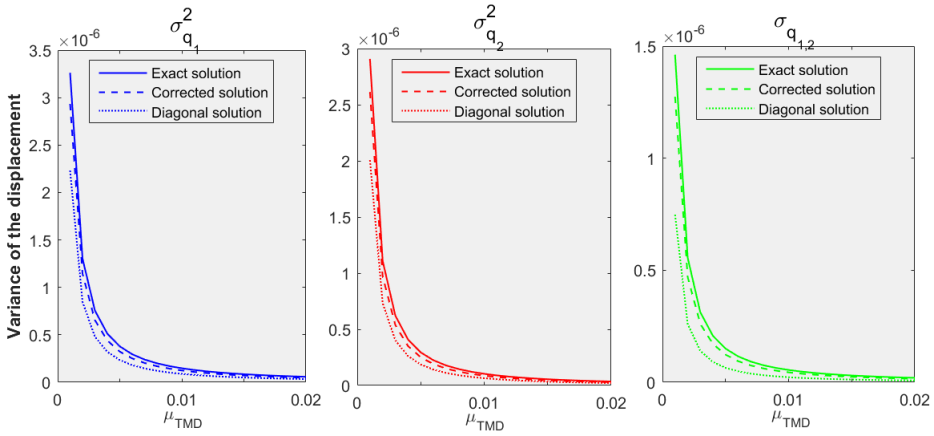

Figure 2.3: Evolution of the variance

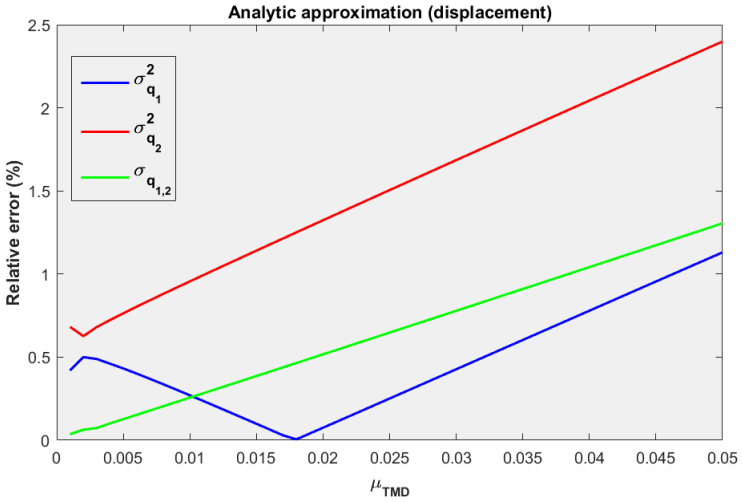

Figure 2.4: Evolution of the relative error of the variance obtained analytically

2.3 Application for acceleration

The design of the dampers is usually made according to the comfort criteria expressed in terms of acceleration. The previous derivations concerned the approximation of the variance of the displacement, the aim here is to attain the variance of the the acceleration.

By using the Fourier transformation, the properties developed concerning the auto-correlation functions, linking the displacement to the acceleration, can be translated in terms of PSD.

$$R_{\ddot{x}\ddot{x}}(\Delta t) = \frac{d^4 R_{xx}(\Delta t)}{d\Delta t^4} \Longrightarrow S_{\ddot{x}\ddot{x}}(\omega) = \omega^4 S_{xx}(\omega) \tag{2.47}$$

Those properties can be useful to compute the spectral moments, that are defined by :

$$m_i = \int_{-\infty}^{+\infty} |\omega|^i S_{x,x}(\omega) d\omega \tag{2.48}$$

Where the order ($i = 0$) corresponds to the variance of the displacement, the order ($i = 2$) to the variance of the velocity, and the order ($i = 4$) to the variance the acceleration. When the spectral densities of the design quantities are established, the process usually consists of calculating the spectral moments, that offer the advantage of being simpler to interpret. Moreover, they don't contain too much information, contrary to the PSDs that are big memory consumers. As soon as the spectral moments are computed, it is advised to get rid of the PSDs as soon as possible.

2.3.1 Determination of the variance

The variance of the acceleration in the mode m is provided by :

$$\sigma^2_{\ddot{q}_{m,m}} = \int_{-\infty}^{+\infty} S_{\ddot{q}_{m,m}}(\omega)\,\mathrm{d}\omega = \int_{-\infty}^{+\infty} \omega^4 \cdot |H^*_{m,m}(\omega)|^2 \cdot S_{p^*_{m,m}}(\omega)\,\mathrm{d}\omega \tag{2.49}$$

Assuming a white-noise approximation, the previous equation becomes simpler :

$$\sigma^2_{\ddot{q}_{m,m}} = S_{p^*_{m,m}} \int_{-\infty}^{+\infty} \omega^4 \cdot |H^*_{m,m}(\omega)|^2\,\mathrm{d}\omega \tag{2.50}$$

The function $|H^*_{m,m}(\omega)|^2$ decreases with $1/\omega^4$, according to (2.26). The multiplication by ω^4 reveals an indeterminacy ($lim_{\omega\to+\infty}\ \omega^4|H(\omega)|^2 \sim \frac{\omega^4}{\omega^4} \to 1 \neq 0$) represented by a constant value for $\omega >>$, which impedes the computation of the integral.

The equation is developed, and written in function of the dimensionless variable

$\Omega = \omega/\omega_m$.

$$\sigma^2_{\ddot{q}_{m,m}} = \frac{S_{p^*_{m,m}}\omega_m}{M^{*2}_{m,m}} \int_{-\infty}^{+\infty} \frac{\Omega^4}{1 + 2(2\xi^{*2} - 1)\Omega^2 + \Omega^4} d\Omega \tag{2.51}$$

Adding and subtracting the quantity $1 + 2(2\xi^{*2} - 1)\Omega^2$ guide to the distinction of two terms where one of them isn't integrable.

$$\sigma^2_{\ddot{q}_{m,m}} = \frac{S_{p^*_{m,m}}\omega_m}{M^{*2}_{m,m}} \int_{-\infty}^{+\infty} 1 - \frac{1 + 2(2\xi^{*2} - 1)\Omega^2}{1 + 2(2\xi^{*2} - 1)\Omega^2 + \Omega^4} d\Omega \tag{2.52}$$

To get rid of the indeterminacy of the first integral, a solution would be to use a white noise defined on a limited band $[-\omega_{max}, \omega_{max}]$, instead of an infinite white noise. While the second integral is computed using Cauchy's residue theorem, since the rational fraction fulfills the applicability conditions [6]. Each integral is treated separately, generating an analytic expression of the variance :

$$\sigma^2_{\ddot{q}_{m,m}} = \frac{S_{p^*_{m,m}}\omega_m}{M^{*2}_{m,m}} \Big(\int_{-\omega_{max}}^{\omega_{max}} 1 \; d\Omega - \int_{-\infty}^{+\infty} \frac{1 + 2(2\xi^{*2} - 1)\Omega^2}{1 + 2(2\xi^{*2} - 1)\Omega^2 + \Omega^4} d\Omega \Big)$$

$$\boxed{\sigma^2_{\ddot{q}_{m,m}} = \frac{S_{p^*_{m,m}}}{M^{*2}_{m,m}} (2\omega_{max} + \frac{\pi\omega_m}{2\xi^*})} \tag{2.53}$$

2.3.2 Determination of the covariance

In parallel, going from the defintion of the covariance of the acceleration provided by the next equation, the purpose is to attain a simple formulation :

$$\sigma_{\ddot{q}_{m,n}} = \int_{-\infty}^{+\infty} S_{\ddot{q}_{m,n}}(\omega)\, \mathrm{d}\omega = \int_{-\infty}^{+\infty} H^*_{m,m}(\omega) \cdot (\omega^4 S_{p^*_{m,n}}(\omega)) \cdot \overline{H^*_{n,n}(\omega)}\, \mathrm{d}\omega \tag{2.54}$$

Assuming a white-noise approximation of the generalized loading, the following simplification is suggested :

$$\sigma_{\ddot{q}_{m,n}} = S_{p^*_{m,n}} \int_{-\infty}^{+\infty} \omega^4 H^*_{m,m}(\omega)\overline{H^*_{n,n}(\omega)}\, \mathrm{d}\omega \tag{2.55}$$

The function to integer delivers the same indeterminacy as for the variance where : $lim_{\omega\to+\infty}\ \omega^4 H^*_{m,m}(\omega)\overline{H^*_{n,n}(\omega)} \sim \frac{\omega^4}{\omega^4} \to 1 \neq 0$. The same strategy is employed in order to identify the integrable part of the function, and integrate the other part on a limited domain.

[6] Applicability conditions of Cauchy's residue theorem : The denominator's polynomial admits complex poles, and is two degrees higher than the numerator's polynomial.

The substitution of the transfer matrices by their expressions provides :

$$\sigma_{\ddot{q}_{m,n}} = \frac{S_{p^*_{m,n}}}{K^*_m K^*_n} \int_{-\infty}^{+\infty} \frac{\omega^4}{(1-(\frac{\omega}{\omega_m})^2 + 2i\xi^*\frac{\omega}{\omega_m})(1-(\frac{\omega}{\omega_n})^2 - 2i\xi^*\frac{\omega}{\omega_n})} d\omega \tag{2.56}$$

The denominator is simplified introducing the variable : $D(H_i) = (1-(\frac{\omega}{\omega_i})^2 + 2i\xi^*\frac{\omega}{\omega_i})$.

The addition and subtraction of the quantity $\omega_m^2\omega_n^2 D(H_m)D(H_n)$, make appear a non-integrable term. Whereas the integrability of the other term needs also to be checked.

$$\sigma_{\ddot{q}_{m,n}} = \frac{S_{p^*_{m,n}}}{K^*_m K^*_n} \int_{-\infty}^{+\infty} \omega_m^2\omega_n^2 + \frac{\omega^4 - \omega_m^2\omega_n^2 D(H_m)D(H_n)}{D(H_m)D(H_n)} d\omega$$

$$= \frac{S_{p^*_{m,n}}}{K^*_m K^*_n} \Big(\int_{-\omega_{max}}^{\omega_{max}} \omega_m^2\omega_n^2 d\omega + \underbrace{\int_{-\infty}^{+\infty} \frac{\omega^4 - \omega_m^2\omega_n^2 D(H_m)D(H_n)}{D(H_m)D(H_n)} d\omega}_{I_2} \Big) \tag{2.57}$$

The polynomial's numerator is of degree 3, as it appears in the following expansion. I_2 is therefore integrable, as the denominator is of degree 4.

$$\omega^4 - \omega_m^2\omega_n^2 D(H_m)D(H_n) = 2i\xi^*(\omega_m - \omega_n)\omega^3 + (\omega_m^2 + \omega_n^2 - 4\xi^{*2}\omega_m\omega_n)\omega^2$$

$$+2i\xi^*\omega_m\omega_n(\omega_m + \omega_n)\omega - \omega_m^2\omega_n^2 \tag{2.58}$$

In order to focus on both natural frequencies ω_m and ω_n simultaneously, a strained coordinate $\omega(\eta)$ is introduced, centered on the mean :

$$\omega = \frac{\omega_m + \omega_n}{2} + \eta\ (\omega_n - \omega_m) = \frac{\omega_m + \omega_n}{2}(1 + 2\varepsilon\eta)$$

With : $\eta = ord(1)$, and $\varepsilon = \frac{\omega_n - \omega_m}{\omega_m + \omega_n}$ a small dimensionless unit that measures the gap between natural frequencies.

In favor of considering a same order of magnitude for the natural frequencies, it is assumed $\varepsilon^2 << 1$. The numerator, in turn, is approximated to the first order. The simplifications guide to the following form of I_2 :

$$I_2 = \frac{1}{4}\Big(\frac{\omega_m + \omega_n}{2}\Big)^4 \int_{-\infty}^{+\infty} \frac{1}{4\eta^2\varepsilon^2 + (\xi^* + i\varepsilon)^2} d\eta = \frac{1}{4}\Big(\frac{\omega_m + \omega_n}{2}\Big)^4 \frac{\pi(\xi^* - i\varepsilon)}{2\varepsilon(\varepsilon^2 + \xi^{*2})} \tag{2.59}$$

(2.57) becomes after simplification :

$$\boxed{\sigma_{\ddot{q}_{m,n}} = \frac{S_{p^*_{m,n}}}{K^*_m K^*_n} \Big(2\omega_{max}\omega_m^2\omega_n^2 + \frac{1}{4}\Big(\frac{\omega_m + \omega_n}{2}\Big)^4 \frac{\pi(\xi^* - i\varepsilon)}{2\varepsilon(\varepsilon^2 + \xi^{*2})} \Big)} \tag{2.60}$$

Stepping back to the modal decomposition, the nodal displacement x is written :

$$\{\ddot{x}\} = \phi\{\ddot{q}\} \tag{2.61}$$

The variance is expressed as the mean of x^2, evidencing a combination of the modal quantities found in (2.28) and (2.32) :

$$\boxed{\sigma_{\ddot{x}}^2 = E[\ddot{x}^2] = \sum_{i=1}^{n} \phi_{i,x}^2 \sigma_{\ddot{q}_i}^2 + 2 \sum_{i=1}^{n} \sum_{j \neq i}^{n} \phi_{i,x}\ \phi_{j,x} \sigma_{\ddot{q}_{i,j}}} \tag{2.62}$$

2.3.3 Comparison with numerical integration

The following figure displays the components of the PSD in the frequency domain. The 'Corrected' curve is associated to the rectification of the uncoupled approach in accordance with the method [9], after one iteration. It shows a better approximation of the 'Exact' curve associated to the coupled approach, in terms of shape and amplitude.

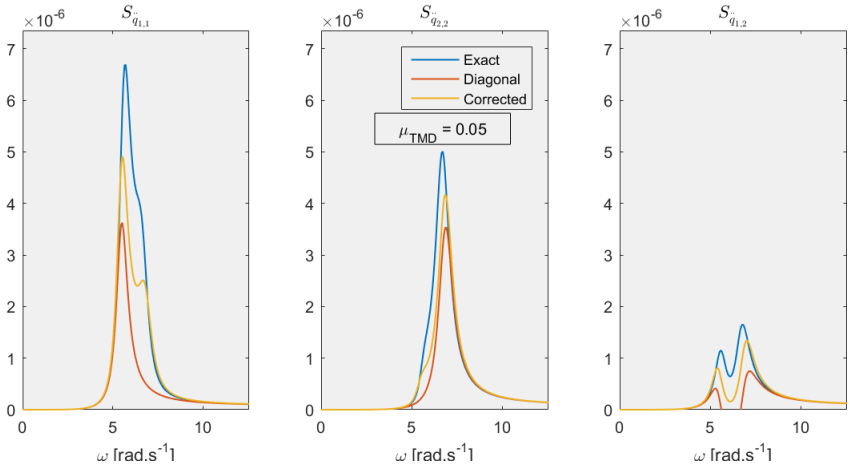

Figure 2.5: PSD of the acceleration for $\mu_{TMD} = 0.05$ in the different configurations

With a simple integration on the frequency domain, the modal variances are achieved

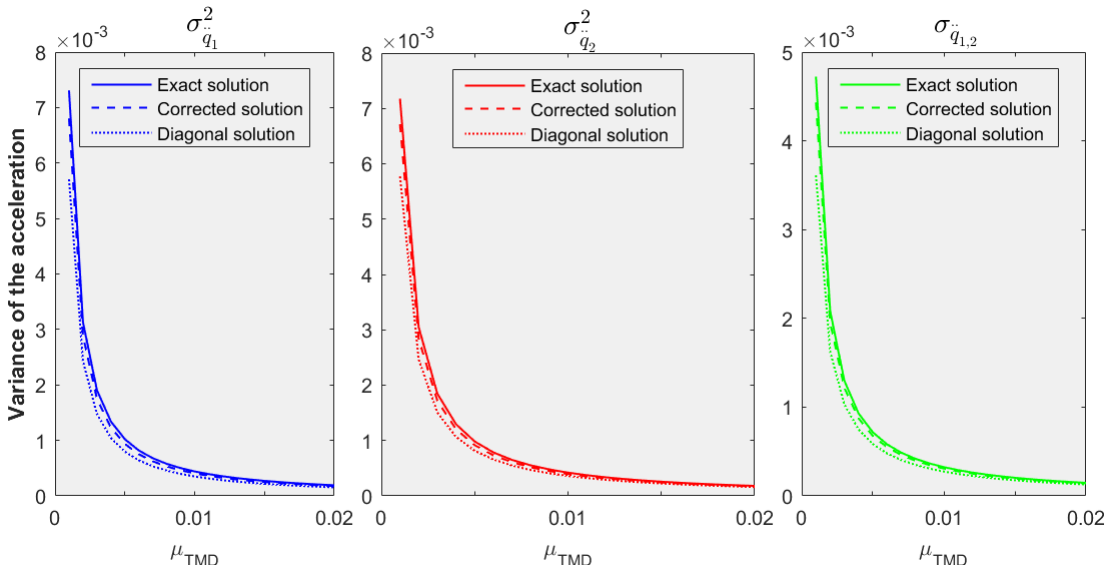

Figure 2.6: Evolution of the variance in function of the mass ratio

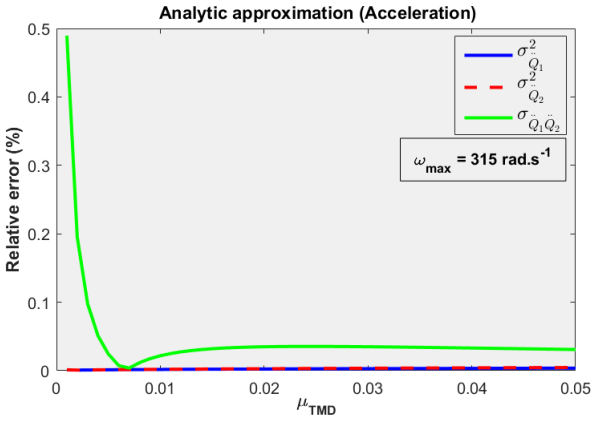

Figure 2.7: Relative error of the analytic expression with respect to the numerical result

For small values of the mass ratio, the accuracy of the analytic approximation of the covariance is questioned. The bandwidth ω_{max} has an influence on the result. In fact, the wider the band the more the curve is shifted downward, and thus the more accurate is the result of the analytic approximation.

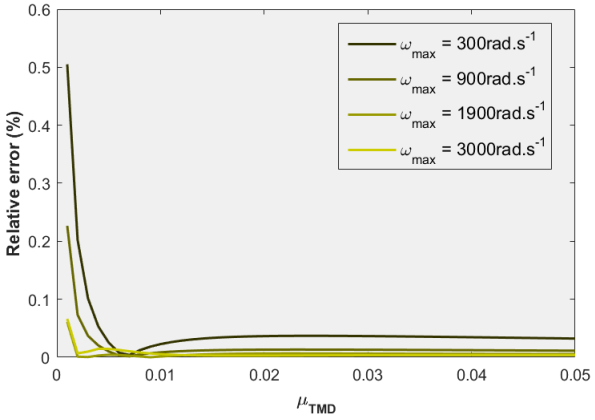

Figure 2.8: Relative error of the analytic expression of $\sigma_{\ddot{q}_{1,2}}$ with respect to the numerical result for increasing values of the bandwidth of the white noise

3 Approximation of the modal properties

This chapter is destined to the dynamic analysis of damped structures considering the coupling effect, and its repercussion on the complexity of the equations. When applying the results of the previous chapter on such structures, it turns out that the analytic expression of variance involves parameters that are not all intuitively obtained, such as the natural frequencies of the damped system, or its equivalent damping ratio. The purpose in this chapter is to seek analytic derivations of those parameters, in order to find a completely explicit form of the variance, involving the mass of the damper, that is crucial for the design.

The first part of the chapter is dedicated to the presentation of the concept of Tuned Mass Damper (TMD), as an example of passive dampers and classical solution to current footbridges. The aim here is to understand and recall the theoretical foundations of damping techniques, which will serve as basis for the developments that will follow.

The second part is consecrated to the analysis of a dynamical system equipped with a TMD. The purpose is to perform an analytic treatment of an SDOF structure as a first step, to be then interested by the transcription of the developments to an MDOF system. The damper's mass considered as a small quantity with respect to the modal masses, a perturbation method is developed using dimensionless variables, that aims to attain analytically the modal characteristics of the coupled system.

3.1 Concept of TMD

The TMD concept was first discovered by Frahm in 1909, to reduce the movement of boats when they were subjected to sea waves. In 1928, a theory was presented in a paper proposed by Ormondroyd and Den Hartog. It suggests the addition of a viscous component in parallel with the spring to permit an absorption of the kinetic energy. Detailed discussion of optimal settings and damping came after in Den Hartog's book on mechanical vibrations.

3.1.1 Description of the TMD

The tuned-mass damper is a device consisting of a heavy mass, a spring and a viscous damper. It is installed at the localized points of the structure in order to reduce its response to dynamic loads. When the vibration outpace vibration comfort limits, the installation of a TMD can be seen as a passive counterweight mechanism for the structure. In other words, when the structure starts to vibrate, the TMD is

excited by the movement, its mass remains always opposed to the movement of the structure, which damps gradually the vibratory movement of the structure. The design of the TMD lies in the tuning of the mass, stiffness and damping of the TMD to the primary structure's dynamic characteristics.

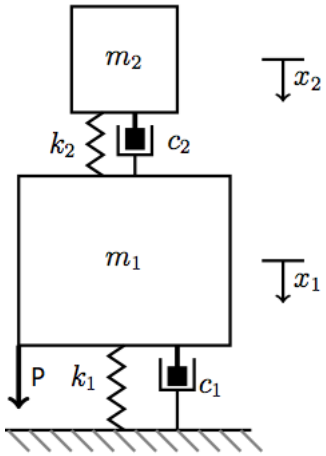

Figure 3.1: Tuned Mass Damper scheme
http://web.mit.edu/jorloff/www/jmoapplets/secondorder/TunedMassDamper.html

The properties of the coupled system are proposed below :

Main structure	**Mass**	m_1
	Stiffness	k_1
	Damping	c_1
	Natural pulsation	$\omega_n = \sqrt{k_1/m_1}$
	Damping ratio	$\xi_1 = c_1/2\sqrt{k_1 m_1}$
TMD	**Mass**	m_2
	Stiffness	k_2
	Damping	c_2
	Natural pulsation	$\omega_{TMD} = \sqrt{k_2/m_2}$
	Damping ratio	$\xi_2 = c_2/2\sqrt{k_2 m_2}$
	Mass ratio	$\mu_{TMD} = m_2/m_1$
	Tuning	$\alpha_{TMD} = \omega_{TMD}/\omega_n$

Table 3.1: Properties of the system structure-TMD

3.1.2 Performance of the TMD

The nominal performance of a TMD is to reduce vibration levels commanded by a single mode. This is why for an MDOF system, the modes are generally decoupled: each mode is treated separately, the damper is tuned to a limited frequency scope surrounding the natural frequency of the mode in question. The TMD is placed where the mode's amplitude is maximum.

3.1.2.1 Tuning :

The TMD's mass is much inferior than the mass of the structure. Generally, the ratio mass μ_{TMD} does not exceed 5% for footbridges. Den Hartog [3] provides the optimal rates for the damping ratio ξ_{TMD} and the tuning α_{TMD} for a given added mass, minimising the FRF (Frequency Response Function). Its adjustment is compared to the ones suggested by Fujino [13], Sadek [7] and Waburton [11], for a random excitation (**Figure 3.2**). All the models describe the same tendency : ξ_{TMD} is a growing function of the ratio mass, and α_{TMD} a decreasing one. The variation of α_{TMD} is not significant, confirming that the TMD covers a limited frequency scope.

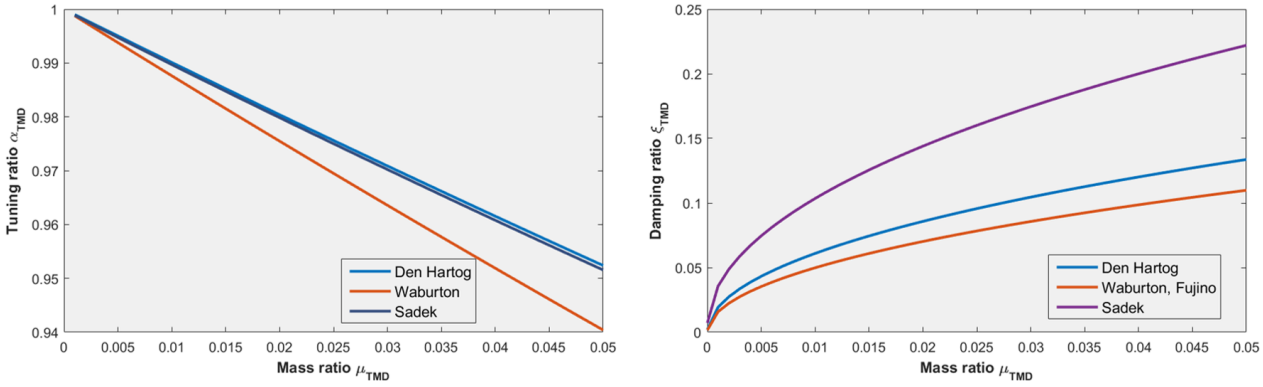

Figure 3.2: Optimum values for the tuning ratio and the damping ratio of the TMD

From the plot of the transfer function, den Hartog's theory [3] pinpoints the existence of 2 invariant points, when varying the frequency ratio α_{TMD}, regardless of the value of the damping ξ_{TMD} conferred on it.

The tuning ratio α_{TMD} is selected so that these 2 fixed points have identical ordinates. Subsequently, the damping ratio ξ_{TMD} can be set to obtain horizontal tangents. The two bumps are decreased equally below the fixed points. The effect of TMD on the transfer function is thus optimized. This model is valid when the structural damping is very small, even neglected. The method gives birth to the following optimal couple of parameters :

$$\begin{cases} \alpha_{TMD} = \frac{1}{1+\mu} \\ \xi_{TMD} = \sqrt{\frac{3\mu}{8(1+\mu)}} \end{cases} \tag{3.1}$$

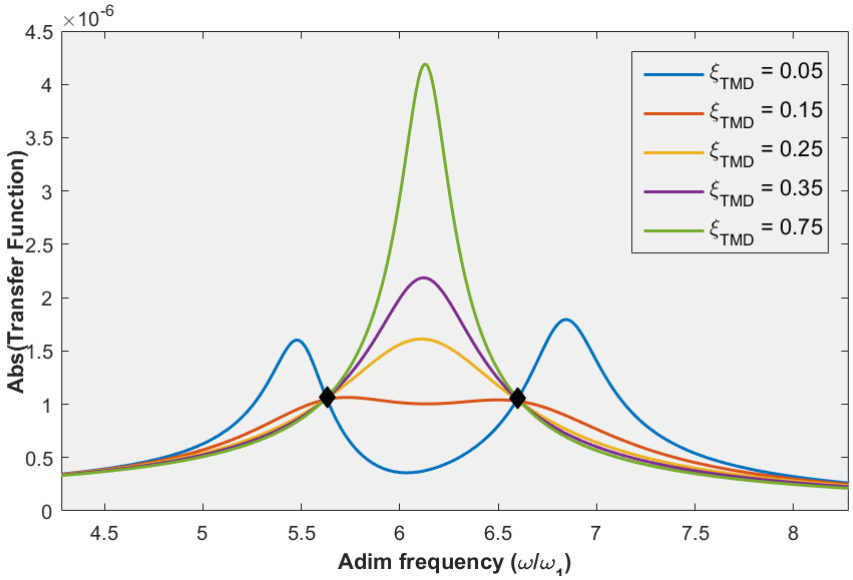

Figure 3.3: Setting of α_{TMD} according to den Hartog's method

3.1.2.2 Deficiency :

A major disadvantage of TMD is its high sensitivity to "detuning". Even if the damper is initially perfectly adjusted, if the frequency of the bridge vary during time, a deregulation is engendered, and the effectiveness of the TMD is jeopardized. Several factors may be the initiator of this problem, such as for instance, the variability of the pedestrian load, or the variability of the structure's properties over time. Consequently, it is important in the design to check the fit of the TMD for a given frequency range rather than a single target frequency.

3.2 Effect of a damper on a SDOF system

→ The elementary model for a structure with a tuned vibration damper, is a 2DOF system. It is used here to develop the theoretical background. The matrix of mass and stiffness are given below :
For the sole purpose of lightening the expressions, a new notation is used for the TMD parameters : $m_{TMD} = m$; $k_{TMD} = k$; $c_{TMD} = c$; $\mu_{TMD} = \mu$; $\omega_{TMD} = \omega_T$; $\xi_{TMD} = \xi_d$

$$\underline{\underline{M}} = \begin{bmatrix} M & 0 \\ 0 & m \end{bmatrix} \; ; \; \underline{\underline{K}} = \begin{bmatrix} K+k & -k \\ -k & k \end{bmatrix} \tag{3.2}$$

3.2.1 Approximation of the natural frequencies

For a primary system subjected to vibrations, the installation of the TMD follows the law : the greater the added mass, the smaller is the amplitude of the response. Besides, another result is observed : when increasing the mass, the transfer function goes from a single-peak curve to a 2-bumps curve as it seen in **Figure 3.4**. The idea is to investigate the location of the bumps, which amounts to the research of the natural frequencies of the coupled system.

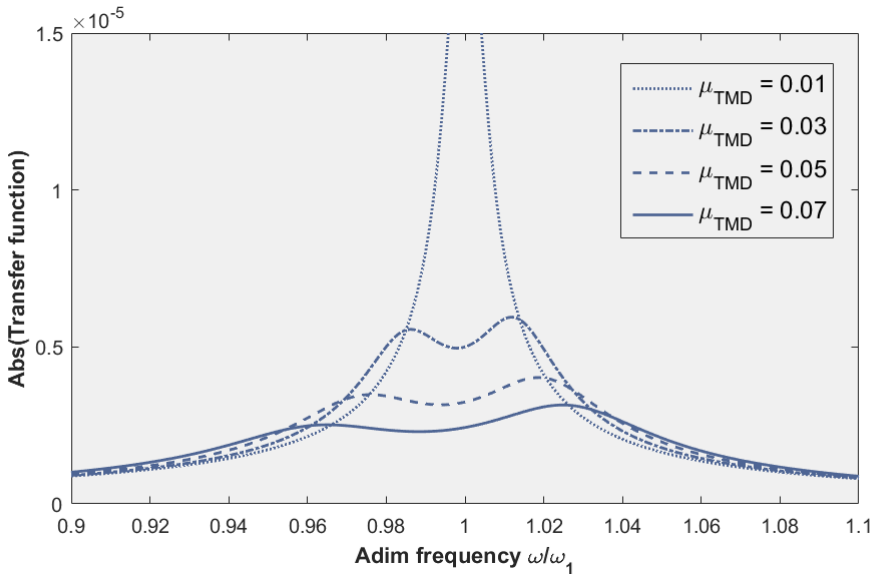

Figure 3.4: Evolution of the transfer function for an increasing mass ratio μ_{TMD}

The analytic development is based on the perturbation method, which consists in the use of the power series expansion of ε, a dimensionless parameter supposed

small, that plays the role of a "scale". The physical parameters are expressed in function of this entity, which transform the variables to extended coordinates. These quantities are essential for the capture of the behavior of the system in the vicinity of the resonance. The result of this development permits the comparison of the contributions of the different parameters, where the parameters that have small effect are spotted and eliminated. The method furnishes equations that are lighter and more explicit, favorable for direct interpretations of the different phenomena involved.

As a starting point, some assumptions have to be made on the order of magnitudes of the different parameters :

- The mass ratio : $\mu = ord(\varepsilon^2)$;
- The damping ratio of the damper : $\xi_{TMD} = ord(\varepsilon)$;
- The tuning ratio of the damper : $\alpha = ord(\varepsilon)$ ($\alpha = \omega_{TMD}/\Omega$: ratio of the natural frequency of the TMD over the natural frequency of the structure) ;

Those assumptions are translated below in order to establish rescaled expressions of the damper's characteristics. New variables are introduced like μ_1 and ν_2 that are both of order 1 ;

$$\begin{cases} m = \mu\ M = (\varepsilon^2\mu_1)M \\ \omega_{TMD} = (1+\varepsilon\nu_2)\Omega \\ k = m\omega_{TMD}^2 = \varepsilon^2\mu_1(1+2\varepsilon\nu_2)K \end{cases}$$

Therefore, with taking ($M = 1$ and $K = 1$) in the sole purpose to lighten the equations, (3.2) become :

$$\underline{\underline{M}} = \begin{bmatrix} 1 & 0 \\ 0 & \varepsilon^2\mu_1 \end{bmatrix} \ ; \ \underline{\underline{K}} = \begin{bmatrix} 1+\varepsilon^2\mu_1(1+2\varepsilon\nu_2) & -\varepsilon^2\mu_1(1+2\varepsilon\nu_2) \\ -\varepsilon^2\mu_1(1+2\varepsilon\nu_2) & \varepsilon^2\mu_1(1+2\varepsilon\nu_2) \end{bmatrix} \tag{3.3}$$

The objective is to look for the natural frequencies and modes associated to the previous mass and stiffness matrix. Before the resolution of the eigenvalues problem $\omega^2\underline{\underline{M}}\underline{\phi} = \underline{\underline{K}}\underline{\phi}$, the mode vector has to be introduced in a way that the structural and TMD terms have the same order of magnitude.

The mode vector is expressed $\underline{\phi} = [\phi_s \ \phi_{TMD}]^T$, where the structural vector $\phi_s = ord(1)$ and $\phi_{TMD} = ord(1/\varepsilon)$. A new variable $\underline{\phi'} = [\phi'_s \ \phi'_{TMD}]^T$ is introduced in order to keep the consistency of the dimensionless development.

$$\underline{\phi} = \begin{bmatrix} \phi_s \\ \phi_{TMD} \end{bmatrix} = \begin{bmatrix} 1 & 0 \\ 0 & 1/\varepsilon \end{bmatrix} \begin{bmatrix} \phi'_s \\ \phi'_{TMD} \end{bmatrix} = \begin{bmatrix} 1 & 0 \\ 0 & 1/\varepsilon \end{bmatrix} \underline{\phi'} \tag{3.4}$$

The change of the basis guide to the transformation of the mass and stiffness matrix :

$$\widetilde{\underline{\underline{M}}} = \begin{bmatrix} 1 & 0 \\ 0 & 1/\varepsilon \end{bmatrix} \underline{\underline{M}} \begin{bmatrix} 1 & 0 \\ 0 & 1/\varepsilon \end{bmatrix} = \underbrace{\begin{bmatrix} 1 & 0 \\ 0 & \mu_1 \end{bmatrix}}_{\underline{\underline{M_0}}} \tag{3.5}$$

$$\begin{aligned} \widetilde{\underline{\underline{K}}} &= \begin{bmatrix} 1 & 0 \\ 0 & 1/\varepsilon \end{bmatrix} \underline{\underline{K}} \begin{bmatrix} 1 & 0 \\ 0 & 1/\varepsilon \end{bmatrix} \\ &= \underbrace{\begin{bmatrix} 1 & 0 \\ 0 & \mu_1 \end{bmatrix}}_{\underline{\underline{K_0}}} + \underbrace{\begin{bmatrix} 0 & -\mu_1 \\ -\mu_1 & 2\nu_2\mu_1 \end{bmatrix}}_{\underline{\underline{K_1}}} \varepsilon + \underbrace{\begin{bmatrix} \mu_1 & -2\nu_2\mu_1 \\ -2\nu_2\mu_1 & 0 \end{bmatrix}}_{\underline{\underline{K_2}}} \varepsilon^2 \end{aligned} \tag{3.6}$$

Stepping back to the resolution of the eigenvalues problem :

$$\omega^2 \underline{\underline{M}}\underline{\phi} = \underline{\underline{K}}\underline{\phi} \Leftrightarrow \lambda \widetilde{\underline{\underline{M}}}\underline{\phi'} = \widetilde{\underline{\underline{K}}}\underline{\phi'} \Leftrightarrow (\widetilde{\underline{\underline{K}}} - \lambda \widetilde{\underline{\underline{M}}})\underline{\phi'} = 0 \tag{3.7}$$

A new dimensionless variable is introduced : $\lambda = \omega^2/\Omega^2$, the power series development is limited to the order ε^1 : $\lambda = \lambda_0 + \varepsilon\lambda_1$. Similarly, the rescaled mode ϕ' is developed : $\underline{\phi'} = \underline{\phi_0} + \varepsilon\underline{\phi_1}$. The replacement of $\underline{\underline{M}}$ and $\underline{\underline{K}}$ gives :

- Order ε^0 :

$$(\underline{\underline{K_0}} - \lambda_0 \underline{\underline{M_0}})\underline{\phi_0} = 0 \tag{3.8}$$

- Order ε^1 :

$$(\underline{\underline{K_0}} - \lambda_0 \underline{\underline{M_0}})\underline{\phi_1} = -(\underline{\underline{K_1}} - \lambda_1 \underline{\underline{M_0}})\underline{\phi_0} \tag{3.9}$$

The result of $f(\lambda_0) = |\underline{\underline{K_0}} - \lambda_0 \underline{\underline{M_0}}| = 0$: $\boxed{\lambda_0 = \{1, 1\}}$

A particular outcome is noticed : the matrix $(\underline{\underline{K_0}} - \lambda_0 \underline{\underline{M_0}})$ is nil, the system is undetermined and the mode shapes $\underline{\phi_0}$ can't be computed at this stage.

Moving on to (3.9), the LHS being equal to zero, as a result of the previous equation, the RHS is equal to zero as well, which leads after the resolution of : $\lambda_1^2 - 2\nu_2\lambda_1 - \mu_1 = 0$: $\boxed{\lambda_1 = \nu_2 \pm \sqrt{\nu_2^2 + \mu_1}}$

This new system represents an uncommon case where the mode shapes associated to the order ε^0, are derived from the system expressed with the eigenvalues associated to the next order. The substitution of λ_0 and λ_1 gives :

$$\lambda = 1 + \varepsilon(\nu_2 \pm \sqrt{\nu_2^2 + \mu_1}) \tag{3.10}$$

To present a notation that is habitual to the reader, a transformation of the dimensionless expression is proposed, involving the physical variables :

$$\boxed{\omega = \Omega \cdot \sqrt{\alpha \pm \sqrt{(\alpha-1)^2 + \mu}}} \tag{3.11}$$

For small values of μ, and as $\alpha = 1/(1+\mu)$ (a result from the analytical developments of [3] and [13]), α is pretty close to the unity. Thus, the term $(\alpha-1)^2$ can be neglected, simplifying the previous expression to :

$$\omega = \Omega \cdot \sqrt{1 \pm \sqrt{\mu}} \tag{3.12}$$

This expression is simpler, stating that the more μ is higher, the more ω moves away from Ω, like it is confirmed by the **Figure 3.5**. Besides, this figure shows the analytic expressions ((3.11) and (3.12)) compared to the eingenvalues computed numerically. The den Hartog adjustment provides more precision especially for high values of μ. The **Figure 3.6**, highlights the increasing tendency of the relative error with respect to the mass ratio, that reaches 2.2% for $\mu = 0.05$.

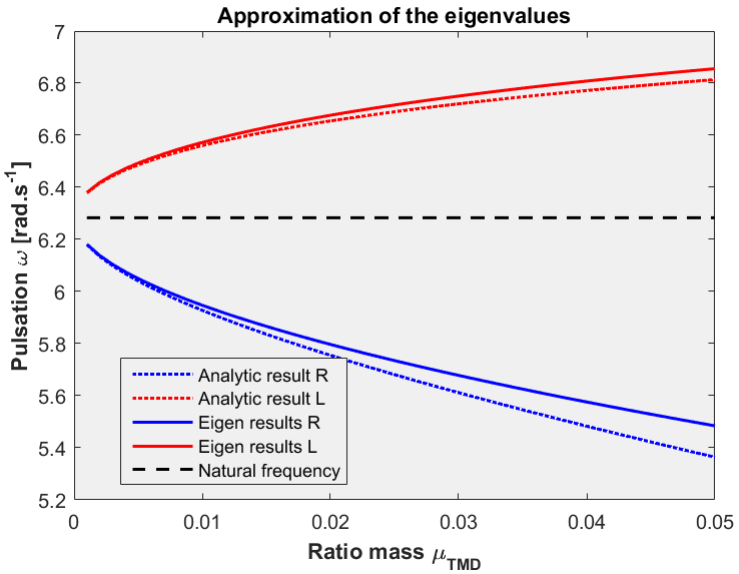

Figure 3.5: Evolution of the analytical expression in function of μ, and comparison with the numerical eigenvalues solution *(R for Right, L for Left)*

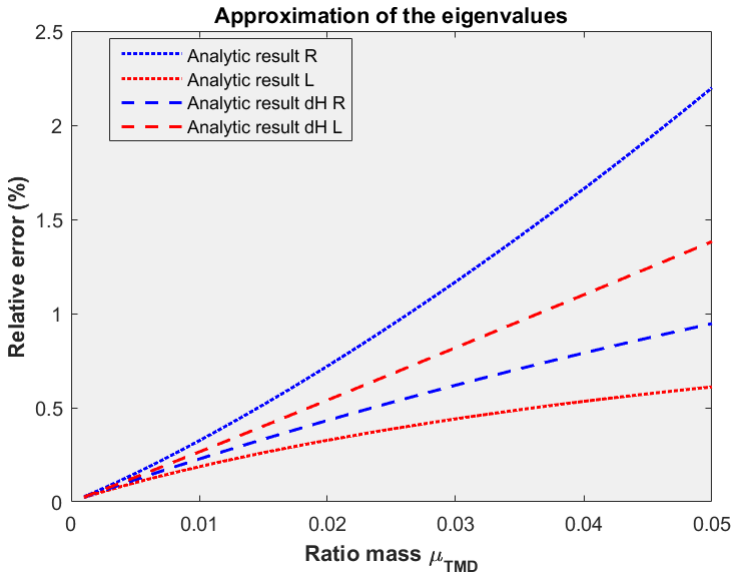

Figure 3.6: Relative error between analytical expression (3.11) and numerical eigenvalues solution in function of μ_{TMD} *(R for Right, L for Left)*

3.2.2 Approximation of the equivalent damping

The purpose of this section is to find an analytic approximation of the equivalent damping after the generalization of the matrices.

For a 2DOF system, composed by a SDOF structure coupled with a TMD, and tuned with den Hartog's adjustment : it is noticed that the equivalent damping ξ_{eq} coincides perfectly to the mean value of ξ_s and ξ_{TMD}. This observation is supported by the analytic expression found by [6] for small values of μ_{TMD}:

$$\xi_{eq} = \frac{(1+\mu)\alpha\xi_{TMD} + \xi_s}{2\sqrt{\alpha}} \tag{3.13}$$

In the case of a Den Hartog adjustment [3], the expression can be simplified. Indeed, considering $\alpha = 1/(1+\mu)$, it is found that :

$$\xi_{eq} = \frac{1}{2}\sqrt{1+\mu}\,(\xi_{TMD} + \xi_s) \tag{3.14}$$

The asymptotic expansion gives a simpler form, showing that for small values of μ_{TMD} (~ 0), the equivalent damping ratio tends to the mean value of ξ and ξ_{TMD}.

$$\xi_{eq} = \frac{1}{2}\,(1+\frac{\mu}{2})\,(\xi_{TMD} + \xi_s) \tag{3.15}$$

A perturbation method is built in order to approximate the previous expression, or at least to reach the same result when μ is small. The strategy is to begin by making

explicit the dimensionless expression of the modal generalized damping $\underline{\underline{C}}^*$, that is directly linked to the damping ratio.

Given the dimensionless form of the eigenvalues found in the Section 3.2.1, the replacement of λ_1 in the system $(\underline{\underline{K_1}} - \lambda_1 \underline{\underline{M_0}})\underline{\phi_0} = 0$ leads to the determination of the eigenvectors $\underline{\phi_0}$:

$$\underline{\underline{\Phi_0}} = \begin{bmatrix} \frac{-\mu_1}{\lambda_1^1} & \frac{-\mu_1}{\lambda_1^2} \\ 1 & 1 \end{bmatrix} \tag{3.16}$$

With : $\lambda_1^1 = \nu_2 + \sqrt{\nu_2^2 + \mu_1}$ and $\lambda_1^2 = \nu_2 - \sqrt{\nu_2^2 + \mu_1}$

The equivalent damping matrix Ξ^* represents the damping ratio associated to the matrices projected on the modes. The diagonal components symbolize the modal damping ratios, while the non-diagonal components speak for the coupling damping ratios.

$$\underline{\underline{\Xi^*}} = \begin{bmatrix} \xi_{1,1}^* & \xi_{1,2}^* \\ \xi_{2,1}^* & \xi_{2,2}^* \end{bmatrix} \tag{3.17}$$

3.2.2.1 Modal damping ratios

Employing the matrices established in (3.5) and (3.6), the generalized matrices can be computed. The projection in the modes $\underline{\phi_0^i} = [-\frac{\mu_1}{\lambda_1^i}\ 1]^T$ provides the diagonal components of the generalized matrices :

$$\begin{cases} M_{i,i}^* = \underline{\phi_0^i}^T \underline{\underline{M_0}}\ \underline{\phi_0^i} = (\frac{\mu_1}{\lambda_1^i})^2 + \mu_1 \\ K_{i,i}^* = \underline{\phi_0^i}^T \underline{\underline{K_0}}\ \underline{\phi_0^i} = (\frac{\mu_1}{\lambda_1^i})^2 + \mu_1 \end{cases}$$

The damping matrix $\underline{\underline{C}}$ is decomposed such that the structural contribution and the contribution of the damper are distinguished : $\underline{\underline{C}} = \underline{\underline{C_s}} + \underline{\underline{C_d}}$

$$\underline{\underline{\widetilde{C}_s}} = \begin{bmatrix} 1 & 0 \\ 0 & 1/\varepsilon \end{bmatrix} \begin{bmatrix} 2\xi_s & 0 \\ 0 & 0 \end{bmatrix} \begin{bmatrix} 1 & 0 \\ 0 & 1/\varepsilon \end{bmatrix} = \underbrace{\begin{bmatrix} 2\xi_s & 0 \\ 0 & 0 \end{bmatrix}}_{\underline{\underline{C_{s,0}}}} \tag{3.18}$$

$$\underline{\underline{\widetilde{C}_d}} = \begin{bmatrix} 1 & 0 \\ 0 & 1/\varepsilon \end{bmatrix} 2\mu_1(1+\varepsilon\nu_2)\xi_{TMD} \begin{bmatrix} \varepsilon^2 & -\varepsilon^2 \\ -\varepsilon^2 & \varepsilon^2 \end{bmatrix} \begin{bmatrix} 1 & 0 \\ 0 & 1/\varepsilon \end{bmatrix}$$

$$\underline{\underline{\widetilde{C}_d}} = \underbrace{\begin{bmatrix} 1 & 0 \\ 0 & 2\mu_1\xi_{TMD} \end{bmatrix}}_{\underline{\underline{C_{d,0}}}} + \underbrace{\begin{bmatrix} 0 & -2\mu_1\xi_{TMD} \\ -2\mu_1\xi_{TMD} & 2\mu_1\nu_2\xi_{TMD} \end{bmatrix}}_{\underline{\underline{C_{d,1}}}} \varepsilon + \underbrace{\begin{bmatrix} 2\mu_1\xi_{TMD} & -2\mu_1\nu_2\xi_{TMD} \\ -2\mu_1\nu_2\xi_{TMD} & 0 \end{bmatrix}}_{\underline{\underline{C_{d,2}}}} \varepsilon^2 \tag{3.19}$$

Similarly to M_0^* and K_0^*, the projection in the modal basis provides :

$$\begin{cases} C_{s,i,i}^* = \underline{\phi_0^i}^T \underline{\underline{C_{s,0}}}\ \underline{\phi_0^i} = 2(\frac{\mu_1}{\lambda_1^i})^2 \xi_s \\ C_{d,i,i}^* = \underline{\phi_0^i}^T \underline{\underline{C_{d,0}}}\ \underline{\phi_0^i} = 2\mu_1 \xi_{TMD} \end{cases}$$

Going from the definition of the damping ratio, it is possible to extract the first order approximation as the following :

$$\boxed{\xi_{i,i}^* = \frac{C_{s,i,i}^* + C_{d,i,i}^*}{2\sqrt{M_{i,i}^* K_{i,i}^*}} = \frac{\mu_1 \xi_s + \lambda_1^{i2} \xi_{TMD}}{\mu_1 + \lambda_1^{i2}}} \tag{3.20}$$

This damping ratio constitutes a kind of weighted average of ξ_s and ξ_{TMD}. It is a good advance since the targeted result is an arithmetic average. Differently, the last formulation contains two solutions, as it contains the quantity $\lambda_1 = \nu_2 \pm \sqrt{\nu_2^2 + \mu_1}$ (a result from 3.10).

To go back to the physical form, ε^2 is introduced up and down giving :

$$\xi_{i,i}^* = \frac{\mu \xi_s + \gamma \xi_{TMD}}{\mu + \gamma} \tag{3.21}$$

With : $\gamma = (\varepsilon \lambda_1)^2 = ((\alpha - 1) \pm \sqrt{(\alpha - 1)^2 + \mu})^2$

The analytic solutions are compared to the exact result procured numerically at **Figure 3.7**. Two ways are used to compute ξ_{eq} numerically :

- Considering the definition of the modal damping :

  $C_{i,i}^* = 2\sqrt{K_{i,i}^* M_{i,i}^*} \xi_{eq})$, where everything is known but ξ_{eq} ;

- Considering the definition of the maximum value of the FRF :
  $max(|H|) = 1/(2K_{i,i}^* \xi_{eq})$

The blue and red curves associated to the numerical outcome give the exact same result, this is why they are not distinguishable. The following table compares the proximity of the different analytic expressions to the numerical result.

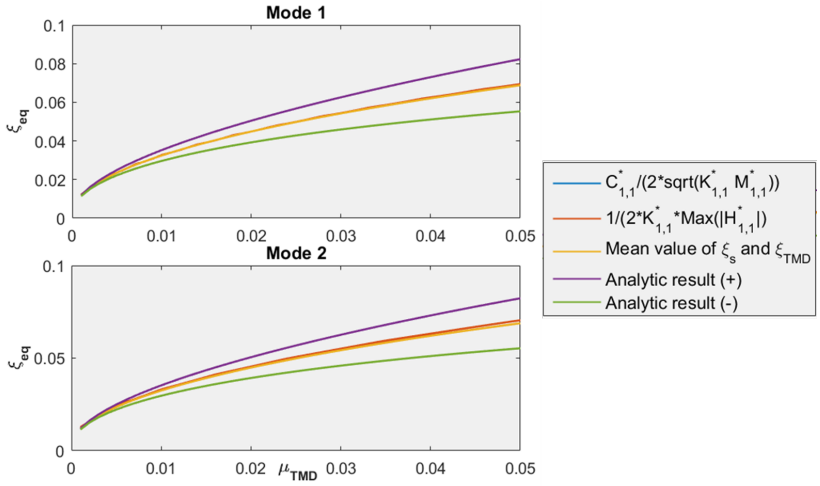

Figure 3.7: Equivalent damping ratio ξ_{eq} in function of μ_{TMD} *(Analytic (+) represents the analytic solution with a (+) in* λ_1*, Analytic (-) with a (-) in* λ_1*)*

Relative error (%)	**Mode 1**	**Mode 2**
JC Miranda's solution [6]	1.32	0.07
Mean value $\frac{\xi_s+\xi_{TMD}}{2}$	1.12	2.34
Analytic (+)	18.28	16.82
Analytic (-)	20.52	21.5

Table 3.2: Relative error with respect to the numerical results for $\mu_{TMD} = 0.05$

The analytic curves present a certain symmetry with respect to the numerical value, as it is showed on FIG. 3.7. It is tempting to suggest that the equivalent damping ratio is none other than the mean value of the analytic couple ((+) and (−)).

Giving a den Hartog's adjustment for the TMD, it can be demonstrated. The tuning ratio α is given in function of μ_{TMD} such that $\alpha = 1/(1+\mu)$. The translation into the dimensionless form is : $1 + \varepsilon\nu_2 = 1/(1+\varepsilon^2\mu_1)$. The substitution of ν_2 in the expression of λ_1^2 gives :

$$\lambda_1^2 = 2(\frac{\mu_1}{1+\varepsilon^2\mu_1})^2\varepsilon^2 + \mu_1 \mp \frac{\mu_1}{1+\varepsilon^2\mu_1}\varepsilon\sqrt{(\frac{\mu_1}{1+\varepsilon^2\mu_1})^2\varepsilon^2 + \mu_1}$$

Similarly to its square root, λ_1^2 contains two values by reason of the last term. The truncation right after the first order brings out only one common value as the result is $\lambda_1^2 = \mu_1$. The replacement in (3.20) gives the targeted result : the arithmetic mean of ξ_s and ξ_{TMD}.

3.2.2.2 Crossed damping ratios

From the above, and maintaining the same reasoning, the coupling components of the generalized matrices $\underline{\underline{M}}$ and $\underline{\underline{K}}$ are derived as follows :

$$\begin{cases} M^*_{i,j} = \underline{\phi^i_0}^T \underline{\underline{M_0}}\ \underline{\phi^j_0} = (\frac{\mu_1}{\lambda^i_1 \lambda^j_1}) + \mu_1 \\ K^*_{i,j} = \underline{\phi^i_0}^T \underline{\underline{K_0}}\ \underline{\phi^j_0} = (\frac{\mu_1}{\lambda^i_1 \lambda^j_1}) + \mu_1 \end{cases}$$

Similarly, the damping matrix non-diagonal elements are defined :

$$\begin{cases} C^*_{s,i,j} = \underline{\phi^i_0}^T \underline{\underline{C_{s,0}}}\ \underline{\phi^j_0} = 2(\frac{\mu_1}{\lambda^i_1 \lambda^j_1})\xi_s \\ C^*_{d,i,j} = \underline{\phi^i_0}^T \underline{\underline{C_{d,0}}}\ \underline{\phi^j_0} = 2\mu_1 \xi_{TMD} \end{cases}$$

The equivalent damping ratio is thus obtained :

$$\boxed{\xi^*_{i,j} = \frac{C^*_{s,i,j} + C^*_{d,i,j}}{2\sqrt{M^*_{i,j} K^*_{i,j}}} = \frac{\mu_1 \xi_s + \lambda^i_1 \lambda^j_1 \xi_{TMD}}{\mu_1 + \lambda^i_1 \lambda^j_1}} \tag{3.22}$$

3.2.3 Validation of the model

It is questionable to what extent the established optimal expressions lead to the optimum in terms of minimization of the variance of the response.

Stepping back to the expression (3.21), that can be written in the following form (by dividing by μ up and down) :

$$\xi^*_{i,i} = \frac{\xi_s + \frac{(\varepsilon\lambda_1)^2}{\mu}\xi_{TMD}}{1 + \frac{(\varepsilon\lambda_1)^2}{\mu}} \tag{3.23}$$

Where :

$$\frac{(\varepsilon\lambda_1)^2}{\mu} = 1 + 2(\frac{\alpha - 1}{\sqrt{\mu}})^2 + 2(\frac{\alpha - 1}{\sqrt{\mu}})\sqrt{(\frac{\alpha - 1}{\sqrt{\mu}})^2 + 1)}$$

The equivalent damping can henceforth be displayed in function of a single dimensional group $A = \frac{\alpha - 1}{\sqrt{\mu}}$.

$$\xi^*_{i,i} = \frac{\xi_s + (1 + 2A^2 + 2A\sqrt{A^2 + 1}))\xi_{TMD}}{1 + (1 + 2A^2 + 2A\sqrt{A^2 + 1}))} \tag{3.24}$$

To tend to the arithmetic value of ξ_s and ξ_{TMD}, and without considering Den Hartog's

adjustment, the following condition has to be fulfilled :

$$1 + 2A^2 + 2A\sqrt{A^2 + 1} = 1 \tag{3.25}$$

The solution of the equation is $A = 0$, a criteria for α can be extracted : $\boxed{\alpha = 1}$. A criteria that is in accordance with den Hartog adjustment for small values of μ.

The following figure displays the variance of the acceleration in the (α, ξ_{TMD}) space (with a mass ratio of 5%.).

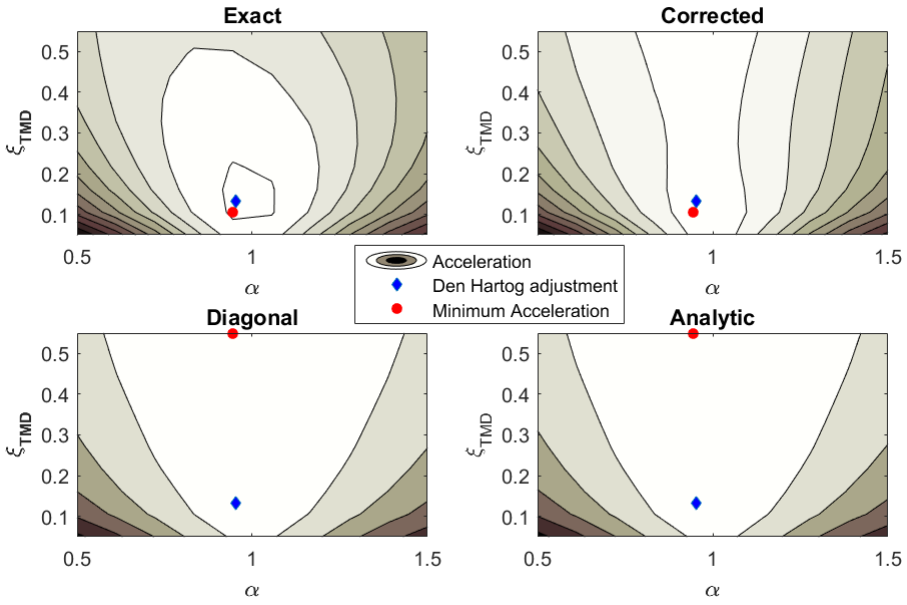

Figure 3.8: Representation of the acceleration's variance in the (α, ξ_{TMD}) space

The 'Corrected' map corresponds to the uncoupled system rectified with [9], the result is obtained after three iterations. It converges well toward the adjustment of Den Hartog (3.1).

For the approached model ('Analytic' plot), the expressions presented above bring an almost optimal value for α. The approached model is built considering the modes uncoupled, it is thus more assimilated to the 'Diagonal' plot.

In terms of ξ_{TMD}, since the adoption of the uncoupled modes hypothesis to procure the analytical expressions of the variance and covariance of the acceleration (respectively reminded (3.26). It is noticed that the acceleration is proportional to $1/\xi^*_{i,i}$ or $1/\xi^*_{i,j}$. Considering the approached expression of the equivalent damping ratio (3.20), the variance and covariance are thus proportional to ξ_{TMD}, the reason behind reaching the minimum acceleration for the maximum value of ξ_{TMD}. The **Figure 3.9** confirms this statement.

$$\begin{cases} \sigma^2_{\ddot{q}_{i,i}} = \frac{S_{p^*_{i,i}}}{M^2_{i,i}}(2\omega_{max} + \frac{\pi\omega_m}{2\xi^*_{i,i}}) \\ \sigma_{\ddot{q}_{i,j}} = \frac{S_{p^*_{i,j}}}{K^*_{i,i}K^*_{j,j}}\left(2\omega_{max}\omega_i^2\omega_j^2 + \frac{1}{4}\left(\frac{\omega_i+\omega_j}{2}\right)^4 \frac{\pi(\xi^*_{i,j}-i\varepsilon)}{2\varepsilon(\varepsilon^2+\xi^{*2}_{i,j})}\right) \end{cases} \tag{3.26}$$

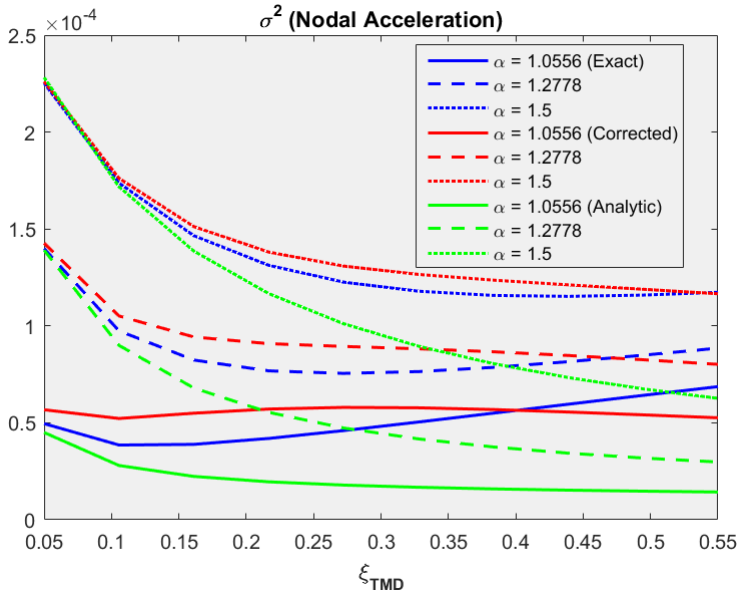

Figure 3.9: Evolution of the acceleration's variance in function of ξ_{TMD}

3.2.3.1 Analytic approximation of the corrected response

The addition of the residual term in an iterative way, has led to the convergence to the exact representation. In what follows, a method based on the developments performed in the previous chapter, is aimed to demonstrate that the residual term is an increasing function of ξ_{TMD}. Actually, the addition to the diagonal outcome would permit to identify an optimum value of ξ_{TMD}.

As reported before, it is known that :

$$S_{\ddot{Q}_c} = S_{\ddot{Q}_d} + S_{\Delta\ddot{Q}} + S_{\ddot{Q}_d\Delta\ddot{Q}} + S_{\Delta\ddot{Q}\ddot{Q}_d}$$

The interaction terms have small impact on $S_{\ddot{Q}_c}$, they are therefore neglected, such as : $S_{\ddot{Q}_c} = S_{\ddot{Q}_d} + S_{\Delta\ddot{Q}}$. Moving to the variances to get : $\sigma_{\ddot{Q}_c} = \sigma_{\ddot{Q}_d} + \sigma_{\Delta\ddot{Q}}$.

The residual term $\Delta\ddot{Q}$ is expressed as a function of ω times $\ddot{Q}_d$:

$$\Delta\ddot{Q} = H^*_d(-\omega D^*_0)\ddot{Q}_d$$

Z^* is a non-diagonal matrix introduced such that :$Z^* = H^*_d(-\omega D^*_0)$, as H^*_d is diagonal and D^*_0 contains only off-diagonal terms of the generalized matrix of damping. Based

on the **Property 2**[7], the PSD can be computed : $S_{\Delta\ddot{Q}} = Z^* S_{\ddot{Q}_d} \overline{Z^*}^T$

From above, the modal variances are obtained, by replacing

$S_{\ddot{Q}_d,n,n}(\omega) = |H^*_{n,n}(\omega)|^2 S_{\ddot{p},n,n}$:

$$\begin{aligned}\sigma^2_{\Delta\ddot{Q},m,m} &= \int_{-\infty}^{+\infty} S_{\Delta\ddot{Q},m,m}(\omega)d\omega \\ &= C^{*2}_{m,n} \int_{-\infty}^{+\infty} \omega^6 |H^*_{m,m}(\omega)|^2 S_{\ddot{Q}_d,n,n}(\omega)d\omega \\ &= C^{*2}_{m,n} S_{\ddot{p},n,n} \underbrace{\int_{-\infty}^{+\infty} \omega^6 |H^*_{m,m}(\omega)|^2 |H^*_{n,n}(\omega)|^2 d\omega}_{I_3} \end{aligned} \tag{3.27}$$

As well as the covariances :

$$\sigma_{\Delta\ddot{Q},m,n} = C^*_{n,m} C^*_{m,n} S_{\ddot{p},m,n} \underbrace{\int_{-\infty}^{+\infty} \omega^6 |H^*_{m,m}(\omega)|^2 |H^*_{n,n}(\omega)|^2 d\omega}_{I_3} \tag{3.28}$$

The denominator is simplified introducing the variable : $D(H_i) = (1 - (\frac{\omega}{\omega_i})^2 + 2i\xi^* \frac{\omega}{\omega_i})$.

$$I_3 = \int_{-\infty}^{+\infty} \omega^6 |H^*_{m,m}(\omega)|^2 |H^*_{n,n}(\omega)|^2 d\omega = \frac{1}{K^{*2}_{m,m} K^{*2}_{n,n}} \int_{-\infty}^{+\infty} \frac{\omega^6}{D(H_m)D(H_n)} d\omega$$

The polynomial's numerator is of degree 6, and its the denominator is of degree 8. Adding and subtracting $\omega_m^4 \omega_n^4 D(H_m)D(H_n)$ allows to get rid of the indeterminacy. This solution is accompanied by using a white noise defined on a limited band $[-\omega_{max}, \omega_{max}]$, instead of an infinite white noise.

$$I_3 = \frac{1}{K^{*2}_{m,m} K^{*2}_{n,n}} \left(\int_{-\omega_{max}}^{+\omega_{max}} \omega_m^4 \omega_n^4 d\omega + \underbrace{\int_{-\infty}^{+\infty} \frac{\omega^6 - \omega_m^4 \omega_n^4 D(H_m)D(H_n)}{D(H_m)D(H_n)} d\omega}_{I_4} \right) \tag{3.29}$$

$$I_4 = \int_{-\infty}^{+\infty} \frac{\omega^6 - \omega_m^4 \omega_n^4 D(H_m)D(H_n)}{D(H_m)D(H_n)} d\omega$$

In order to focus on both natural frequencies ω_m and ω_n simultaneously, a strained

[7] **Property 2 :** Knowing $[S_x]$ the PSD associated to the random process $\{X(\omega)\}$ and the transfer matrix $[H(\omega)]$, the PSD $[S_y]$ of the random process $\{Y(\omega)\}$ defined by : $\{Y(\Omega)\} = [H(\omega)]\{X(\omega)\}$ is also known : $[S_y] = [H(\omega)][S_x][\overline{H(\omega)}]^T$

coordinate $\omega(\eta)$ is introduced, centered on the mean :

$$\omega = \frac{\omega_m + \omega_n}{2}(1 + 2\varepsilon\eta)$$

With : $\eta = ord(1)$, and $\varepsilon = \frac{\omega_n - \omega_m}{\omega_m + \omega_n}$ a small dimensionless unit that measures the gap between natural frequencies.

In favor of considering a same order of magnitude for the natural frequencies, it is assumed $\varepsilon^2 << 1$. The numerator, in turn, is approximated to the first order. The simplifications guide to the following form of I_4 :

$$I_4 = (\frac{\omega_m + \omega_n}{2})^6 \frac{1}{16\xi^{*2}} \int_{-\infty}^{+\infty} \frac{1}{2(1 + 4\eta^2)\varepsilon^2 + \xi^2} d\eta \tag{3.30}$$

I_5 is computed using Cauchy's residue theorem, since the rational fraction fulfills the applicability conditions [8]. I_3 is reconstructed such that : $I_3 = I_4 + I_5$.

$$I_5 = \int_{-\infty}^{+\infty} \frac{1}{2(1 + 4\eta^2)\varepsilon^2 + \xi^2} d\eta = \frac{2\sqrt{2}\pi\varepsilon}{\sqrt{\xi^2 + 2\varepsilon^2}} \tag{3.31}$$

The substitution in (3.27) and (3.28) provides the analytic formulation of the variance and covariance.

$$\boxed{\sigma^2_{\Delta Q,\ddot{m},m} = \frac{C^{*2}_{m,n} S_{\ddot{p},n,n}}{K^{*2}_{m,m} K^{*2}_{n,n}} (2\omega_{max}\omega_m^4\omega_n^4 + (\frac{\omega_m + \omega_n}{2})^6 \frac{1}{16\xi^{*2}} \frac{2\sqrt{2}\pi\varepsilon}{\sqrt{\xi^{*2} + 2\varepsilon^2}})} \tag{3.32}$$

$$\boxed{\sigma_{\Delta Q,\ddot{m},n} = \frac{C^{*}_{n,m} C^{*}_{m,n} S_{\ddot{p},m,n}}{K^{*2}_{m,m} K^{*2}_{n,n}} (2\omega_{max}\omega_m^4\omega_n^4 + (\frac{\omega_m + \omega_n}{2})^6 \frac{1}{16\xi^{*2}} \frac{2\sqrt{2}\pi\varepsilon}{\sqrt{\xi^{*2} + 2\varepsilon^2}})} \tag{3.33}$$

The paragraph **3.2.2.2**, furnishes the analytic expression of the off-diagonal terms of C^*, that are by the way proportional to ξ_{TMD} : $C^*_{m,n} = \frac{2\mu_1^2}{\lambda_1^m \lambda_1^n}\xi_s + 2\mu_1\xi_{TMD}$

In fine, the nodal variance $\sigma^2_{\ddot{x}}$ make appear two contributions of ξ_{TMD}: ξ^2_{TMD} thanks to the first term of the modal variance (and covariance too), and $1/\xi_{TMD}$ in the second term.

[8] Applicability conditions of Cauchy's residue theorem : The denominator's polynomial admits complex poles, and is two degrees higher than the numerator's polynomial.

3.3 Effect of a damper on a MDOF system

3.3.1 Approximation of the natural frequencies

→ A 3DOF system is now treated : a 2DOF structure assembled with a damper. The matrix of mass and stiffness are given below :

$$\underline{\underline{M}} = \begin{bmatrix} M_1 & 0 & 0 \\ 0 & M_2 & 0 \\ 0 & 0 & m \end{bmatrix} \; ; \; \underline{\underline{K}} = \begin{bmatrix} K_1 & 0 & 0 \\ 0 & K_2 & 0 \\ 0 & 0 & 0 \end{bmatrix} + k \begin{bmatrix} \varphi_1^2 & \varphi_1\varphi_2 & -\varphi_1 \\ \varphi_1\varphi_2 & \varphi_2^2 & -\varphi_2 \\ -\varphi_1 & -\varphi_2 & 1 \end{bmatrix} \quad (3.34)$$

The TMD is taken tuned to the first structural mode, which leads to : $m = \varepsilon^2\mu_1 M_1$ and $k = \varepsilon^2\mu_1(1 + 2\varepsilon\nu_2)K_1$. Dimensionless parameters are introduced to link the two structural modes : $\beta = \Omega_2/\Omega_1$ and $\overline{M_2} = M_2/M_1$. The first parameter measures the distance between the two structural frequencies, its dimensionless form is : $\beta = 1 + b\varepsilon$, with $b = ord(1)$. This form allows to limit the range of study to values of the parameter β near 1, and with the objective to attain good approximations for β reaching $1,2$ at least.

Taking ($M_1 = 1$, $K_1 = 1$), the substitution in 3.34 gives :

$$\underline{\underline{M}} = \begin{bmatrix} 1 & 0 & 0 \\ 0 & \overline{M_2} & 0 \\ 0 & 0 & \varepsilon^2\mu_1 \end{bmatrix}$$

$$\underline{\underline{K}} = \begin{bmatrix} 1 & 0 & 0 \\ 0 & \beta^2\overline{M_2} & 0 \\ 0 & 0 & \varepsilon^2\mu_1 \end{bmatrix} + \varepsilon^2\mu_1(1 + 2\varepsilon\nu_2) \begin{bmatrix} \varphi_1^2 & \varphi_1\varphi_2 & -\varphi_1 \\ \varphi_1\varphi_2 & \varphi_2^2 & -\varphi_2 \\ -\varphi_1 & -\varphi_2 & 1 \end{bmatrix} \quad (3.35)$$

In analogy with the system 2×2, and in order to maintain a consistency in the dimensionless development, the matrices are now written in the new eigenvector basis. The change of basis is operated by the introduction of the matrix $\underline{\underline{A}}$ such that :

$$\underline{\underline{A}} = \begin{bmatrix} 1 & 0 & 0 \\ 0 & 1 & 0 \\ 0 & 0 & 1/\varepsilon \end{bmatrix}$$

The form of the mass and stiffness matrices, after the development of the dimensionless form gives :

$$\underline{\underline{\widetilde{M}}} = \underline{\underline{A}}^T \underline{\underline{M}}\ \underline{\underline{A}} = \underbrace{\begin{bmatrix} 1 & 0 & 0 \\ 0 & \overline{M_2} & 0 \\ 0 & 0 & \mu_1 \end{bmatrix}}_{\underline{\underline{M_0}}} \tag{3.36}$$

$$\underline{\underline{\widetilde{K}}} = \underline{\underline{A}}^T \underline{\underline{K}}\ \underline{\underline{A}} = \underbrace{\begin{bmatrix} 1 & 0 & 0 \\ 0 & \overline{M_2} & 0 \\ 0 & 0 & \mu_1 \end{bmatrix}}_{\underline{\underline{K_0}}} + \underbrace{\begin{bmatrix} 0 & 0 & -\mu_1\varphi_1 \\ 0 & 2b\overline{M_2} & -\mu_1\varphi_2 \\ -\mu_1\varphi_1 & -\mu_1\varphi_2 & 2\nu_2 \end{bmatrix}}_{\underline{\underline{K_1}}} \varepsilon + ord(\varepsilon^2) \tag{3.37}$$

Maintaining the power series expansion of $\lambda = \omega^2/\Omega^2$ and $\underline{\phi}'$ limited to the order ε^1. Similarly to the system 2×2, the eigenvalue problem $(\underline{\underline{\widetilde{K}}} - \lambda\underline{\underline{\widetilde{M}}})\underline{\phi}' = 0$ gives rise to 2 equations :

- Order ε^0 : $(\underline{\underline{K_0}} - \lambda_0\underline{\underline{M_0}})\underline{\phi_0} = 0$

$f(\lambda_0) = |\underline{\underline{K_0}} - \lambda_0\underline{\underline{M_0}}| = 0$ admits as solution $\boxed{\lambda_0 = \{1, 1, 1\}}$.

- Order ε^1 : $(\underline{\underline{K_1}} - \lambda_1\underline{\underline{M_0}})\underline{\phi_0} = 0$

The resolution of the eigenvalue problem $f(\lambda_1) = |\underline{\underline{K_1}} - \lambda_1\underline{\underline{M_0}}| = 0$ leads to an equation of 3rd degree :

$$\boxed{\lambda_1^3 - 2(b+\nu_2)\lambda_1^2 + (4b\nu_2 - \mu_1(\varphi_1^2 + \frac{\varphi_2^2}{\overline{M_2}}))\lambda_1 + 2\mu_1\varphi_1^2 b = 0} \tag{3.38}$$

Three solutions are derived, where each one of them represents one of the three modes. The reconstruction of $\lambda = \lambda_0 + \varepsilon\lambda_1$, and the comparison with the exact values guide to the association of the values of λ_1 with the right modes.

Going from the equation (3.38), and considering the following set of parameters, an equation of 2^{nd} degree is derived : $\lambda_1^2 - 2\nu_2\lambda_1 - \mu_1 = 0$. This equation is the one generating the solutions of λ_1 in the 2DOF system. The consistency of the equation is thus verified.

Dataset 1			
β	$\overline{M_2}$	φ_1	φ_2
1	1	1	0

Table 3.3: Dataset 1

Nevertheless, unlike the 2×2 system, the analytic form of λ_1 is not established in an explicit way. For now, it is declared as unknown.

3.3.2 Approximation of the equivalent damping

Based on the dimensionless form of the eigenvalues found in the section 3.3.1, the replacement of λ_1 in the system $(\underline{\underline{K_1}} - \lambda_1 \underline{\underline{M_0}})\underline{\phi_0} = 0$ leads to the definition of the eigenvectors matrix $\underline{\underline{\Phi_0}}$:

$$\underline{\underline{\Phi_0}} = \begin{bmatrix} -\frac{\mu_1\varphi_1}{\lambda_1^1} & -\frac{\mu_1\varphi_1}{\lambda_1^2} & -\frac{\mu_1\varphi_1}{\lambda_1^3} \\ -\frac{\mu_1\varphi_2}{(\lambda_1^1-2b)\overline{M_2}} & -\frac{\mu_1\varphi_2}{(\lambda_1^2-2b)\overline{M_2}} & -\frac{\mu_1\varphi_2}{(\lambda_1^3-2b)\overline{M_2}} \\ 1 & 1 & 1 \end{bmatrix} \tag{3.39}$$

Based on that, the generalized matrices can be computed. The projection on each mode provides diagonal elements :

$$\begin{cases} M^*_{i,i} = \underline{\phi_0^{iT}}\ \underline{\underline{M_0}}\ \underline{\phi_0^i} = (\frac{\mu_1\varphi_1}{\lambda_1^i})^2 + \frac{1}{\overline{M_2}}(\frac{\mu_1\varphi_2}{\lambda_1^i-2b})^2 + \mu_1 \\ K^*_{i,i} = \underline{\phi_0^{iT}}\ \underline{\underline{K_0}}\ \underline{\phi_0^i} = (\frac{\mu_1\varphi_1}{\lambda_1^i})^2 + \frac{\beta^2}{\overline{M_2}}(\frac{\mu_1\varphi_2}{\lambda_1^i-2b})^2 + \mu_1 \end{cases}$$

The damping matrix is decomposed such that the structural contribution and the contribution of the damper are distinguished :

$$\widetilde{\underline{\underline{C_s}}} = \underline{\underline{A}}^T \underline{\underline{C_s}}\ \underline{\underline{A}} = \underbrace{\begin{bmatrix} 2\xi_s & 0 & 0 \\ 0 & 2\overline{M_2}\xi_s & 0 \\ 0 & 0 & 0 \end{bmatrix}}_{\underline{\underline{C_{s,0}}}} + \underbrace{\begin{bmatrix} 0 & 0 & 0 \\ 0 & 2b\overline{M_2}\xi_s & 0 \\ 0 & 0 & 0 \end{bmatrix}}_{\underline{\underline{C_{s,1}}}} \varepsilon + ord(\varepsilon^2) \tag{3.40}$$

$$\widetilde{\underline{\underline{C_d}}} = \underline{\underline{A}}^T \underline{\underline{C_d}}\ \underline{\underline{A}} = 2\varepsilon^2\mu_1(1+\varepsilon\nu_2)\xi_{TMD} \begin{bmatrix} \varphi_1^2 & \varphi_1\varphi_2 & -\frac{1}{\varepsilon}\varphi_1 \\ \varphi_1\varphi_2 & \varphi_2^2 & -\frac{1}{\varepsilon}\varphi_2 \\ -\frac{1}{\varepsilon}\varphi_1 & -\frac{1}{\varepsilon}\varphi_2 & \frac{1}{\varepsilon^2} \end{bmatrix} \tag{3.41}$$

$$\widetilde{\underline{\underline{C_d}}} = \underbrace{\begin{bmatrix} 0 & 0 & 0 \\ 0 & 0 & 0 \\ 0 & 0 & 2\mu_1\xi_{TMD} \end{bmatrix}}_{\underline{\underline{C_{d,0}}}} + \underbrace{\begin{bmatrix} 0 & 0 & -2\mu_1\xi_{TMD}\varphi_1 \\ 0 & 0 & -2\mu_1\xi_{TMD}\varphi_2 \\ -2\mu_1\xi_{TMD}\varphi_1 & -2\mu_1\xi_{TMD}\varphi_2 & 2\mu_1\nu_2\xi_{TMD} \end{bmatrix}}_{\underline{\underline{C_{d,1}}}} \varepsilon$$

$$+ord(\varepsilon^2) \tag{3.42}$$

Similarly to $M^*_{i,i}$ and $K^*_{i,i}$, the projection in the modal basis provides :

$$\begin{cases} C^*_{s,i,i} = \underline{\phi^{iT}_0}\ \underline{\underline{C_{s,i,i}}}\ \underline{\phi^i_0} = 2\Big((\frac{\mu_1\varphi_1}{\lambda_1})^2 + \frac{1}{\overline{\overline{M_2}}}(\frac{\mu_1\varphi_2}{\lambda^i_1-2b})^2\Big)\xi_s \\ C^*_{d,i,i} = \underline{\phi^{iT}_0}\ \underline{\underline{C_{d,0}}}\ \underline{\phi_0} = 2\mu_1\xi_{TMD} \end{cases}$$

The first order approximation of the damping ratio is subsequently computed :

$$\boxed{\xi^*_{i,i} = \frac{C^*_{s,i,i} + C^*_{d,i,i}}{2\sqrt{M^*_{i,i}K^*_{i,i}}} = \frac{\mu_1((\frac{\varphi_1}{\lambda^i_1})^2 + \frac{1}{\overline{\overline{M_2}}}(\frac{\varphi_2}{\lambda^i_1-2b})^2)\xi_s + \xi_{TMD}}{\mu_1((\frac{\varphi_1}{\lambda^i_1})^2 + \frac{1}{\overline{\overline{M_2}}}(\frac{\varphi_2}{\lambda^i_1-2b})^2) + 1}} \tag{3.43}$$

Based on the same reasoning as in the 2×2 system, the coupling elements of the matrix are found :

$$\boxed{\xi^*_{i,j} = \frac{\mu_1(\frac{\varphi_1^2}{\lambda^i_1\lambda^j_1} + \frac{1}{\overline{\overline{M_2}}}\frac{\varphi_2^2}{(\lambda^i_1-2b)(\lambda^j_1-2b)})\xi_s + \xi_{TMD}}{\mu_1(\frac{\varphi_1^2}{\lambda^i_1\lambda^j_1} + \frac{1}{\overline{\overline{M_2}}}\frac{\varphi_2^2}{(\lambda^i_1-2b)(\lambda^j_1-2b)}) + 1}} \tag{3.44}$$

The expression of ξ^* has henceforth a lot of meaning, it represents a weighted average of ξ_s and ξ_{TMD}, like it has been discovered previously. However it involves a complex quantity that is the sum of two positive terms $\Gamma = \Gamma_1 + \Gamma_2$, where :

$$\Gamma_1 = (\frac{\mu_1\varphi_1}{\lambda^i_1})^2,\ \Gamma_2 = \frac{1}{\overline{\overline{M_2}}}(\frac{\mu_1\varphi_2}{\lambda_1 - 2b})^2$$

A way of validating the expression (3.44), is to verify if its consistent with the results of the 2DOF system. Indeed, considering the set of parameters aforementioned, the expression found is the one established in 2DOF system section.

Given its definition, the extreme values of ξ^* are naturally ξ_s and ξ_{TMD}.

- ξ^* tends to ξ_s when $\lambda_1 \to 0 \Leftrightarrow \Gamma_1$ is dominant, and when $\lambda_1 \to 2b \Leftrightarrow \Gamma_2$ is dominant ;
- ξ^* tends to ξ_{TMD} when $\lambda_1 \to \infty \Leftrightarrow \Gamma_1$ and Γ_2 are both small. The intention is to maximize the damping ratio, in this way the last case is the optimal one.
- The optimum to be reached is therefore the one for which the 2 quantities have an equal importance, which constitutes an intermediate case : $\Gamma_1 = \Gamma_2$. In other words, the TMD tuned on the first mode, comes to an influence in the second mode. A criteria can be established on the position of the TMD :

$$\boxed{\frac{\varphi_1}{\varphi_2} = (1 + \frac{2b}{\lambda^i_1 - 2b})\frac{1}{\sqrt{\overline{\overline{M_2}}}}} \tag{3.45}$$

The equation (3.44) also reveals that the result of $\xi^*_{i,i}$ remains the same if φ_2 is multiplied by $\sqrt{\theta}$ and $\overline{M_2}$ by θ. It turns out that it is conform to the reality, according to the next figure. The exact result of the equivalent damping remains unchanging from a configuration to another.

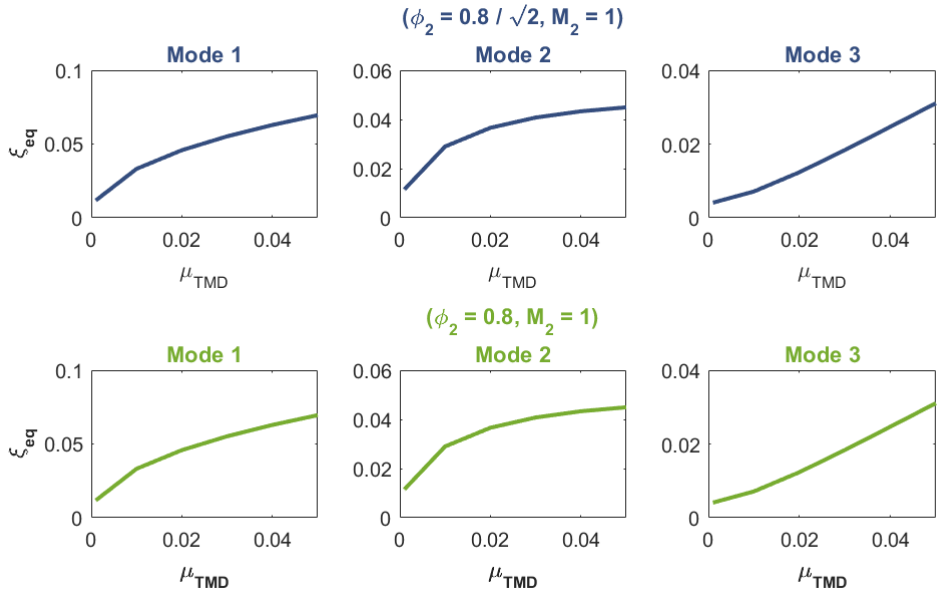

Figure 3.10: Comparison of the exact result in the two configurations

In order to understand in depth the behavior of Γ, it is required to evaluate the sensitivity of λ_1 in function of principal parameters such as μ, β, $\overline{M_2}$, φ_1 and φ_2.

In the phase of research, it has been developed an alternative method which is similar to the current one, except that the parameter β has been considered of $ord(1)$ without any other restriction. It may have a negative impact on the precision of the solution. This argument is reinforced by the following figure, that displays the natural frequencies along the ratio mass.

Keeping β free is also not an interesting choice, as if β exceeds a certain value, the coupling effect between the modes disappears, which may question the global strategy of the method.

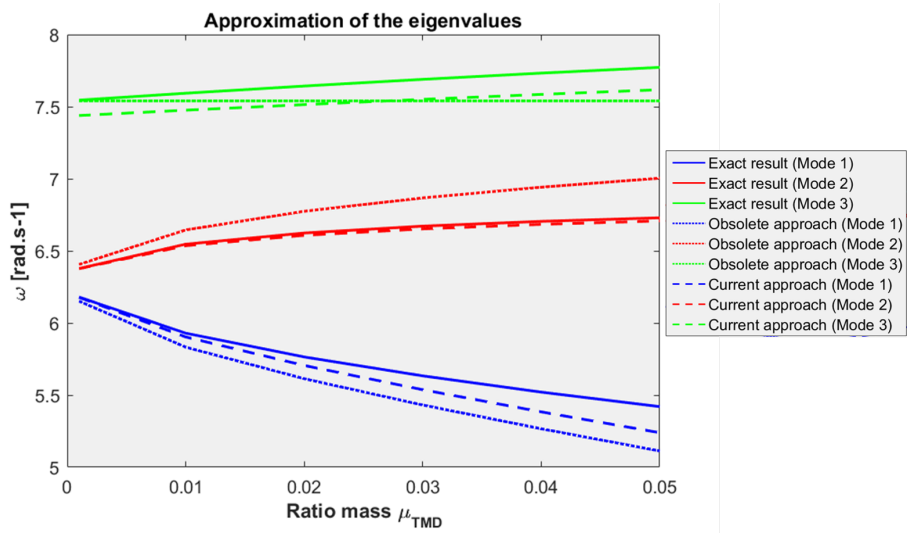

Figure 3.11: Comparison of the current approach vs. the obsolete approach (Natural frequencies) ($\beta = 1.2, \overline{M_2} = 1$)

On the other hand, the obsolete method (available in Appendix A3) presents a good approximation of the eigenvalues as it has been observed before, but not satisfying results for the approximation of the damping ratio, except the first mode (**Figure 3.12**). More importantly, it provides an analytic expression of λ_1, likely to help understand the contribution of each parameter.

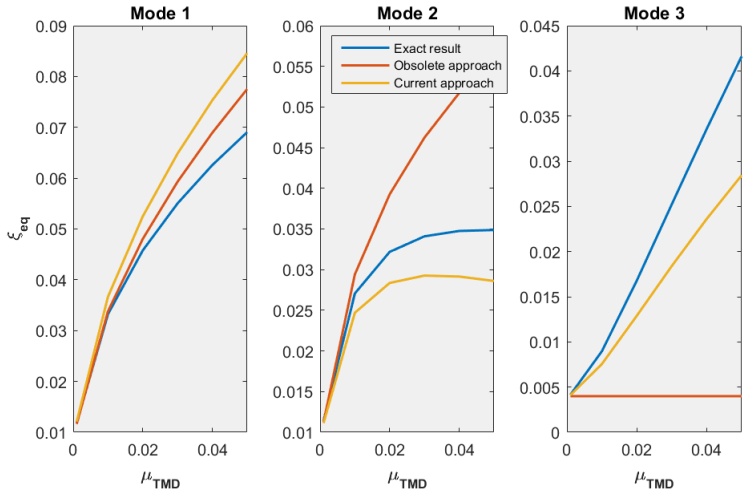

Figure 3.12: Comparison of the current approach vs. the obsolete approach (Equivalent damping ratios) ($\beta = 1.15, \overline{M_2} = 1$)

The sensitivity investigation :

In what follows, a consultation of the unknown λ_1 is performed, in order to detect how it is influenced by the evolution of the other parameters of the problem.

- **Influence of μ**

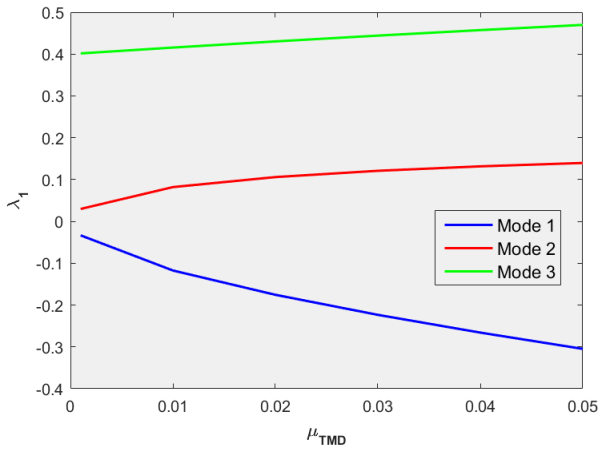

Figure 3.13: Variation of λ_1 in function of μ

The figure reveals the behavior observed in **Figure 3.4**. Indeed, when μ grows, the transfer function is attenuated and the distance between the peak locations grows. Other, λ_0 being equal to 1 in the three modes, it is λ_1 that reveals the evolution of the locations of the FRF's poles, where the red curve would represent the location of the common pole of the transfer functions, in a case of an optimum setting of the TMD.

In absolute value, λ_1 is a growing function of μ. It evolves as a square-root function of μ for the first and second mode, which is confirmed by the analytic solution found with the previous approach. On the other hand, the variation in the third mode is linear, with a shift from 0.

- **Influence of β**

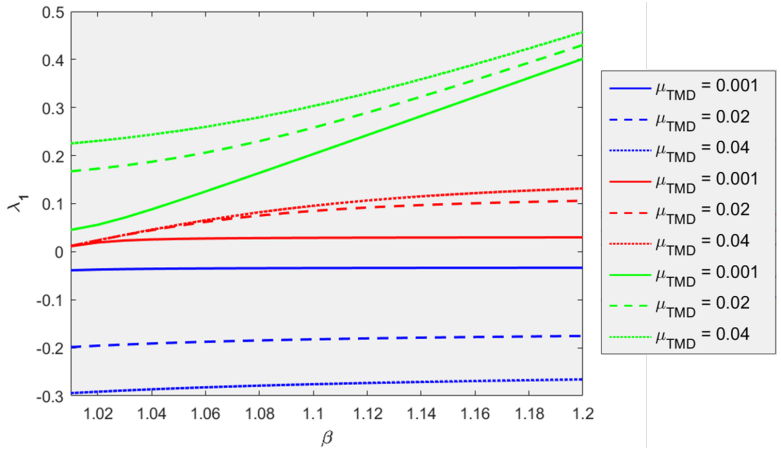

Figure 3.14: Variation of λ_1 in function of β, for different values of μ_{TMD}

It is showed in the figure that for the three modes, λ_1 increases with β. Also that, β influences more the behaviour of the third mode. At $\beta = 1$ there are only two bumps : the modes are located at the same natural frequency, then when β increases, the number of peaks goes from 2 to 3 : the first at the left of the first natural frequency, the second at the right of the second frequency, then the third between them. The green curve represents the second one, if β goes to far right, the third root will naturally follow it. In parallel, and since the TMD is tuned to the first mode, the common pole (in red) remains nearer to the first root.

Observation : *A series of trial and error has been performed, it has been discovered that the shift in the third mode at $\mu = 0$* (**Figure (3.13)**) *follows a linear progression for increasing β, through the function $2(\beta - 1)$* (**Figure (3.15)**).

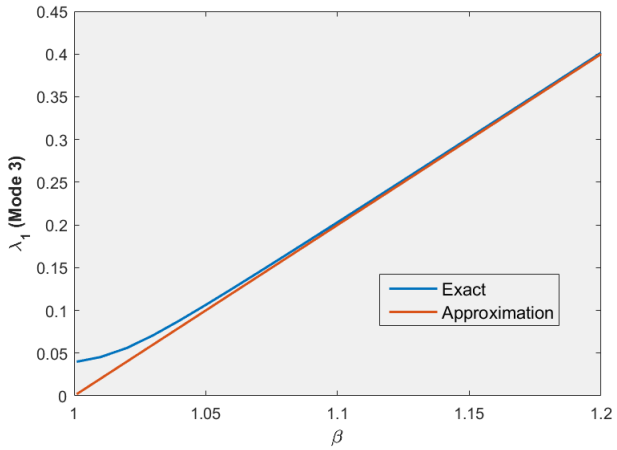

Figure 3.15: Variation of λ_1 (Third Mode) for $\mu = 0$ in function of β

- **Influence of $\overline{M_2}$**

  The variation along $\overline{M_2}$: λ_1 is increasing in the first two modes, and decreasing in the third one. For the three curves, λ_1 tends to a constant for higher values of $\overline{M_2}$: it is no longer sensitive.

  It is also observed that the variability grows as μ grows : going from constant tendency for small values of μ, to square-root distribution.

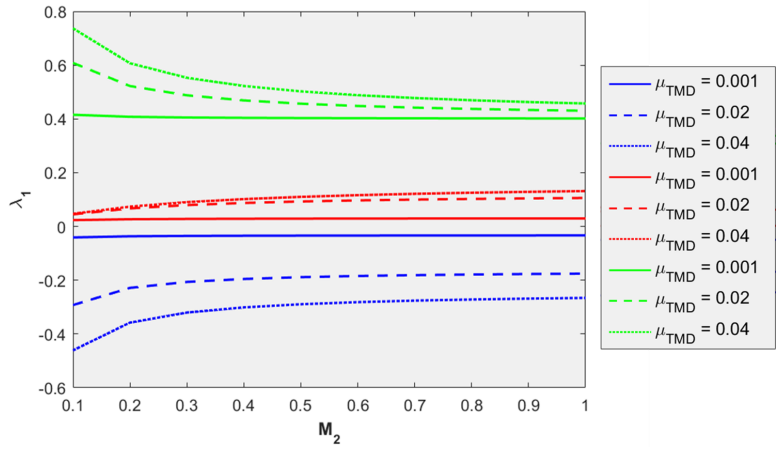

Figure 3.16: Variation of λ_1 in function of $\overline{M_2}$, for different values of μ_{TMD}

- **Influence of α**

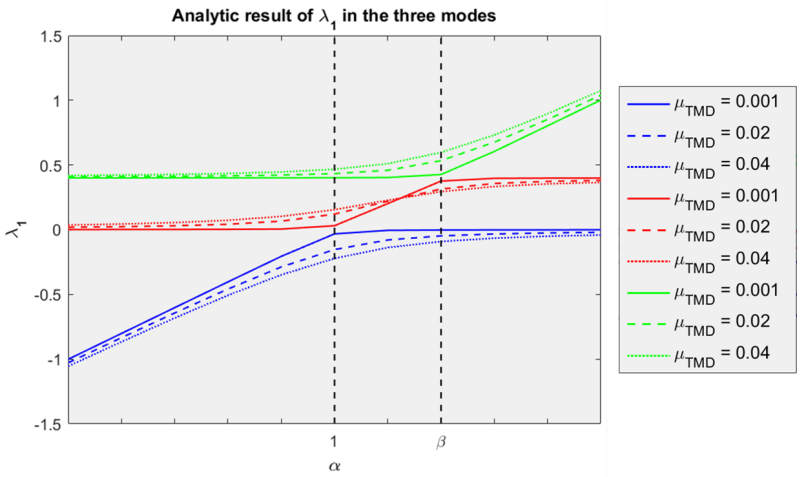

Figure 3.17: Variation of λ_1 in function of α

The evolution of the roots is marked by slope failures, evidencing three segments $[0, 1]$, $[1, \beta]$ and $[\beta, +\infty]$. The second plot (in red) is particularly marked by 2 slope failures (at $\alpha = 1$ and $\alpha = \beta$), while the other curves just one. The function knows a horizontal asymptote for $\alpha >>$ in the first mode, and a horizontal asymptote for $\alpha <<$ in the third mode. Whereas in the second, an asymptote when $\alpha >>$ and when $\alpha <<$. If the TMD is tuned other than in

the interval $[1, \beta]$, the distance between the eigenvalues becomes wider, and the modal coupling disappears.

- **Influence of** (φ_1, φ_2)

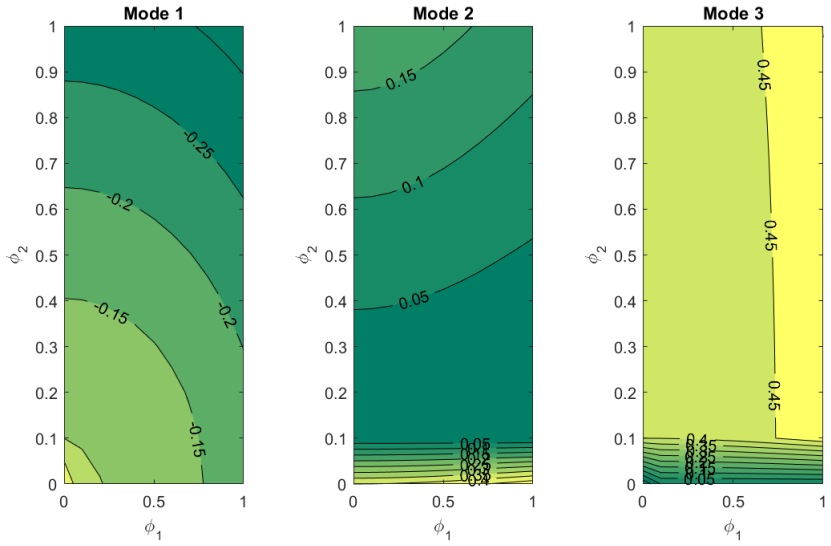

Figure 3.18: Variation of λ_1 in function of (φ_1, φ_2)

In the first mode, λ_1 is sensitive to the combined variation of φ_1 and φ_2. Whereas in the second and the third mode, the distribution is vertical for small values of φ_2. Subsequently, the distribution becomes diagonal for the second mode (similarly to the first mode), and horizontal for the third mode.

Inverse strategy

Until now, the method goes in the direction of predicting the behavior of the response. In other words, the inputs μ, ξ_{TMD} and α are known, and the goal is to verify if the analytic model reproduces well the reality, and if the acceleration's outcome is below the threshold.

In the inverse thinking, the acceleration $\sigma_{\ddot{x}}$ is limited by a threshold $\sigma_{\ddot{x},lim}$, the goal becomes the research of the values of the entry parameters. As reported by the first chapter, the variance of the acceleration is a function of ω (thus of λ_1), and ξ^* that is in itself a function of λ_1. Writing the comfort criteria $\sigma_{\ddot{x}} < \sigma_{\ddot{x},lim}$, it can be deduced a criteria on λ_1. Once this criteria determined, conditions can be derived for the 6 parameters (μ, β, α, φ_1, φ_2, and $\overline{M_2}$), given that λ_1 is function of these.

However working in such a large space (6 dimensions) inevitably requires the development of a strategy. The coefficients from the cubic equation (3.38), are combinations of the previous parameters. Besides, the roots of the equation can be expressed in function of these coefficients (Theorem of Cardano [12]). For these

reasons, the coefficients can be introduced as the new parameters of the problem, converting the problem to a 3 dimensions space (p_0,p_1,p_2).

$$\lambda_1^3 + p_2\lambda_1^2 + p_1\lambda_1 + p_0 = 0 \tag{3.46}$$

The construction of these new variables requires the determination of their domain of definition.

Start		**New**	
Parameter	**Range**	**Parameter**	**Range**
μ	$[0, 0.05]$	p_0	$[0, 0.1]$
β	$[1, 2]$		
α	$[0, 2]$	p_1	$[-4.55, 4]$
$\overline{M_2}$	$[0.1, 2]$		
φ_1^2	$[0.1]$	p_2	$[-4, 2]$
φ_2^2	$[0.1]$		

Table 3.4: Domain of definition of the new parameters

The following figures illustrate λ_1 in the spaces (p_2,p_1), (p_1,p_0) and (p_2,p_0), keeping the last variable fixed.

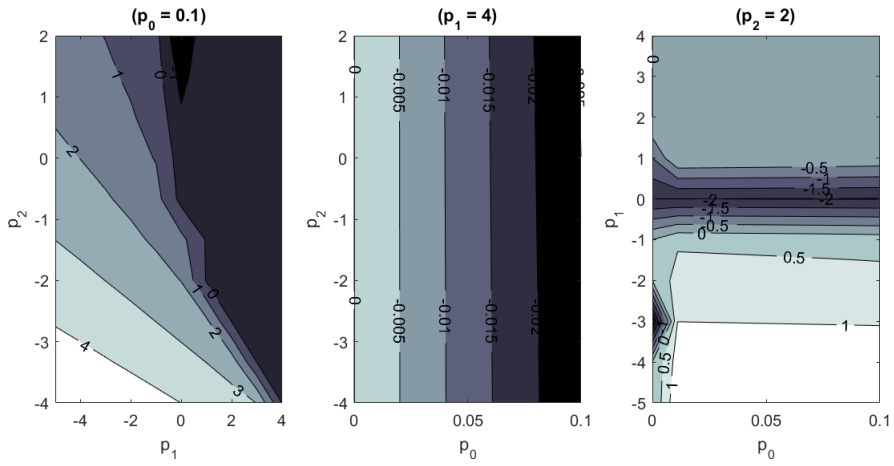

Figure 3.19: Influence of (p_0,p_1,p_2) on the first root of λ_1

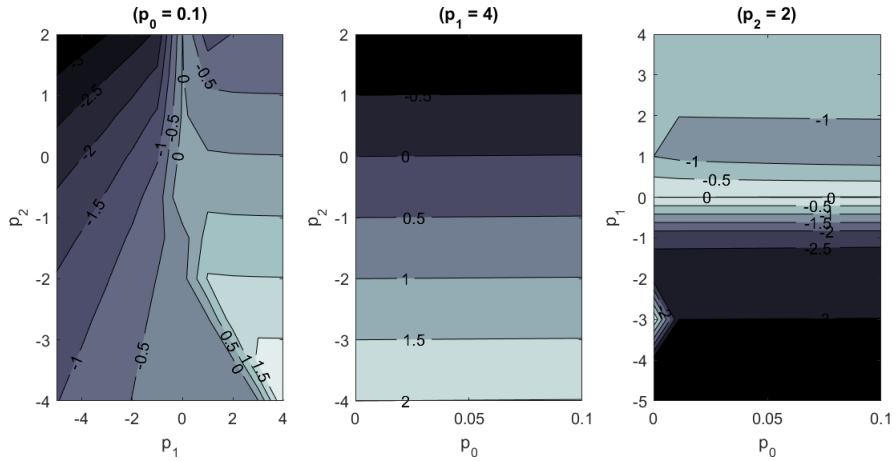

Figure 3.20: Influence of (p_0,p_1,p_2) on the second root of λ_1

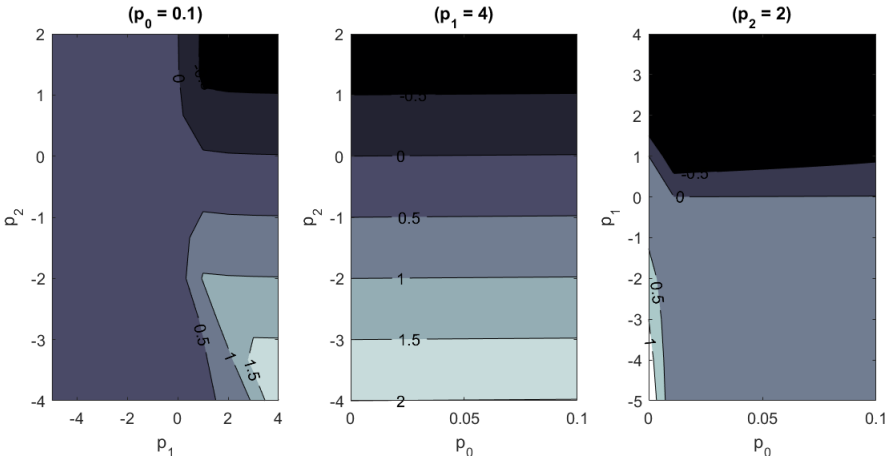

Figure 3.21: Influence of (p_0,p_1,p_2) on the third root of λ_1

All what remains is to compose a set of the 6 parameters such that the criteria on $lambda_1$ is fulfilled. The aim of these 'maps' is to offer the widest possible flexibility to the designer, by proposing a solution that is not unique, as it was until now.

4 Application on a case study

4.1 Presentation of the case study

The example that will be treated in this chapter is the footbridge of Mantes Limay in Paris (France). This new footbridge dedicated to pedestrians and cyclists in an ecoresponsible prospect. It will connect the city centre of Mantes-la-Jolie to the city centre of Limay, restoring the continuity of the old bridge of Mantes.

A dynamic study will be carried out under crowd load without damper at first, and with a TMD afterwards. The purpose is to predict the behavior of the structure with the analytic model developed through the two previous chapters.

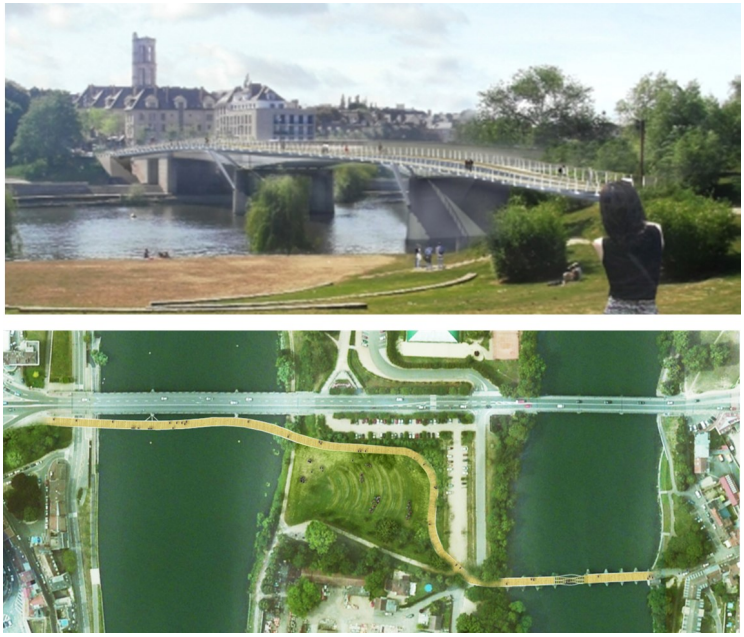

Figure 4.1: Architectural view of the footbridge of Mantes Limay (Paris)
http://www.smso.fr/index.php/lacces-aux-berges-et-a-leau/les-passerelles/14-lacces-aux-berges-et-a-leau/les-passerelles/242-passerelle-de-mantes-limay

4.1.1 Modelling and modal parameters

The footbridge is treated like a 2D-member is composed by 3 spans with a total length of $L = 203\ m$, a width of $l = 6\ m$ and a mass $M_0 = 150\ t$. Its dimensions are described in the **Figure 4.2**.

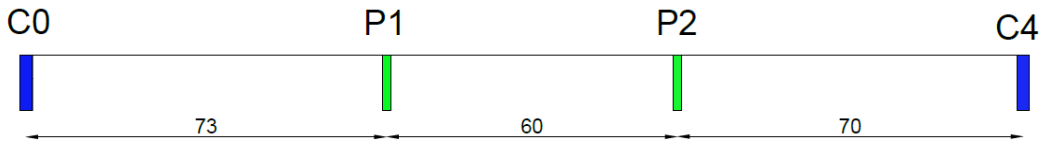

Figure 4.2: Dimensions of the footbridge

It is assumed that a study has already been conducted to identify the natural characteristics of the bridge within the lateral direction. The obtained first and second natural frequencies are $[f_1, f_2] = [1\ Hz,\ 1.12\ Hz]$. The mode shapes associated are shown on the **Figure 4.3**.

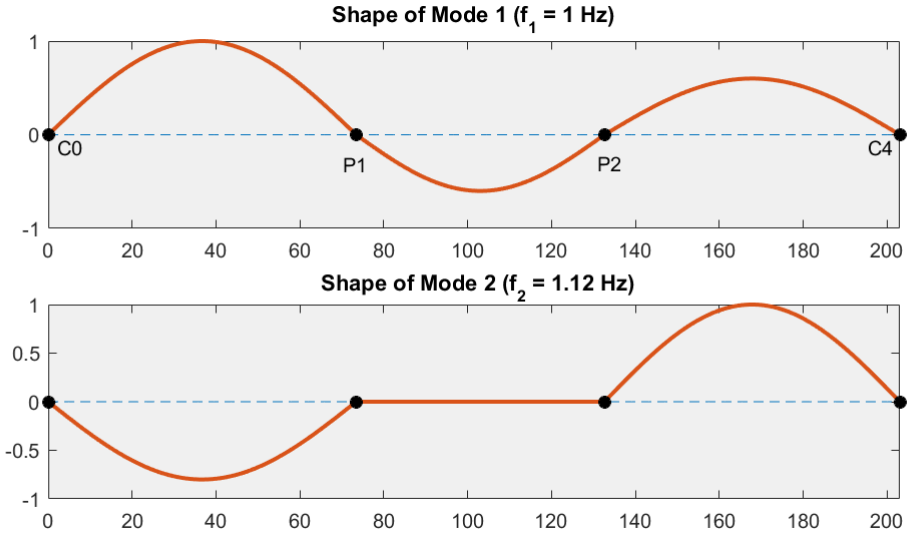

Figure 4.3: Mode shapes $\phi_i(x)$

The footbridge is constituted by a metallic deck, the average value of the critical damping ratio is $\xi_s = 0.4\%$. The modal mass is the same in the first and second mode, and they are both equal to the mass of the structure $M_{i,i} = M_0$. In the modal base, the stiffness matrix is also diagonal, where $\underline{\underline{K}} = diag(\omega_i^2 \cdot M_{i,i})$. An assumption is made for the viscosity matrix considering it diagonal as well, where $\underline{\underline{C}} = diag(2 \cdot M_{i,i} \cdot \omega_i \cdot \xi_i)$. The structure is load along the first DOF. The equation of motion is written below :

$$\begin{bmatrix} M_{1,1} & 0 \\ 0 & M_{2,2} \end{bmatrix} \begin{bmatrix} \ddot{x}_1 \\ \ddot{x}_2 \end{bmatrix} + \begin{bmatrix} C_{1,1} & 0 \\ 0 & C_{2,2} \end{bmatrix} \begin{bmatrix} \dot{x}_1 \\ \dot{x}_2 \end{bmatrix} + \begin{bmatrix} K_{1,1} & 0 \\ 0 & K_{2,2} \end{bmatrix} \begin{bmatrix} x_1 \\ x_2 \end{bmatrix} = \begin{bmatrix} p_1 \\ 0 \end{bmatrix} \tag{4.1}$$

The absolute value of the FRF is represented below bringing out the peaks related to the natural frequencies f_1 and f_2.

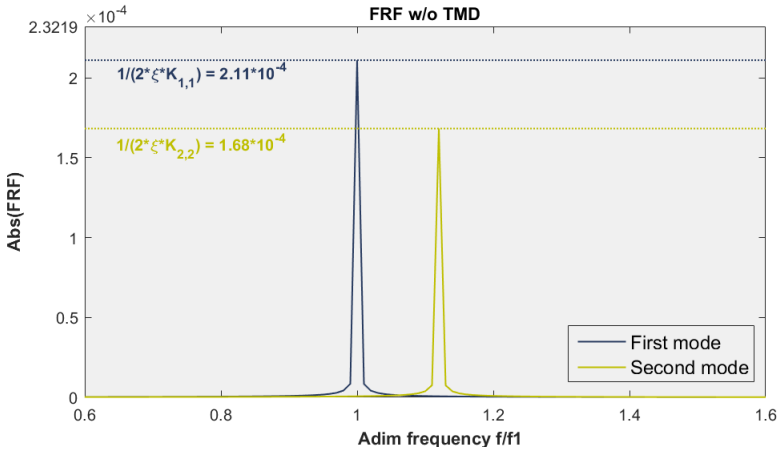

Figure 4.4: FRF without damper

4.1.2 Computation of the Loading

Deterministic Loading

4.3.1 - Frequency range classification

In both vertical and horizontal directions, there are four frequency ranges, corresponding to a decreasing risk of resonance:
Range 1: maximum risk of resonance.
Range 2: medium risk of resonance.
Range 3: low risk of resonance for standard loading situations.
Range 4: negligible risk of resonance.
Table 2.3 defines the frequency ranges for vertical vibrations and for longitudinal horizontal vibrations. Table 2.4 concerns transverse horizontal vibrations.

Frequency	0	1	1.7	2.1	2.6	5
Range 1						
Range 2						
Range 3						
Range 4						

Table 2.3: Frequency ranges (Hz) of the vertical and longitudinal vibrations

Frequency	0	0.3	0.5	1.1	1.3	2.5
Range 1						
Range 2						
Range 3						
Range 4						

Table 2.4: Frequency ranges (Hz) of the transverse horizontal vibrations

Figure 4.5: Frequency range classification for all types of resonance risks (extracted from the Sétra Guideline [8])

The Owner of the project is the one who specifies the class of the footbridge, coming out of the definition of the level of traffic. It is considered a pedestrian density d of 0.8 m^{-2} associated to the case of a dense crowd (category II), leading to a number of pedestrian $N = d \times S = 1000$.

The Owner has also to establish the comfort requirement to reach, this condition

is generally translated in terms of acceleration. In the transversal direction, the pedestrian comfort limit is 0.10 m/s^2, in order to avoid the "lock-in" effect that may occur in the range 0.10 m/s^2 to 0.15 m/s^2.

The crowd load applied to the system is computed according to the Sétra Guideline [8]. A load per unit area is obtained according to the following equation :

$$p(t) = d \times (35N) \times cos(2\pi f_0 t) \times 10.8 \times \sqrt{\frac{\xi}{n}} \times \psi \tag{4.2}$$

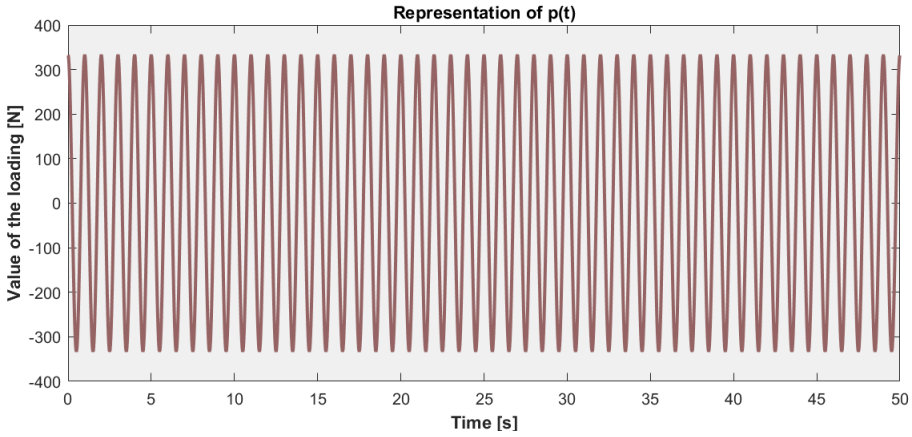

Figure 4.6: Representation of the harmonic loading modelling the crowd excitation

Stochastic loading

The loading is now modeled with a white noise. As a reminder it is the realization of a random process in which the PSD is the same for all frequencies of the bandwidth.

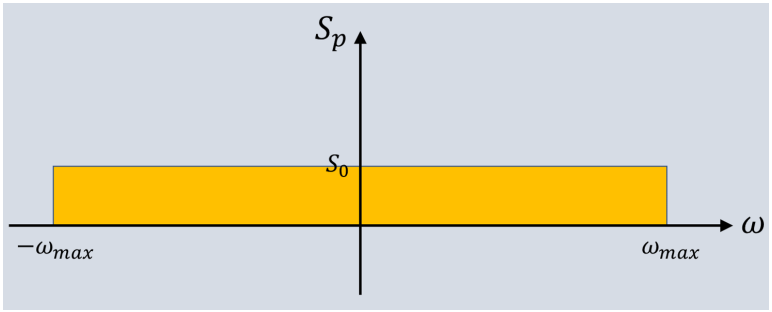

Figure 4.7: Power spectral density of the loading

In favor of keeping the same energy as the deterministic determined loading, S_0 is computed from $\sigma_P^2 = (\sqrt{2}P_h)^2$, such that σ_P^2 is the energy of the harmonic signal, and P_h its amplitude. This energy is now equalized to the energy of the white noise,

representing also the integral of the PSD, providing :

$$S_0 = \frac{\sigma_P^2}{2\omega_{max}}$$

The following table display the set of parameters used to obtain the spectral excitation. Where N_{step} is the number of step considered, and dt is the time step. ω_{max} is defined as the half of the pulsation of Nyquist $\omega_{max} = \omega_{Ny}/2$, where $\omega_{Ny} = 2\pi/dt$.

Set of parameters	
N_{step}	5000
$dt[s]$	0.01
$\sigma_P[N]$	470.3
$\omega_{max}[rad.s^{-1}]$	315
S_0	352

In the interest of generating $p(t) = \sum_{n=-\infty}^{n=+\infty} \mathcal{P}_n e^{in\Omega t}$ the time domain signal associated to this PSD, it is needed to work with Fourier transformation. Since the loading $p(t)$ is considered real, a restriction must be verified on the coefficients $\mathcal{P}_n$. Indeed, the restriction is that $p(t)$ must necessarily be equal to its combined complex $p(t) = p(t)$:

$$\sum_{n=-\infty}^{+\infty} \mathcal{P}_n e^{in\Omega t} = \sum_{n=-\infty}^{+\infty} \overline{\mathcal{P}_n} e^{-in\Omega t} = \sum_{n=-\infty}^{+\infty} \overline{\mathcal{P}_{-n}} e^{in\Omega t} \tag{4.3}$$

In order to conserve the result of the sum as real, the condition $\mathcal{P}_n = \overline{\mathcal{P}_{-n}}$ has to be verified.

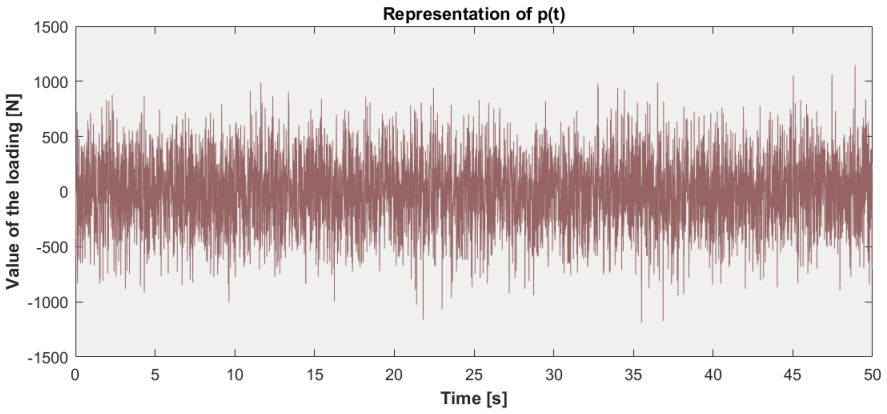

Figure 4.8: Loading $p(t)$ extracted from the PSD

4.1.3 Integration of the TMD

The introduction of a damper add another DOF to the system. The TMD is characterized by its mass m_{TMD}, its damping c_{TMD}, and its spring k_{TMD}.

The proximity of the natural frequencies expressed by $\beta = \frac{f_2 - f_1}{f_1}$ goes in agreement with the strategy that consists in the damping of 2 modes with a single TMD.

The mass, viscosity and stiffness matrix are changed : the dimensions are increased (2×2 to 3×3), and apart from the mass matrix they are no longer diagonal, as it is noticed in the following expressions.

$$\underline{\underline{\widetilde{M}}} = \begin{bmatrix} M_{1,1} & 0 & 0 \\ 0 & M_{2,2} & 0 \\ 0 & 0 & m \end{bmatrix} \tag{4.4}$$

$$\underline{\underline{\widetilde{C}}} = \begin{bmatrix} C_{1,1} & 0 & 0 \\ 0 & C_{2,2} & 0 \\ 0 & 0 & 0 \end{bmatrix} + c_{TMD} \begin{bmatrix} \varphi_1^2 & \varphi_1\varphi_2 & -\varphi_1 \\ \varphi_1\varphi_2 & \varphi_2^2 & -\varphi_2 \\ -\varphi_1 & -\varphi_2 & 1 \end{bmatrix} \tag{4.5}$$

$$\underline{\underline{\widetilde{K}}} = \begin{bmatrix} K_{1,1} & 0 & 0 \\ 0 & K_{2,2} & 0 \\ 0 & 0 & 0 \end{bmatrix} + k_{TMD} \begin{bmatrix} \varphi_1^2 & \varphi_1\varphi_2 & -\varphi_1 \\ \varphi_1\varphi_2 & \varphi_2^2 & -\varphi_2 \\ -\varphi_1 & -\varphi_2 & 1 \end{bmatrix} \tag{4.6}$$

The nodal FRF associated to these new matrices is the written :

$$\underline{\underline{\widetilde{H}}}(\omega) = (-\underline{\underline{\widetilde{M}}}\omega^2 + i\omega\underline{\underline{\widetilde{C}}} + \underline{\underline{\widetilde{K}}})^{-1} \tag{4.7}$$

The **Figure 4.9** highlights the evolution of the transfer function $\underline{\underline{\widetilde{H}}}$, for a TMD tuned on the first natural frequency.

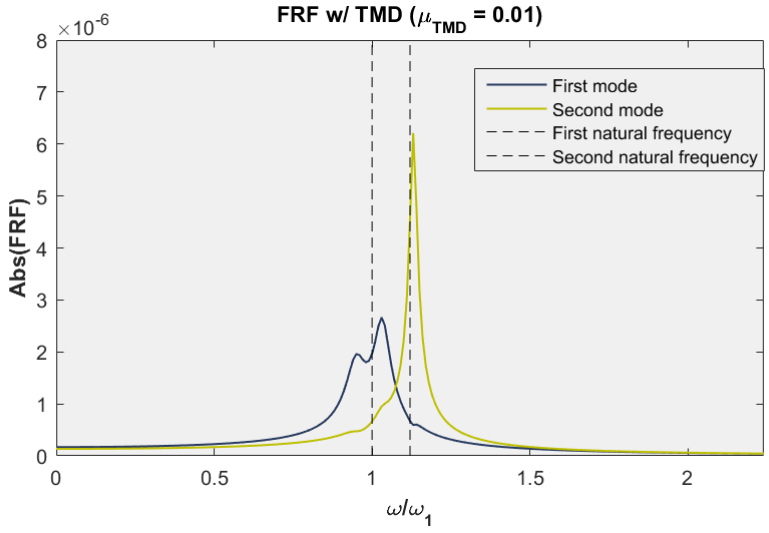

Figure 4.9: FRF after implementation of the TMD

Generalization of the matrices

The matrices $\widetilde{\underline{\underline{M}}}$, $\widetilde{\underline{\underline{K}}}$ and $\widetilde{\underline{\underline{C}}}$ are generalized, the new equation of motion and FRF expression is the following :

$$\underline{\underline{M}}^* \cdot \begin{bmatrix} \ddot{q}_1 \\ \ddot{q}_2 \\ \ddot{q}_3 \end{bmatrix} + \underline{\underline{C}}^* \cdot \begin{bmatrix} \dot{q}_1 \\ \dot{q}_2 \\ \dot{q}_3 \end{bmatrix} + \underline{\underline{K}}^* \cdot \begin{bmatrix} q_1 \\ q_2 \\ q_3 \end{bmatrix} = \begin{bmatrix} p_1^*(t) \\ 0 \\ 0 \end{bmatrix} \tag{4.8}$$

The structure is excited on its first DOF, by means of the white noise aforementioned. The PSD of this loading is $[S_P]$ such that :

$$[S_P] = \begin{bmatrix} S_0 & 0 & 0 \\ 0 & 0 & 0 \\ 0 & 0 & 0 \end{bmatrix} \tag{4.9}$$

The modal forces associated are derived from : $[S_{p^*}] = [\Phi]^T [S_p][\Phi]$

4.1.4 Response of the system

Deterministic loading

The system is a particular, the addition of a 0.01 is sufficient to go below the threshold of $0.1 m/s^2$

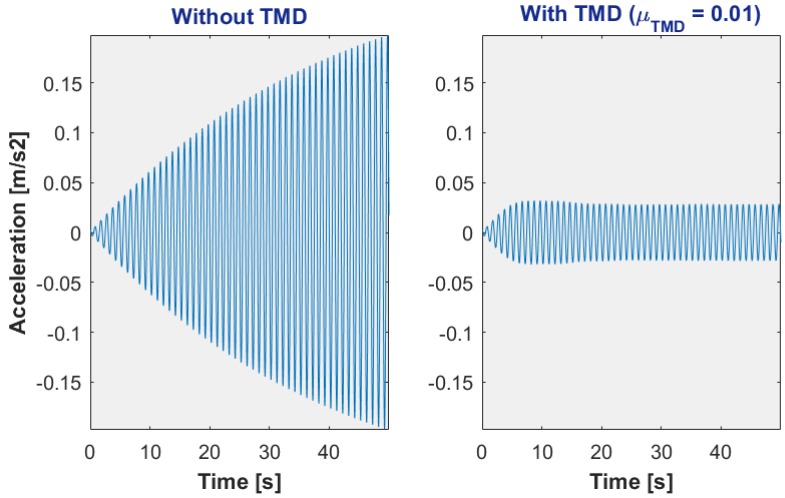

Figure 4.10: The response of the system : nodal acceleration in function of time with and without TMD

The next figure evidences the excitation frequency associated to the maximum of acceleration. To clarify the observation, a cross-section (**Figure 4.12**) is performed at $x = 168m$, with an increased mass ratio.

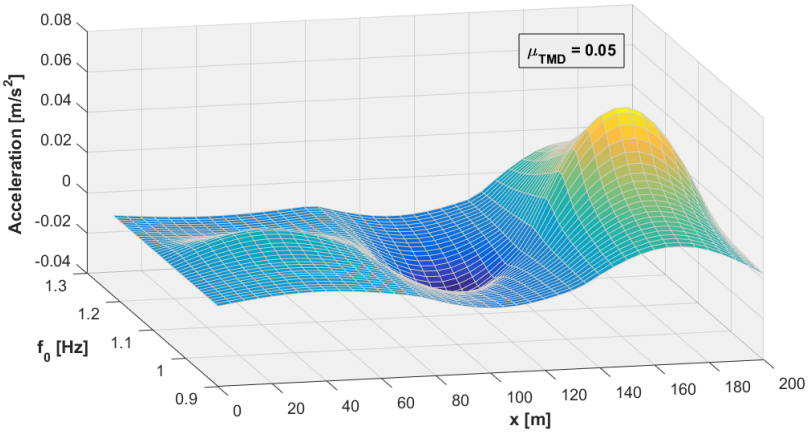

Figure 4.11: Acceleration in function of the frequency of the excitation f_0 and the longitudinal distance x

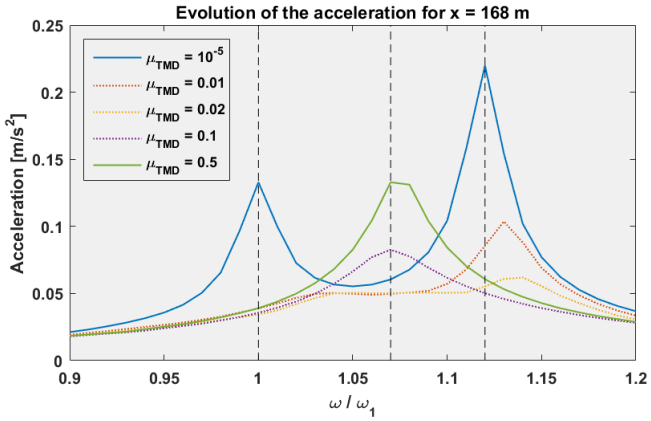

Figure 4.12: Acceleration in function of the frequency of solicitation f_0 ; at $x = 168m$

A perturbation technique has been employed by Loore [5] for the development of an analytic approximation of the FRF (4.11). A close-up in the vicinity of the resonance has been performed using an extended coordinate :

$$\hat{\omega} = \frac{\omega}{\omega_1} = 1 + \varepsilon\eta \tag{4.10}$$

with $\eta = ord(1)$

Thanks to the method developed, it is possible to make fall the singularity present in the approximation in the first order of the FRF.

$$\underline{\underline{H_1^*}}(\hat{\omega}) = \left[2\underline{\underline{\mu}}(\underline{\underline{\beta}} - \hat{\omega}\underline{\underline{I}} + i\underline{\underline{\Xi}}) - \frac{\mu_{TMD}\underline{\phi}^T\underline{\phi}}{2(\alpha - \hat{\omega} + i\xi_{TMD})}\right]^{-1} \tag{4.11}$$

Where :

$$\underline{\underline{\mu}} = \begin{bmatrix} 1 & 0 \\ 0 & M_2^*/M_1^* \end{bmatrix}, \ \underline{\underline{\beta}} = \begin{bmatrix} 1 & 0 \\ 0 & \omega_2/\omega_1 \end{bmatrix}, \ \underline{\underline{\Xi}} = \begin{bmatrix} \xi_1 & 0 \\ 0 & \xi_2 \end{bmatrix} \tag{4.12}$$

To present a notation that is habitual to the reader, a transformation of the dimensionless expression is proposed, where the variables are known :

$$\boxed{\underline{\underline{H_1^*}}(\omega) = \left[2[\underline{\underline{K}}^* - \underline{\underline{M}}^* \underline{\underline{\Omega}}\omega] + \omega_1 \underline{\underline{C}}^* - \frac{m_{TMD} \underline{\phi}^T \underline{\phi}}{2(\omega_{TMD} - \omega + i\omega_1 \xi_{TMD})}\right]^{-1}} \tag{4.13}$$

Where :

$$\underline{\underline{\Omega}} = \begin{bmatrix} \omega_1 & 0 \\ 0 & \omega_2 \end{bmatrix} \tag{4.14}$$

The analytic formulation of the transfer function allows to interpret the evolution of the acceleration in **Figure 4.12**, from 2 peaks to a single one. The discussion is presented by distinguishing 3 cases for μ_{TMD} :

- **Low values :** Two peaks are observed, the maximum values are reached at :

$$\boxed{\hat{\omega} = 1 \ ; \ \hat{\omega} = 1 + \beta} \tag{4.15}$$

- **High values :** A single peak is highlighted, the maximum value is reached for :

$$\boxed{\hat{\omega} = \hat{\omega}^* = \frac{\phi_2^2 + (1+\beta)\mu_2\phi_1^2}{\phi_2^2 + \mu_2\phi_1^2}} \tag{4.16}$$

  this value represents a sort of weighted mean between 1 and $1+\beta$. When the modes are equal, $\hat{\omega}$ tends to $1+\beta/2$ which is exactly the middle between 1 and $1+\beta$.

- **Intermediate values :** The peaks located at the poles 1 and $1+\beta$ decrease to reach a minimum value, then a transition to a single peak is observed located at the pole $\hat{\omega}^*$, followed by a rise in amplitude.

4.2 Results

In this section, the expression of the variance coming from the first chapter is completed by the results of the analytic development of the modal properties coming from the second chapter, giving rise to an expression completely analytic. The purpose is to show that the model obtained predicts appropriately the behavior of the response.

4.2.1 Approximation of the modal properties

4.2.1.1 Approximation of the eigenvalues

The following figure compares the analytic expression of the eigenvalues to the exact outcome of the equation $f(\omega^2) = |\underline{\underline{K}} - \omega^2 \underline{\underline{M}}| = 0$. The dashed curves converge well to the solid ones, with a relative error growing with μ_{TMD}. The approximation of the first mode presents the biggest error, sticking to the **Figure 4.14**. Concerning the third mode, a shift appears with respect to the numerical computation : the curves do not start from the same value. The relative errors, all modes confused, remain below 3.5% for $\mu_{TMD} \leq 5\%$

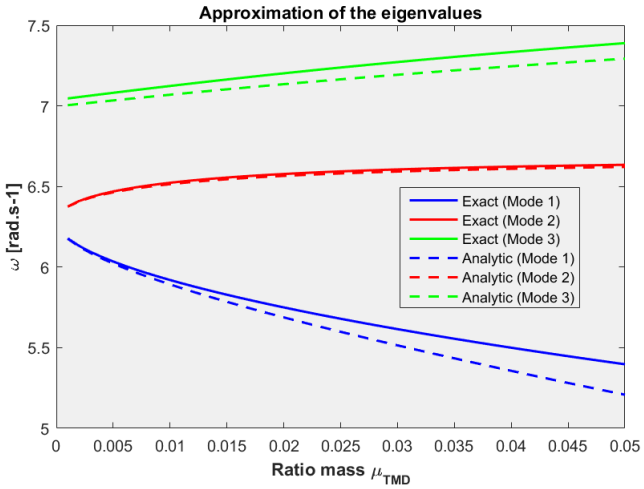

Figure 4.13: Evolution of the analytic result in function of μ_{TMD}, and comparison with the numerical eigenvalues solution

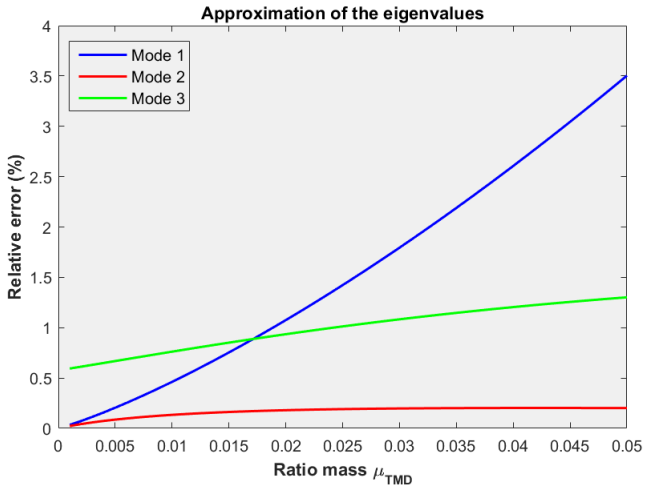

Figure 4.14: Relative error of the analytic expression with respect to numerical eigenvalues solution in function of μ_{TMD}

4.2.1.2 Approximation of the damping ratio

Moving to the equivalent damping ratio, where the exact and analytic results of the $\xi^*_{i,i}$ are represented in the **Figure 4.15**. Here again, the analytic function reproduces well the shape, but not in terms of amplitude. The errors (computed and plotted in the next figure) are increasing along μ_{TMD}, reaching 23% in the first mode, 16% in the second and 30% in the third for a mass ratio of 5%.

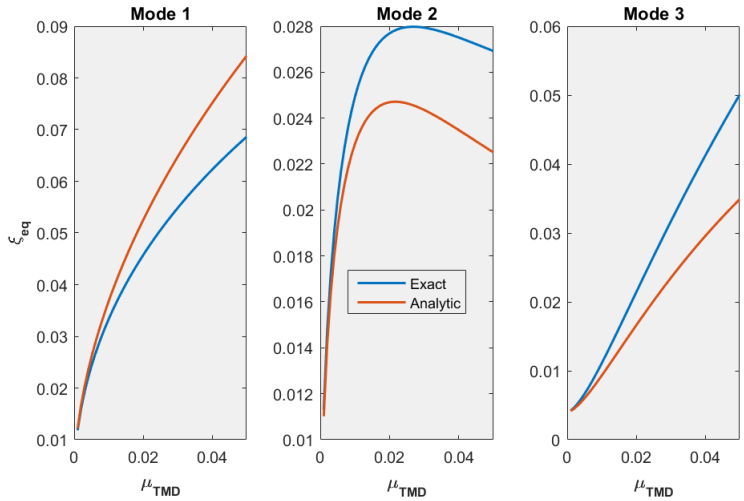

Figure 4.15: Evolution of the analytic result in function of μ_{TMD}, and comparison with the numerical equivalent damping ratio

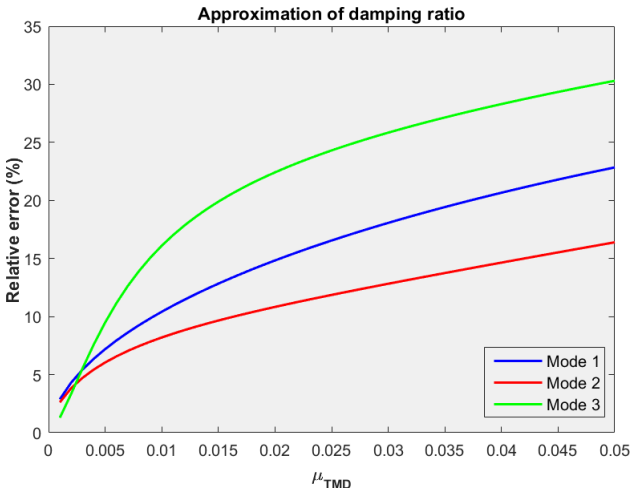

Figure 4.16: Relative error of the analytic expression with respect to the numerical outcome of the equivalent damping ratio in function of μ_{TMD}

4.2.2 Approximation of the variance

The green curves speak for the correction of the uncoupled approach (blue curves) after one iteration of the method [9]. The PSDs are therefore well approximated, for diagonal and non-diagonal components of $S_{\ddot{q}}$, according to **Figure 4.17** and **4.18**.

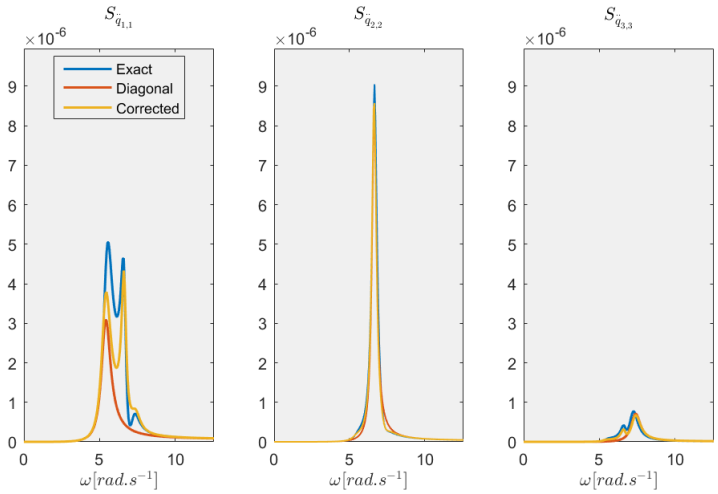

Figure 4.17: PSD of Modal acceleration (diagonal components)

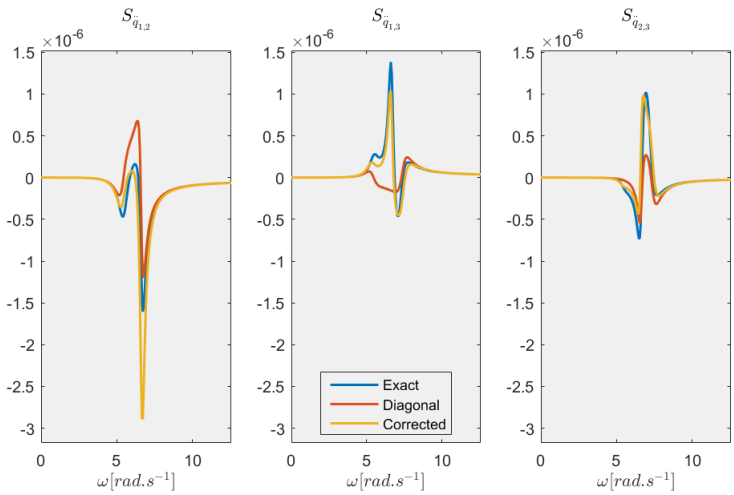

Figure 4.18: PSD of Modal acceleration (non-diagonal components)

The analytic outcomes of the variance and covariance coming from the first chapter, are linked to the uncoupled approach, hence they are compared to the 'Diagonal' curves. This time, the natural frequencies and the damping ratios that emerge from it, are replaced by the outcomes of the second chapter.

The variance computed through the integration of the PSD is depicted. According to the following figure, it is coherent to the variance measured from the time simulation of the response.

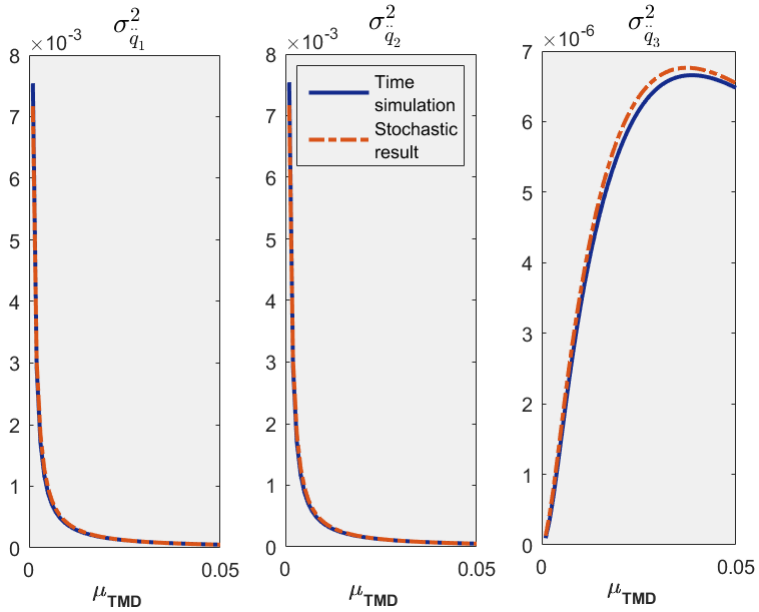

Figure 4.19: Comparison of the stochastic result of the variance of acceleration with respect to the variance measured from the time simulation

The following figures depict the error of measured on the expressions of variance and covariance. For a mass ratio 5%, the error attains as maximum : 12%.

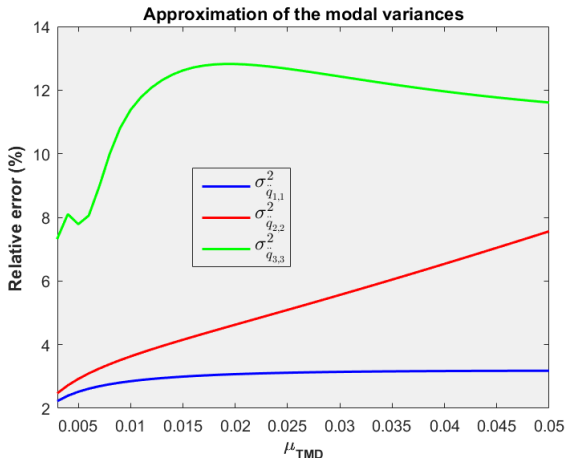

Figure 4.20: Relative error of the analytic expression of the modal variances with respect to the exact outcome solution in function of μ_{TMD}

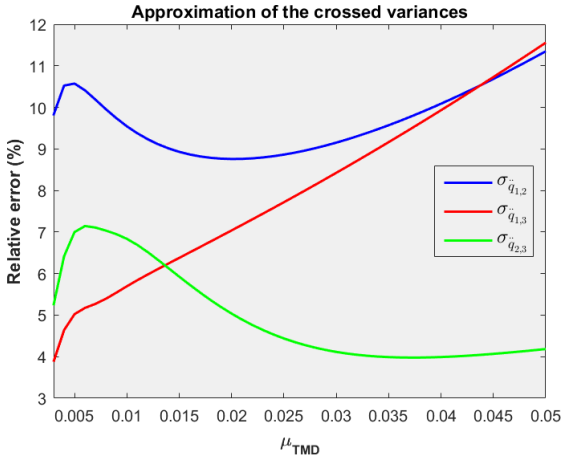

Figure 4.21: Relative error of the analytic expression of the crossed variances with respect to the exact outcome in function of μ_{TMD}

In the **Figure 4.22**, the nodal variance associated to the first DOF is plotted in the different configurations. The error related to the analytic variance at 5% of mass, is estimated at : 16%.

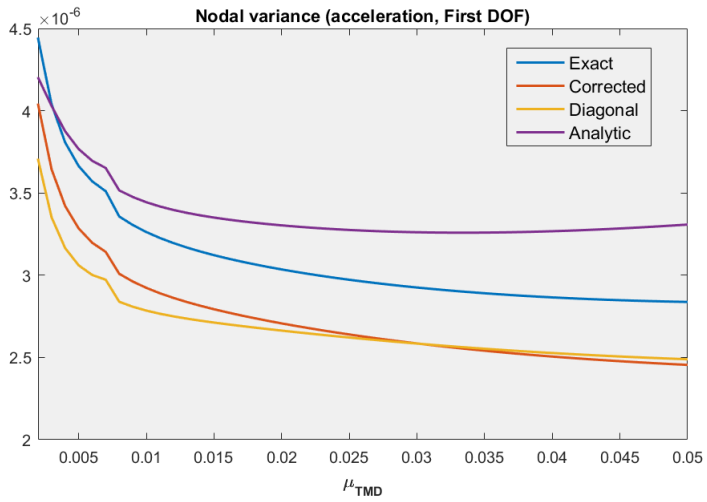

Figure 4.22: Evolution of the nodal variance in function of μ_{TMD}

Like it was done in the SDOF system, a validation of the model is proposed. The variance of the acceleration is represented in the (α, ξ_{TMD}) domain for the first DOF (the loaded DOF).

The 'Corrected' map corresponds to the uncoupled system rectified with [9], the result is obtained after three iterations. It converges well towards the exact result. The 'Analytic' map reproduces well the shape of the exact solution, as it depicts the white region containing the minimal values of the variance. The α optimum is also well approximated ($\alpha_{opt} = 1.056$). However, the criteria on ξ_{TMD} ($\xi_{opt} = 0.67$) is not conform.

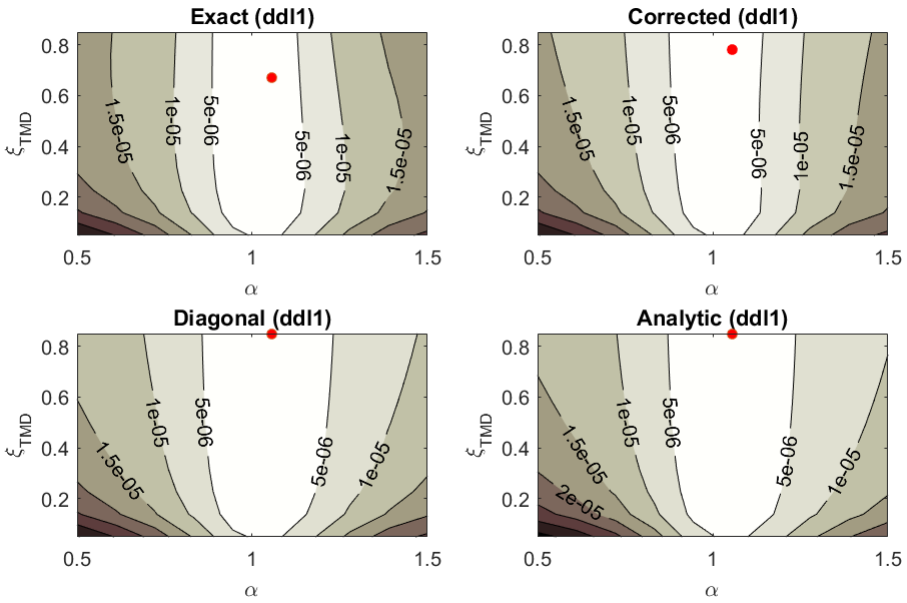

Figure 4.23: Representation of the variance of the acceleration in the (α, ξ_{TMD}) space

4.3 Conclusion of the application

The method is revealed to be satisfactory, as it imitates in a precise way the dynamic behavior of an MDOF structure subjected to lateral vibrations. It provides a forecast of the response, and offers a good approximation of the optimum domain (α, ξ_{TMD}).

5 Conclusion

For footbridges subjected to crowd-induced vibrations, an estimation of the response is requested for the assessment of the dynamic behaviour. When the vibrations go beyond the comfort limits, the main structure can be equipped with a TMD to reduce the vibration levels. The damper sees its properties tuned to the properties of the footbridge. Optimal values are available in the literature for SDOF strutures, where the natural frequency and damping ratio of the device are defined in function of the input of the problem : the mass ratio between the damper and the primary system.

This work focuses on the definition of the response thanks a spectral analysis using stochastic operators, with the loading and the response designated by random variables. Perturbation techniques has been employed to point out the interactions between multiple modes (modal coupling). Based on assumptions on the order of magnitudes of the different parameters, dimensionless formulations have been derived for complex equations. The mentioned techniques proved to be a perfectly effective tool in simplifying the basic problem. The formulas derived are simple, rich in information, and with a scope that is quite general.

The document aims attention to the importance of modal coupling in the evaluation of the criteria for bridge comfort. It proposes a complete analytic method permitting to predict the response of a damped structure using a single TMD to dampen 2 modes simultaneously, which is not feasible with simplistic methods neglecting the effect of coupling.

The generalization proposed could also make it possible to study the problems of seismic or wind in buildings of high height. The proposed expression may, beyond the use to which it is to be put, constitute a study object or a perfectly general tool for characterizing the coupled dynamics of any structure comprising a damper. Moreover, the overall approach followed here could also be applied in the case of the use of several TMD, or even more sophisticated dampers, which still opens the door to many additional investigations.

The personal contributions have involved :

- The computation of the acceleration variance and covariance analytic formula based on Denoël's displacement results [10] ;
- The adaptation of the method proposed by Denoël [9] (Method aiming to rectify the uncoupled approach outcome, using the asymptotic expansion of the transfer function), for the case of a normalization for a unitary maximum, and the proposition of an analytic expression of the correction ;

- The establishment of the first order approximation of the eigenvalues and the equivalent damping ratios for SDOF and MDOF structures, treating with the modal basis (employment of generalized matrices).

References

[1] V. Denoël. *Analyse de structures soumises au vent turbulent : de l'approche stochastique fréquentielle au dynamique transitoire non linéaire*, volume 1. Faculté des Sciences appliquées, Université de Liège (Plateforme Matheo http://hdl.handle.net/2268/13006), 2003.

[2] V. Denoël. *Analyse de structures 2 (Syllabus Master I)*, volume 1. Faculté des Sciences appliquées, Université de Liège, 2017.

[3] J. P. D. Hartog. *Mechanical Vibrations*, volume 4th edition. McGraw-Hill, New York, 1956.

[4] S. Hicks, M. Feldmann, C. Heinemeyer, M. Lukic, E. Caetano, A. Cunha, A. Goldack, A. Keil, M. Schlaich, A. Smith, O. Hechler, R. Obiala, F. Galanti, and P. Waarts. *Human-induced vibration of steel structures (Hivoss)*. European Research Area - European Commission, 2010.

[5] T. Loore. *Effet du couplage modal sur le contrôle du comportement vibratoire de passerelles*, volume 1. Faculté des Sciences appliquées, Université de Liège (Plateforme Matheo http://hdl.handle.net/2268.2/4556), 2018.

[6] J. C. Miranda. *A method for tuning tuned mass dampers for seismic applications*, volume 42, 1103-1110. Earthquake eng. struct. dyn., 2012.

[7] Sadek F, Mohraz B. *A method of estimating the parameters of tuned mass dampers for seismic applications*, volume 26:617-35. Earthquake eng. struct. dyn., 1997.

[8] Service d'Études Techniques des Routes et Autoroutes (Sétra). *Technical guide - Footbridges: Assessment of vibrational behaviour of footbridges under pedestrian loading*. Ministère des Transports, de l'Equipement, du Tourisme, et de la Mer (France), 2006.

[9] Vincent Denoël, Hervé Degée. *Asymptotic expansion of slightly coupled modal dynamic transfer functions*, volume (328):1-8. Journal of Sound and Vibration, 2009.

[10] Vincent Denoël. Multiple timescale spectral analysis. *Probabilistic Engineering Mechanics*, (39) 69–86. 2015.

[11] G. B. Warburton. *Optimum absorber parameters for minimizing vibration response*, volume 9 :251–262. Earthquake eng. struct. dyn., 1981.

[12] Weisstein, Eric W.. Cubic Formula (Theorem of Cardano). *MathWorld–A Wolfram Web Resource* http://mathworld.wolfram.com/CubicFormula.html.

[13] Yozo Fujino, Masato Abé. *Design formulas for tuned mass dampers based on a perturbation technique*, volume 22, 833-854. Earthquake Engineering And Structural Dynamics, 1993.

Appendix

A1 Variance of displacement

The purpose is to demonstrate thanks to a perturbation technique the mathematical sentence below, that declares the variance of the displacement, giving a white noise loading of intensity S_0 for an SDOF system.

$$\sigma_q^2 = S_0 \int_{-\infty}^{+\infty} |H(\omega)|^2 d\omega = \frac{S_0}{K^2} \cdot \frac{\pi \omega_m}{2\xi} \tag{.1}$$

Starting from k_2, that is defined as the following integral : with the introduction of a new variable $K(\omega) = |H(\omega)|^2$ illustrating the kernel of the problem.

$$k_2 = \int_{-\infty}^{+\infty} K(\omega)\ d\omega;\ K(\omega) = \frac{1}{K^2} \frac{1}{(1 - (\frac{\omega}{\omega_m})^2)^2 + (2\xi \frac{\omega}{\omega_m})^2} \tag{.2}$$

The kernel can be expressed as the sum of a background component and a residual one $K(\omega) = \widetilde{K}(\omega) + \mathcal{K}(\omega)$.

The background component $\widetilde{K}(\omega)$ corresponds to the kernel evaluated in the low-frequency range. Making ω tend to 0, an approximation in the vicinity of the origin is obtained : $\widetilde{K}(\omega) \sim \frac{1}{K^2}$.

The residual component represents the quantity needed to recover the exact value of the kernel. The shape of the kernel highlights the presence of two peaks corresponding to the natural frequency and its negative image. A local approximation near the natural frequency is sought, which induces the introduction of the strained coordinate : $\omega = (1 + \xi\eta)\omega_m$, where ξ is the damping ratio and $\eta = ord(1)$. ξ constitutes a small quantity (order of magnitude lower than the other terms), it represents also a characteristic of the resonant peak, since the peak's width is of order $\xi\omega_m$.

$$\mathcal{K}(\omega(\eta)) = K(\omega) - \frac{1}{K^2} = \frac{1}{K^2}(\frac{1}{(1 - (1 + \xi\eta)^2)^2 + (2\xi(1 + \xi\eta))^2} - 1)$$

A simplification is made on the last equation :

$$\mathcal{K}(\omega(\eta)) = \frac{1}{K^2\xi^2} \frac{(1 + \xi\eta)^2(1 - 2\xi\eta - (4 + \eta^2)\xi^2)}{4(1 + \eta^2) + 4\xi\eta(2 + \eta^2) + \xi^2\eta^2(4 + \eta^2)}$$

To focus on only one peak at a time, an approximation can be obtained by assuming $\xi << 1$, which results in the suppression of the terms containing $\xi\eta$. The resulted $\mathcal{K}$

represents a first residual, since it is associated to the peak of frequency ω_m.

$$\mathcal{K}(\omega(\eta)) = \frac{1}{K^2\xi^2}\frac{1}{4(1+\eta^2)}$$

The expression is now lighter, with a degree 2 in the denominator instead of degree 4. The residual is now integrable, its integral is simple to compute :

$$k_{2,r_1} = \int_{-\infty}^{+\infty} \mathcal{K}(\omega(\eta))\ \xi\omega_m d\eta = \frac{1}{K^2}\cdot\frac{\pi\omega_m}{4\xi}$$

The close-up on the second peak provides the second residual, and since the peaks are similar, it can be written that : $k_{2,r_2} = k_{2,r_1}$. Finally, the variance is deduced :

$$\boxed{\sigma_q^2 = S_0 \cdot k_{2,r} = S_0 \cdot (2 \times k_{2,r_1}) = \frac{S_0}{K^2}\cdot\frac{\pi\omega_m}{2\xi}}$$

A2 Covariance of displacement

The purpose is to demonstrate thanks to a perturbation technique the mathematical sentence below, that declares the covariance of the displacement, giving a white noise loading of intensity S_0 for an MDOF system.

$$\sigma_{q_{m,n}} = \frac{1}{K_m K_n}\ Re\Big(\frac{S_{p_{m,n}}(\omega_m) + S_{p_{m,n}}(\omega_n)}{2}\frac{\omega_m + \omega_n}{2}\frac{\pi(\xi - i\varepsilon)}{2(\varepsilon^2 + \xi^2)}\Big) \tag{.3}$$

Starting from k_2, that is defined as the following integral : with the introduction of a new variable $K(\omega) = H_m(\omega)\overline{H_n(\omega)}^T$ illustrating the kernel of the problem.

$$k_2 = \int_{-\infty}^{+\infty} S_{p_{m,n}}(\omega)K(\omega)\ d\omega;$$

$$K(\omega) = \frac{1}{K_m K_n}\frac{1}{[1 - (\frac{\omega}{\omega_m})^2 + 2i\xi\frac{\omega}{\omega_m}][1 - (\frac{\omega}{\omega_n})^2 - 2i\xi\frac{\omega}{\omega_n}]} \tag{.4}$$

The kernel can be expressed as the sum of a background component and a residual one $K(\omega) = \widetilde{K}(\omega) + \mathcal{K}(\omega)$.

The background component $\widetilde{K}(\omega)$ corresponds to the kernel evaluated in the low-frequency range. Making ω tend to 0, an approximation in the vicinity of the origin is obtained : $\widetilde{K}(\omega) \sim \frac{1}{K_m K_n}$.

The residual component represents the quantity needed to recover the exact value of the kernel. The shape of the kernel highlights the presence of ...

$$\mathcal{K}(\omega(\eta)) = K(\omega) - \frac{1}{K^2} = \frac{1}{K^2}(\frac{1}{(1 - (1 + \xi\eta)^2)^2 + (2\xi(1 + \xi\eta))^2} - 1)$$

A local approximation is sought that permits the close-up on both natural frequencies simultaneously. This induces the introduction of the strained coordinate $\omega(\eta)$ that is centered on the average of the natural frequencies :

$$\omega = \frac{\omega_m + \omega_n}{2} + \eta\ (\omega_n - \omega_m) = \frac{\omega_m + \omega_n}{2}(1 + 2\varepsilon\eta)$$

With : $\eta = ord(1)$, and $\varepsilon = \frac{\omega_n - \omega_m}{\omega_m + \omega_n}$ a small dimensionless parameter that measures the gap between natural frequencies.

Stepping back to the residual component, the following equation represents its development with the introduction of the new coordinate :

$$\mathcal{K}(\omega(\eta)) = \frac{1}{K_m K_n}\frac{1 + 2\varepsilon^2 + 4i\xi(-2\varepsilon + \varepsilon^3)}{D};$$

With :

$$D = 8\varepsilon^2(-\varepsilon^2+6i\xi\varepsilon+2)\eta^2+8\varepsilon(-i\xi\varepsilon^3-\varepsilon^2+4i\xi\varepsilon+2\xi^2)\eta+(\varepsilon^4-4i\xi\varepsilon^3-4\varepsilon^2+8i\xi\varepsilon+4\xi^2)$$

To focus exclusively on the case where the natural frequencies are of the same order of magnitude, an approximation can be obtained by imposing $\varepsilon^2 << 1$. The condition contains the cases : $\varepsilon < \xi$ where the peaks are joined, and $\varepsilon > \xi$ where the peaks are separated. The result is the suppression of the terms of order ε^3.

$$\mathcal{K}(\omega(\eta)) = \frac{1}{4K_mK_n}\frac{1}{(4\eta^2-1)\varepsilon^2+2i\xi\varepsilon+\xi^2}$$

The expression is now lighter, with a degree 2 in the denominator instead of degree 4. On the other hand, it is performed a Taylor expansion of the PSD, such that :

$$S_{p_{m,n}}(\omega(\eta)) = S_p(\frac{\omega_m+\omega_n}{2}) + S'_p(\frac{\omega_m+\omega_n}{2})(\omega_n-\omega_m)\eta + ord(\eta^2)$$

The PSD is approximated to its first term giving :

$$S_{p_{m,n}}(\omega(\eta)) \approx S_p(\frac{\omega_m+\omega_n}{2}) \simeq \frac{S_p(\omega_m)+S_p(\omega_n)}{2}$$

Finally, the residual is integrable. Its integral $k_{2,r}$ is decomposed such that $k_{2,r} = k_{2,r_1} + k_{2,r_2}$, where k_{2,r_1} captures the resonant peaks on the positive side of the frequency domain, and k_{2,r_2} its complex conjugate.

$$k_{2,r_1} = \int_{-\infty}^{+\infty} S_p(\omega(\eta))\mathcal{K}(\omega(\eta))\ \frac{\omega_m+\omega_n}{2}2\varepsilon\ d\eta$$

$$= \frac{1}{4K_mK_n}\frac{S_p(\omega_m)+S_p(\omega_n)}{2}\frac{\omega_m+\omega_n}{2}\underbrace{\int_{-\infty}^{+\infty}\frac{2\varepsilon}{4\eta^2\varepsilon^2+(\xi+i\varepsilon)^2}\ d\eta}_{I_1}$$

I_1 is obtained performing Cauchy's residue theorem, since the applicability conditions are fulfilled by the rational fraction :

- The denominator admit complex poles where at least one of them has a positive imaginary part ;
- The degree of the numerator + 2 $\leq$ The degree of the denominator ;

$$I_1 = \frac{\pi(\xi-i\varepsilon)}{(\varepsilon^2+\xi^2)} \tag{.5}$$

The replacement of I_1 in k_{2,r_1} gives :

$$k_{2,r_1} = \frac{1}{K_mK_n}\frac{S_p(\omega_m)+S_p(\omega_n)}{2}\frac{\omega_m+\omega_n}{2}\frac{\pi(\xi-i\varepsilon)}{4(\varepsilon^2+\xi^2)} \tag{.6}$$

Finally the addition of the contribution of k_{2,r_2} provides the wanted result of $k_{2,r}$:

$$\boxed{k_{2,r} = \frac{1}{K_m K_n}\ Re\Big(\frac{S_{p_{m,n}}(\omega_m) + S_{p_{m,n}}(\omega_n)}{2}\frac{\omega_m + \omega_n}{2}\frac{\pi(\xi - i\varepsilon)}{2(\varepsilon^2 + \xi^2)}\Big)}$$

A3 Approximation of the eigenvalues (Alternative method)

$$\underline{\underline{\widetilde{M}}} = \underline{\underline{A}}^T \underline{\underline{M}}\ \underline{\underline{A}} = \underbrace{\begin{bmatrix} 1 & 0 & 0 \\ 0 & \overline{M_2} & 0 \\ 0 & 0 & \mu_1 \end{bmatrix}}_{\underline{\underline{M_0}}} \tag{.7}$$

$$\underline{\underline{\widetilde{K}}} = \underline{\underline{A}}^T \underline{\underline{K}}\ \underline{\underline{A}} = \underbrace{\begin{bmatrix} 1 & 0 & 0 \\ 0 & \beta^2\overline{M_2} & 0 \\ 0 & 0 & \mu_1 \end{bmatrix}}_{\underline{\underline{K_0}}} + \underbrace{\begin{bmatrix} 0 & 0 & -\mu_1\varphi_1 \\ 0 & 0 & -\mu_1\varphi_2 \\ -\mu_1\varphi_1 & -\mu_1\varphi_2 & 2\nu_2 \end{bmatrix}}_{\underline{\underline{K_1}}} \varepsilon + ord(\varepsilon^2) \tag{.8}$$

Limiting the power series expansions to the order ε^1. Similarly to the system 2×2, the eigenvalue problem $(\underline{\underline{\widetilde{K}}} - \lambda\underline{\underline{\widetilde{M}}})\underline{\phi'} = 0$ give birth to 2 equations :

- Order ε^0 : $(\underline{\underline{K_0}} - \underline{\underline{M_0}}\lambda_0)\underline{\phi_0} = 0 \Rightarrow \lambda_0 = \{1, 1, \beta^2\}$
- Order ε^1 : $(\underline{\underline{K_1}} - \lambda_1\underline{\underline{M_0}})\underline{\phi_0} = 0 \Rightarrow \lambda_1 = \{0, \nu_2 \pm \sqrt{\nu_2^2 + \mu_1(\varphi_1^2 + \frac{\varphi_2^2}{\overline{M_2}})}\}$

The obtained formula of λ remains coherent with the result found in the 2DOF system. It represents a generalization, the EQUATION (3.10) is met when the following parameters are set :

Set of parameters			
β	$\overline{M_2}$	φ_1	φ_2
1	1	1	0

3 eigenvalues are expected from a 3DOF system. However, the analytic development provides 6 possible combinations of $\lambda = \lambda_0 + \varepsilon\lambda_1$. When exploring the different cases, the case $\lambda_1 = 0$ seems to state that one of the eigenvalues λ remains constant, even when μ increases. This case is not possible, it is thus eliminated, leaving 4 possibilities for λ.

$$\lambda = \begin{cases} 1 + \varepsilon(\nu_2 \pm \sqrt{\nu_2^2 + \mu_1(\varphi_1^2 + \frac{\varphi_2^2}{\overline{M_2}})} \\ \beta^2 + \varepsilon(\nu_2 \pm \sqrt{\nu_2^2 + \mu_1(\varphi_1^2 + \frac{\varphi_2^2}{\overline{M_2}})} \end{cases}$$

$$\omega = \begin{cases} \Omega_1\sqrt{\alpha + \sqrt{(\alpha-1)^2 + \mu(\varphi_1^2 + \frac{\varphi_2^2}{\overline{M_2}})}} \\ \Omega_1\sqrt{\beta^2 + \alpha - 1 + \sqrt{(\alpha-1)^2 + \mu(\varphi_1^2 + \frac{\varphi_2^2}{\overline{M_2}})}} \end{cases}$$

$$\omega = \begin{cases} \Omega_1 \sqrt{1 + \sqrt{\mu(\varphi_1^2 + \frac{\varphi_2^2}{M_2})}} \\ \Omega_1 \sqrt{\beta^2 + \sqrt{\mu(\varphi_1^2 + \frac{\varphi_2^2}{M_2})}} \end{cases}$$